NASA/CR—2000-209813

Acoustic and Aerothermal Performance Test of the Axisymmetric Coannular Ejector Nozzle

Volume II—Acoustic Performance

William Herkes
The Boeing Commerical Airplane Group, Seattle, Washington

February 2000

The NASA STI Program Office . . . in Profile

Since its founding, NASA has been dedicated to the advancement of aeronautics and space science. The NASA Scientific and Technical Information (STI) Program Office plays a key part in helping NASA maintain this important role.

The NASA STI Program Office is operated by Langley Research Center, the Lead Center for NASA's scientific and technical information. The NASA STI Program Office provides access to the NASA STI Database, the largest collection of aeronautical and space science STI in the world. The Program Office is also NASA's institutional mechanism for disseminating the results of its research and development activities. These results are published by NASA in the NASA STI Report Series, which includes the following report types:

- TECHNICAL PUBLICATION. Reports of completed research or a major significant phase of research that present the results of NASA programs and include extensive data or theoretical analysis. Includes compilations of significant scientific and technical data and information deemed to be of continuing reference value. NASA's counterpart of peer-reviewed formal professional papers but has less stringent limitations on manuscript length and extent of graphic presentations.

- TECHNICAL MEMORANDUM. Scientific and technical findings that are preliminary or of specialized interest, e.g., quick release reports, working papers, and bibliographies that contain minimal annotation. Does not contain extensive analysis.

- CONTRACTOR REPORT. Scientific and technical findings by NASA-sponsored contractors and grantees.

- CONFERENCE PUBLICATION. Collected papers from scientific and technical conferences, symposia, seminars, or other meetings sponsored or cosponsored by NASA.

- SPECIAL PUBLICATION. Scientific, technical, or historical information from NASA programs, projects, and missions, often concerned with subjects having substantial public interest.

- TECHNICAL TRANSLATION. English-language translations of foreign scientific and technical material pertinent to NASA's mission.

Specialized services that complement the STI Program Office's diverse offerings include creating custom thesauri, building customized data bases, organizing and publishing research results . . . even providing videos.

For more information about the NASA STI Program Office, see the following:

- Access the NASA STI Program Home Page at ***http://www.sti.nasa.gov***

- E-mail your question via the Internet to help@sti.nasa.gov

- Fax your question to the NASA Access Help Desk at (301) 621-0134

- Telephone the NASA Access Help Desk at (301) 621-0390

- Write to:
  NASA Access Help Desk
  NASA Center for AeroSpace Information
  7121 Standard Drive
  Hanover, MD 21076

NASA/CR—2000-209813

Acoustic and Aerothermal Performance Test of the Axisymmetric Coannular Ejector Nozzle

Volume II—Acoustic Performance

William Herkes
The Boeing Commerical Airplane Group, Seattle, Washington

Prepared under Contract NAS3–25963

National Aeronautics and
Space Administration

Glenn Research Center

February 2000

Available from

NASA Center for Aerospace Information
7121 Standard Drive
Hanover, MD 21076
Price Code: A06

National Technical Information Service
5285 Port Royal Road
Springfield, VA 22100
Price Code: A06

Table of Contents

List of Figures

References

1. Zaman, K. B. M. Q., "Streamwise Vorticity Generation and Mixing Enhancement in Free Jets by 'Delta–Tabs'," AIAA Paper 93–3253, AIAA Shear Flow Conference, July, 1993.
2. Samimy, M., M. F. Reeder, and K. B. M. Q. Zaman, "Supersonic Jet Mixing Enhancement by Vortex Generations," AIAA Paper 91–2263, AIAA/SAE/ASME/ASEE 17th Joint Propulsion Conference, June, 1991.
3. Ahuja, K. K., "Mixing Enhancement and Jet Noise Reduction Through Tabs plus Ejectors," AIAA Paper 93–4347, 15th AIAA Aeroacoustics Conference, October, 1993.
4. Kobayashi, H., H. Oinuma, T. Sawamura, and E. Outa, "Effects of Tabs on Supersonic Underexpanded Cold and Heated Jet Noise Suppression and Jet Thrust Loss," AIAA Paper 93–4348, 15th AIAA Aeroacoustics Conference, October, 1993.
5. Samimy, M., K. B. M. Q. Zaman, and M. F. Reeder, "Effect of Tabs on the Flow and Noise Field of an Axisymmetric Jet," *AIAA Journal*, Vol. 31, No. 4, pp. 609–619, April, 1993.
6. Ahuja, K. K., J. P, Manes, K. C. Massey, and A. B Calloway, "An Evaluation of Various Concepts of Reducing Supersonic Jet Noise," AIAA Paper 90–3982, 13th AIAA Aeroacoustics Conference, October, 1990.
7. Ahuja, K. K., and W. H. Brown, "Shear Flow Control by Mechanical Tabs," AIAA Paper 89–0994, 2nd AIAA Shear Flow Conference, March, 1989.
8. Amiet, Roy K., "Correction of Open Jet Wind Tunnel Measurements for Shear Layer Refraction," AIAA Paper 75–532, AIAA 2nd Aeroacoustics Conference, March, 1975.
9. Tam, C. K. W., and H. K. Tanna, "Shock Associated Noise of Supersonic Jets from Convergent–Divergent Nozzles," *J. Sound and Vibration*, Vol. 81, pp. 337–358, 1982.
10. Tam, C. K. W., "Stochastic Model Theory of Broadband Shock Associated Noise from Supersonic Jets," *J. Sound and Vibration*, Vol. 116(2), pp. 265–302, 1987.
11. Tam, C. K. W., "Broadband Shock–Associated Noise from Supersonic Jets in Flight," *J. Sound and Vibration*, Vol. 151(1), pp. 131–147, 1991.

Nomenclature

EPNL	Effective Perceived Noise Level
LSAF	Low–speed Aeroacoustic Facility
ACE	Axisymmetric Coannular Ejector (nozzle)
npr	nozzle pressure ratio
PNL	Perceived Noise Level
RC	Round Convergent (nozzle)
spl	sound pressure level
SAR	Suppressor Area Ratio (mixing duct cross–sectional area / primary throat area)

Summary

Technology development is underway throughout the High Speed Research community to support the introduction of a high–speed civil transport early in the next century. One of the main goals of this technology development is to ensure that the airplane noise levels are environmentally acceptable. Jet noise is considered to be the dominating noise source and various suppression devices are being developed to address this noise source. The Boeing Commercial Airplane Group has developed an ejector–suppressor nozzle that would be used on a low–bypass (between approximately 0.5 and 1.0) mixed flow turbofan engine. This nozzle, known as the Axisymmetric Coannular Ejector (ACE) nozzle, is a plug nozzle with an ejector designed to provide aspiration of about 20 % of the engine flow (Figure S1). A variety of mixing enhancers were designed to promote mixing of the engine and the aspirated flows. These included delta tabs (Figure S2), tone–injection rods, and wheeler ramps. They were tested at various locations on the nozzle and in various combinations as shown in Figure S3.

Model–scale acoustic and propulsion performance testing of the ACE nozzle was conducted in the Boeing Low–speed Aeroacoustic Facility (LSAF). This facility consists of a free–jet wind tunnel with its test section in an anechoic chamber (Figure S4). Acoustic data were collected using microphones on both both 4.7 and 20–foot sidelines. This report addresses the acoustic aspects of the testing. The main acoustic objectives of this test were to: 1) evaluate the Effective Perceived Noise Level (EPNL) attenuation attainable from the ACE nozzle; and 2) evaluate the effectiveness of a number of different mixing enhancer designs.

Broadband shock–associated noise is seen for the ACE nozzle for nozzle pressure ratios of 3.0 and above. For the ACE nozzle without ejector, the delta tabs on the primary eliminated this shock–associated noise at npr 4.0 (Figure S5) and reduced it at other npr's. None of the other mixing enhancer configurations, either with or without ejectors, showed any effect on the shock–associated noise. However, the contribution of the broadband shock–associated noise to the EPNL was small, at most half an EPNdB, and the reductions that were achieved did not have any significant impact on the EPNL.

The effect of the mixing enhancers on jet–mixing noise tend to follow certain characteristic trends, as shown in Figure S6 and described as follows: The delta tabs on the primary nozzle generally reduce the low– to mid–frequency (about 500 to 10 kHz model–scale) jet–mixing noise by 2 to 4 dB, and increase the high frequency (over 10 kHz) jet–mixing noise by 5 dB or more, relative to the other three primary nozzle configurations (i.e., the baseline nozzle, the tone–injection rods, and the wheeler ramps), which all give almost identical results. The high–frequency noise increase is not seen for the highest power settings (npr's 3.5 and 4.0) or the highest noise emission angles (e.g., 140°). These trends are generally seen for all three ejector shroud configurations (i.e., no ejector, baseline ejector, and ejector with tabs).

The model–scale measured data were extrapolated to sideline and cutback flight conditions. Results of these extrapolations, on an EPNL basis, are shown in Figure S7 for the sideline case. These results can be plotted as functions of npr, of jet velocity, or of thrust, as shown in Figure S7. Plotting versus thrust allows for any thrust loss associated with particular configurations to be accounted for. The figure shows that the EPNLs for the various ACE nozzle configurations are all fairly close. The primary delta tabs with ejector shroud configurations generally have the lowest levels, while the baseline primary generally has the highest levels.

The greatest attenuation levels were achieved for the configuration of delta tabs on the primary nozzle with an ejector shroud installed – either the baseline or the tabbed ejector. Figure S8 shows that there is up to two EPNdB more attenuation with the primary delta tabs relative to the other three primary nozzle configurations (i.e., baseline nozzle, tone–injection rods, and wheeler ramps) when compared on an npr basis. The exact benefit depends on the extrapolation condition and the power setting. The other three primary configurations give attenuation levels within an EPNdB of each other. Which of these other primary configurations gives the greatest attenuation depends on the shroud configuration, the extrapolation condition, and the power setting.

Figures S9 and S10 summarize the noise reductions achieved by the various ACE nozzle configurations, relative to the RC nozzle, at the sideline and cutback flight conditions and power settings. For sideline flight conditions and power settings delta tabs on the primary nozzle, with either ejector installed, give the greatest attenuation, 5.3 EPNdB relative to the RC nozzle when compared on an npr basis (Figure S9). Without an ejector the primary tabs gave 4.7 EPNdB attenuation. The various other configurations (i.e., all those without primary tabs, including the baseline primary nozzle, the tone–injection rods, and the wheeler ramps) performed fairly similarly, achieving between 3.5 and 4.2 EPNdB attenuation. The effect of comparing ACE and RC nozzles on a thrust basis, i.e., accounting for the reduced thrust of the ACE nozzle relative to the RC at the same gas conditions, is to reduce the attenuation levels by between 1 and 1 $^1/_2$ EPNdB. For cutback flight conditions and power settings all the configurations tested performed fairly similarly, giving between 0.6 and 1.6 EPNdB attenuation relative to the RC nozzle when compared on an npr basis (Figure S10). The effect of comparing ACE and RC nozzles cutback levels on a thrust basis is to reduce the attenuation levels by about half an EPNdB.

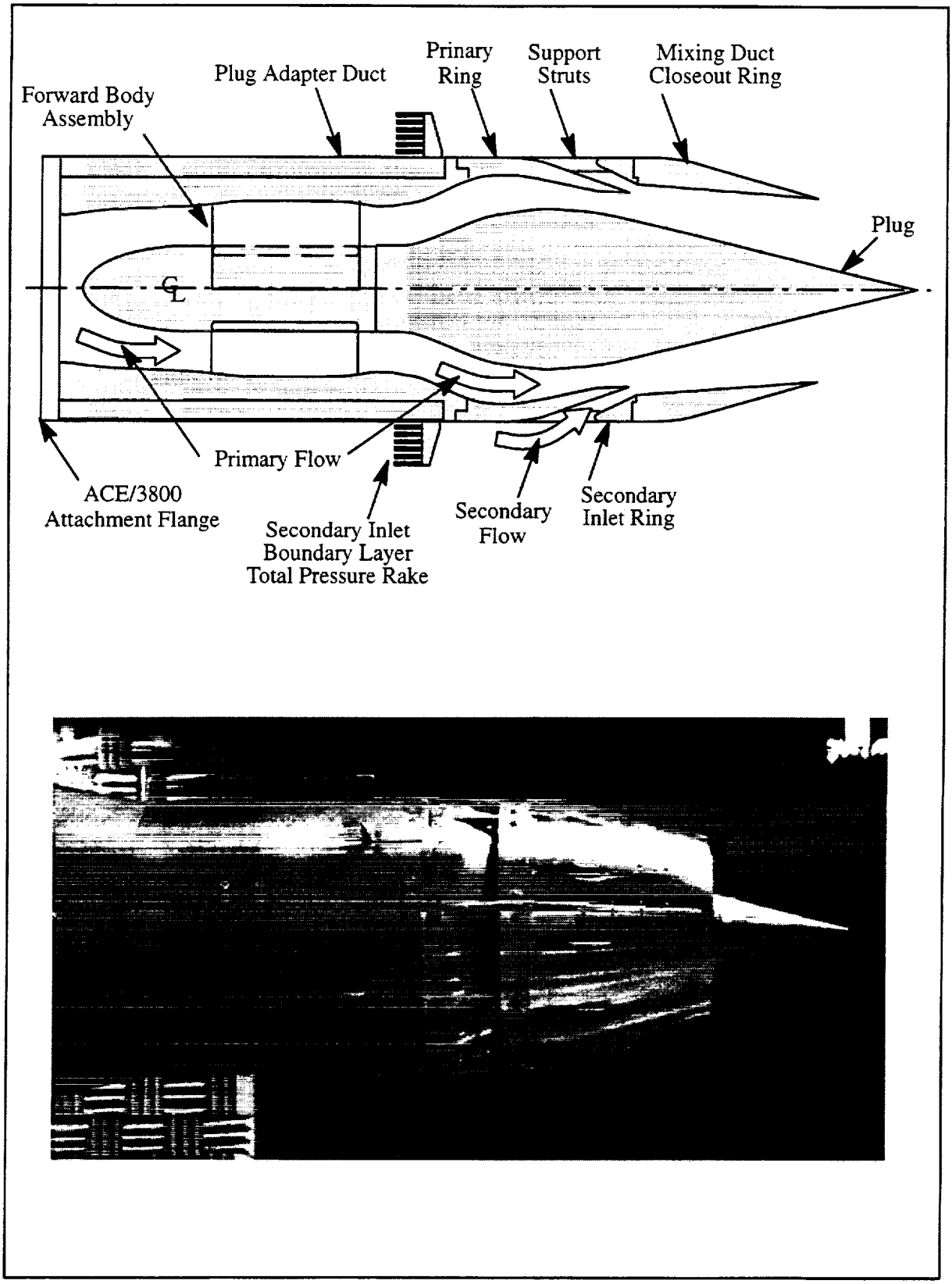

Figure S1. ACE Nozzle

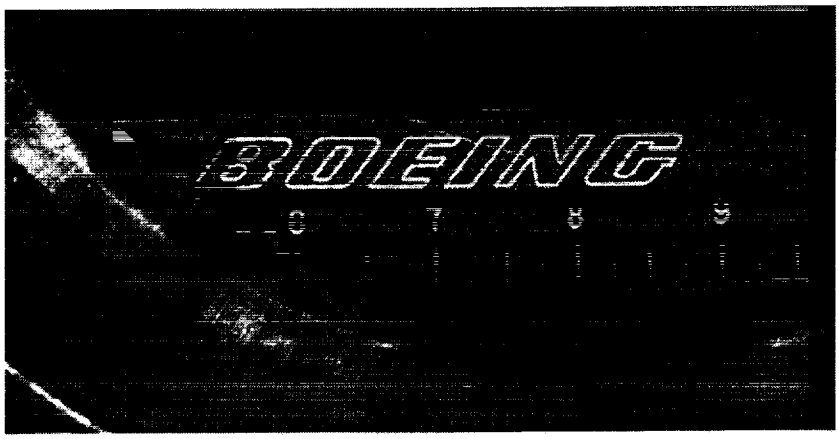

Figure S2. Primary Ring with Delta Tabs

Ejector Shroud	Primary Nozzle: baseline	tabs	rods	wheeler ramps
none	tunnel off and on config'n. 510	tunnel on config'n. 520	(not tested) config'n. 530	tunnel on config'n. 540
baseline	tunnel off and on config'n. 511	tunnel on config'n. 521	tunnel on config'n. 531	tunnel on config'n. 541
tabs	tunnel on config'n. 512	tunnel on config'n. 522	tunnel on config'n. 532	tunnel on config'n. 542

Figure S3. Test Matrix: Nozzle Configurations and Tunnel Conditions

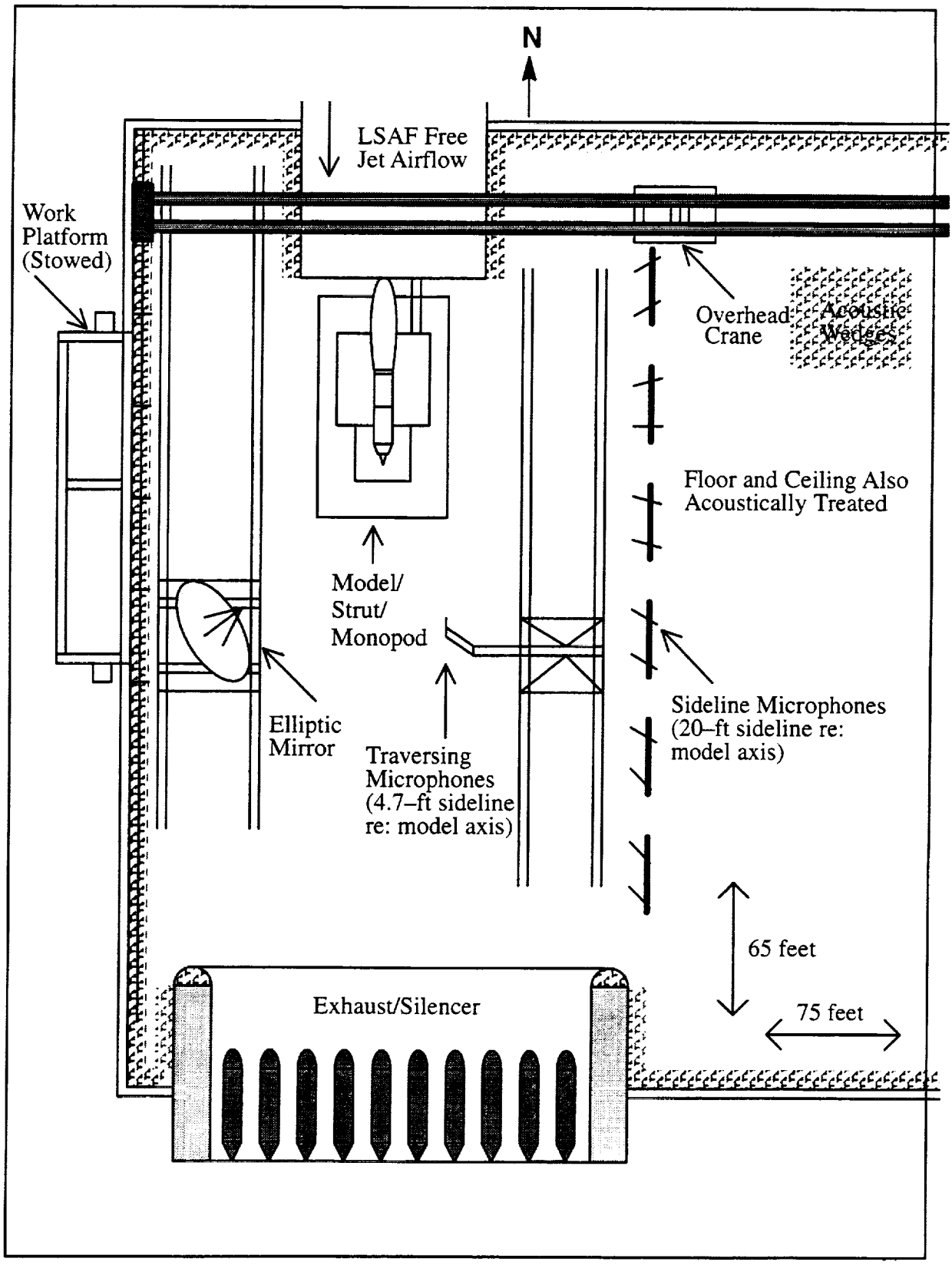

Figure S4. Drawing of the LSAF

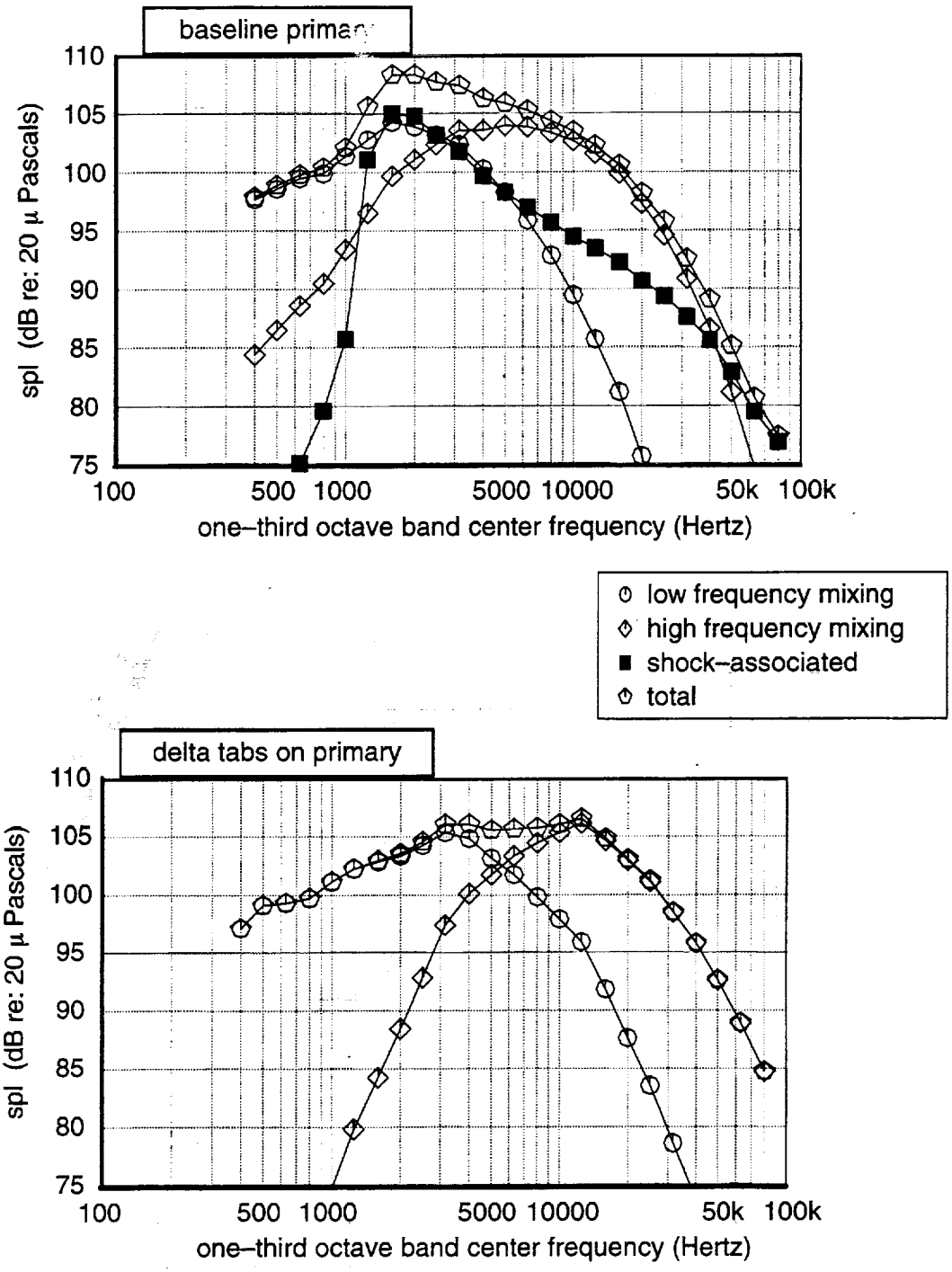

Figure S5. Shock–associated Noise Spectra: npr 4.0, 60–degree Microphone, No Ejector model scale, tunnel Mach 0.245, 20–ft mics

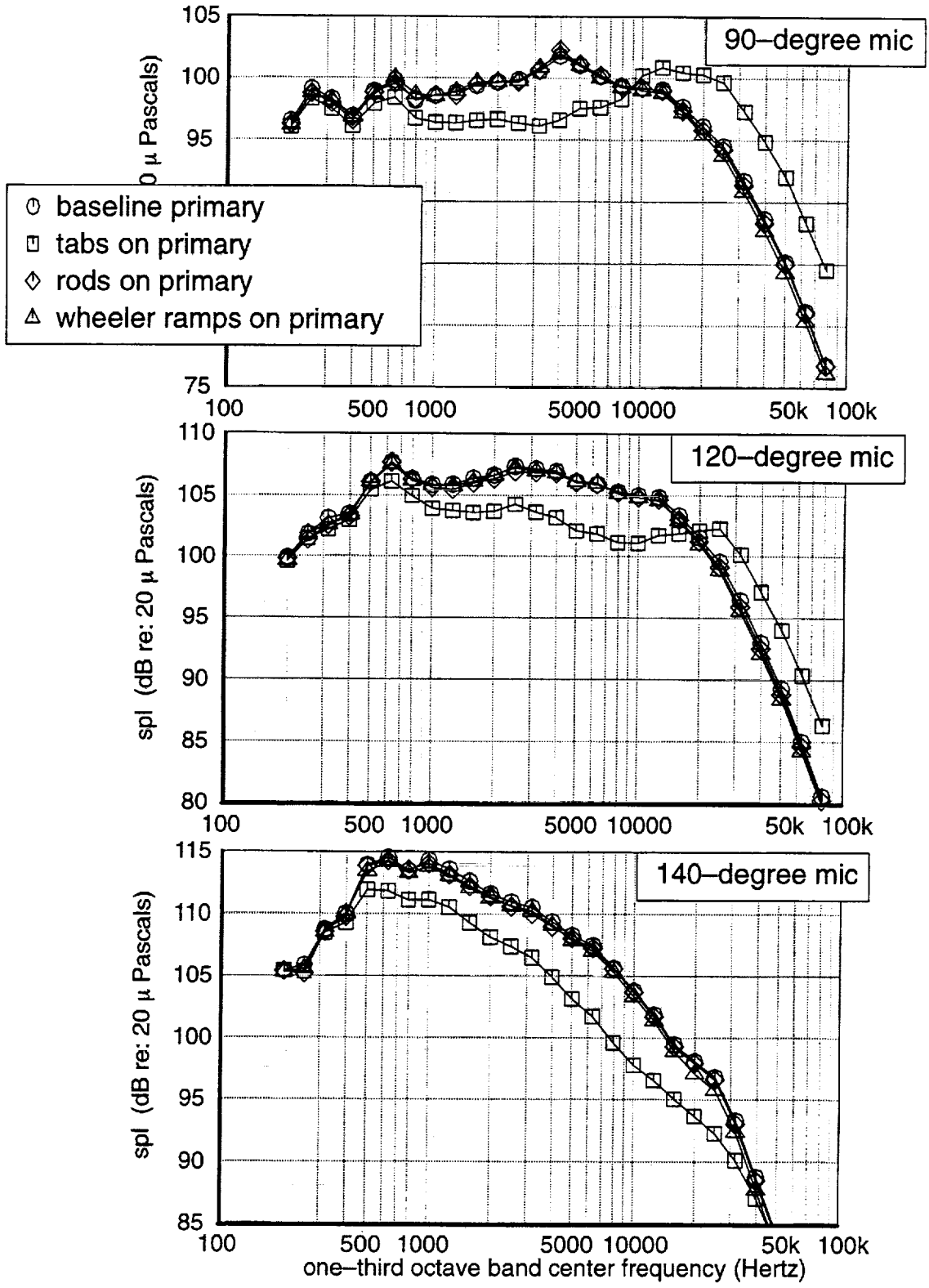

Figure S6. Model–scale Spectra: Tabs on Ejector, Various Primaries, NPR 2.5 20–ft sideline mics, tunnel Mach 0.245

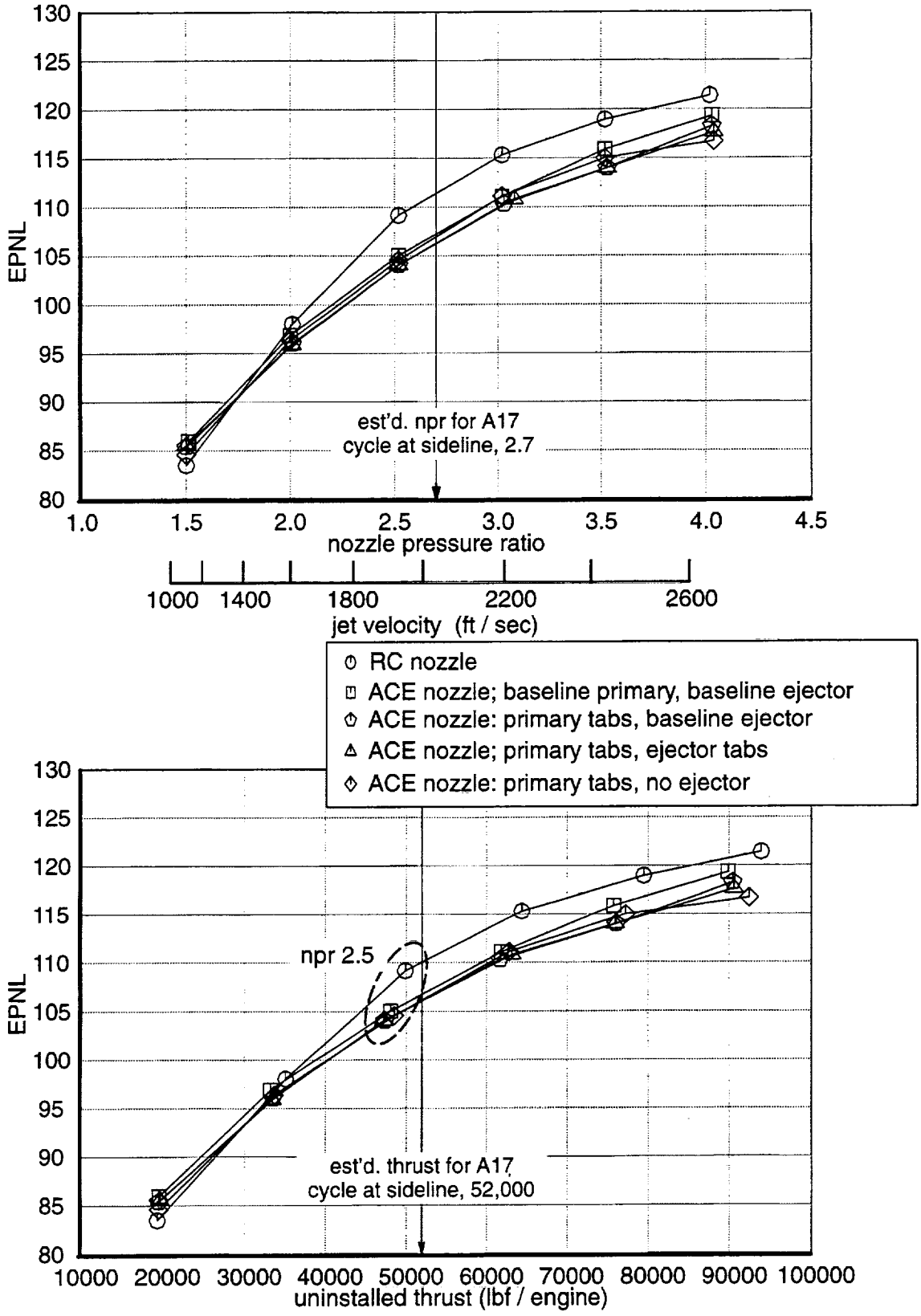

Figure S7. EPNLs for RC Nozzle and Selected ACE Nozzle Configurations at Sideline tunnel Mach 0.245, 20–ft mics

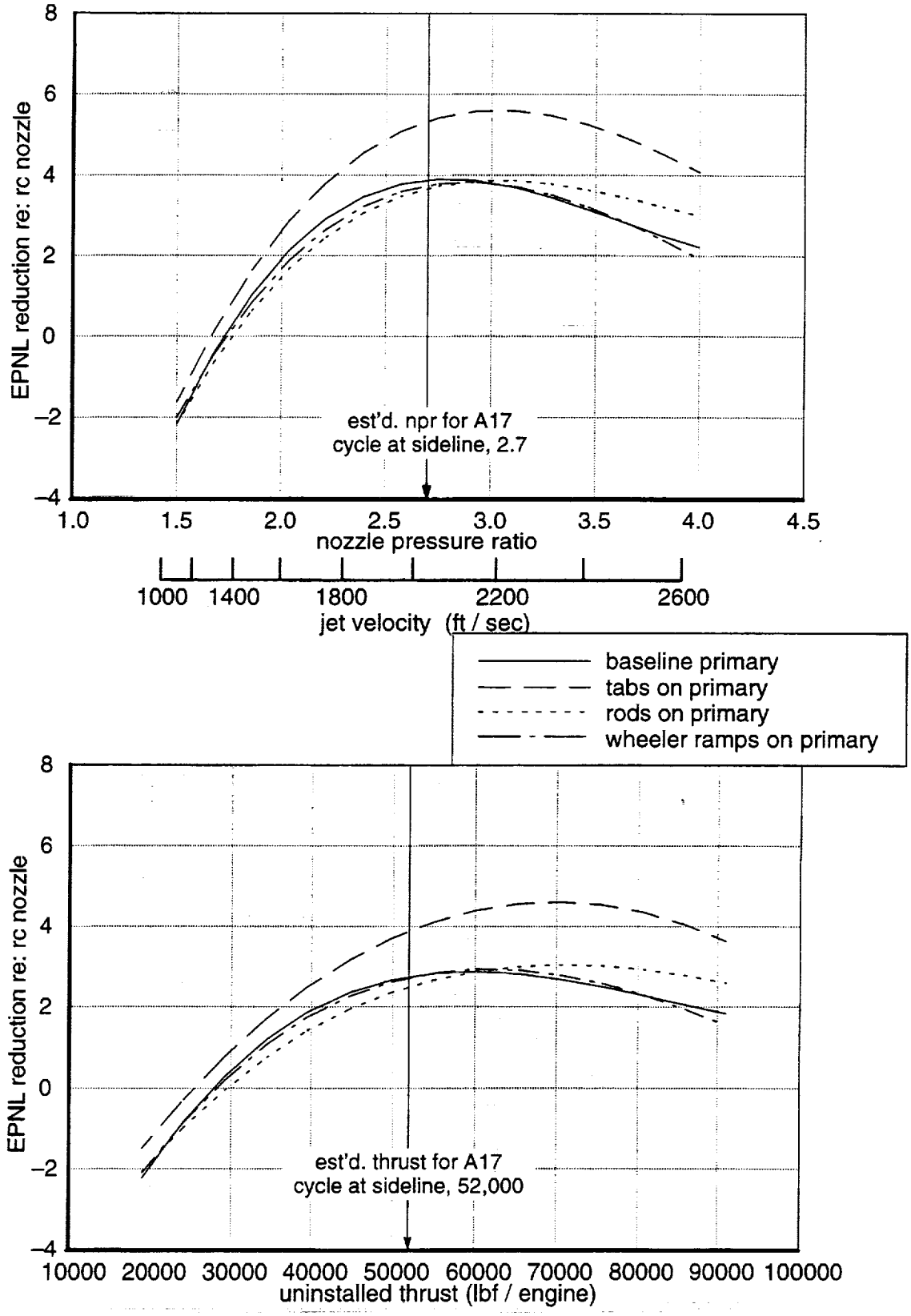

Figure S8. EPNL Reduction, Tabs on Ejector Shroud at Sideline
tunnel Mach 0.245, 20–ft mics, corrected data

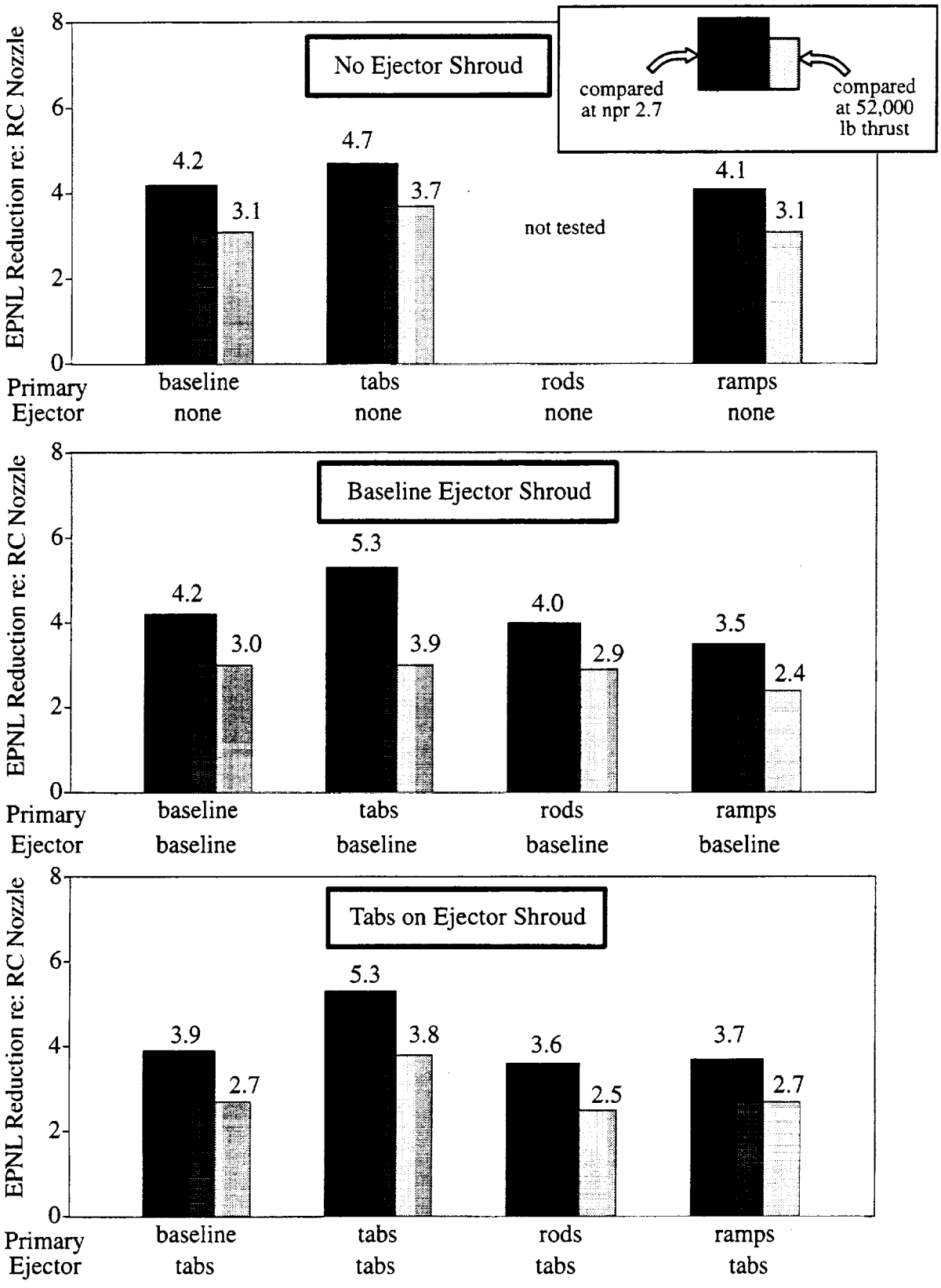

Figure S9. Summary of EPNL Results, Extrapolation to Sideline Condition tunnel Mach 0.245, 20–ft mics, corrected data

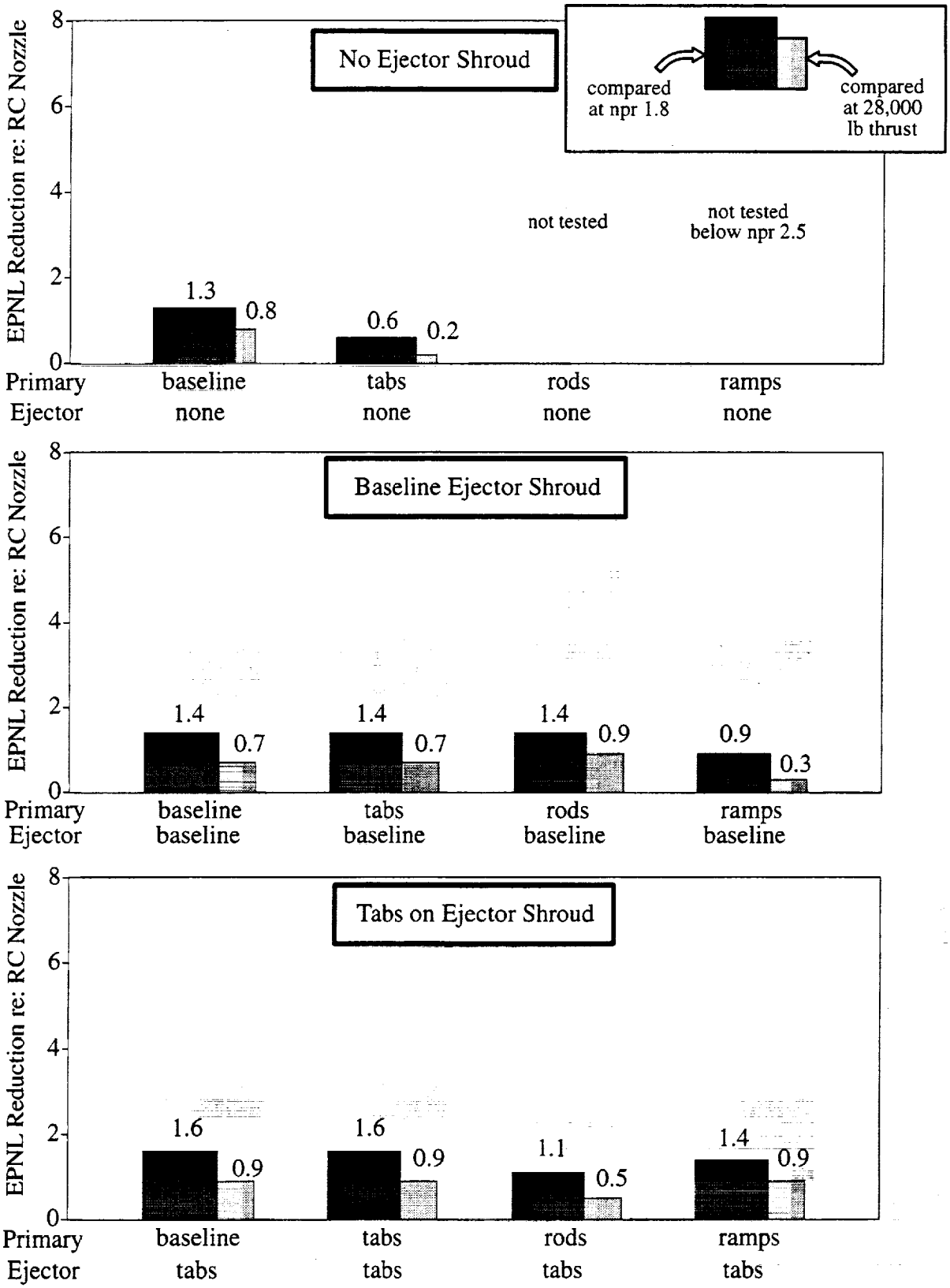

Figure S10. Summary of EPNL Results, Extrapolation to Cutback Condition tunnel Mach 0.245, 20–ft mics, corrected data

1. Introduction

Technology development is underway throughout the High Speed Research community to support the introduction of a high–speed civil transport early in the next century. One of the main goals of this technology development is to ensure that the airplane noise levels are environmentally acceptable.

Jet noise is considered to be the dominating noise source and various suppression devices are being developed to address this noise. The choice of a jet noise suppressor is dependent upon the engine cycle of the airplane, which determines the amount of suppression required. The Boeing Commercial Airplane Group has developed an ejector–suppressor nozzle that would be used on a low–bypass (between approximately 0.5 and 1.0) mixed flow turbofan engine. This nozzle, known as the Axisymmetric Coannular Ejector (ACE) nozzle, is a plug nozzle with an ejector designed to provide aspiration of about 20 % of the engine flow. The principle of an ejector nozzle is that the high–velocity primary flow is mixed (to some degree depending on the shroud length) with an aspirated flow before being exhausted into the lower velocity ambient flow. This reduces the higher velocity gradients, and stronger noise sources, associated with the direct mixing of the primary and the ambient flows.

A variety of mixing enhancers were designed to promote mixing of the engine and the aspirated flows. These included delta tabs, tone–injection rods, and wheeler ramps. The principle of these various devices is to create vorticity that increases the aspiration, and increases the degree to which the primary and aspirated are mixed. These mixing enhancers were designed for different locations on the ACE nozzle: on the primary nozzle protruding into the primary flow; on the primary nozzle protruding into the aspirated flow; and on the ejector nozzle protruding into the aspirated flow. Zaman (Reference 1) has postulated on the specific mechanisms causing the counter–rotating streamwise vortices shed from delta tabs. A number of researchers have shown them to be effective in increasing aspiration and mixing (References 1 and 2) and in reducing noise (References 2 through 7).

Model–scale acoustic and propulsion performance testing of the ACE nozzle was conducted in the Boeing Low–speed Aeroacoustic Facility. This report addresses the acoustic aspects of the test, and the accompanying volume addresses the propulsion aspects. The main acoustic objectives of this test were to: 1) evaluate the EPNL attenuation attainable from the ACE nozzle; and 2) evaluate the effectiveness of a number of different mixing enhancer designs.

2. Description of the Facility, Instrumentation, and Data Acquisition

2.1. Low–speed Aeroacoustic Facility

Testing was done in the Boeing Low–speed Aeroacoustic Facility (LSAF). This facility consists of a free–jet wind tunnel with its test section in an anechoic chamber. A drawing of the LSAF is shown in Figure 1 and a photograph in Figure 2. The free–jet exit measures nine feet high by 12 feet wide, with corner fillets. The anechoic chamber measures 65 feet long by 75 feet wide by 30 feet wide. It is lined with foam wedges, making it anechoic for broadband noise above 200 Hertz. The free–jet flow exits the LSAF through a 19–foot by 19–foot exhaust collector, passes through a duct silencer, and is then turned upward by a deflector.

The free–jet flow is supplied by two centrifugal fans operating in parallel, with a combined flow of 2000 pounds per second at the Mach 0.25 LSAF design point. Each fan has a 107–inch wheel with ten backward–inclined airfoil blades, and is powered by a 5200–horse-power synchronous motor. Tunnel speed is controlled by variable–frequency motor speed controls, operated remotely from the LSAF control room, over the Mach number range of 0.05 to 0.25. The maximum fan speed, corresponding to Mach 0.25, is 945 rpm.

2.2. Model–jet Flow Simulator

The model jet airflow was generated by the Boeing 3800 model–jet flow simulator. Drawings of the 3800 simulator are shown in Figures 3 and 4, and photographs in Figures 2 and 5. For this study the simulator was located two feet to the east of the tunnel centerline, as shown in Figure 1, to allow for locating a traversing microphone structure in the flowfield. While this simulator has a dual–flow capability only the primary flow was used in the present study. High pressure dry air is supplied to the simulator at a total pressure of 300 pounds per square inch, with a maximum continuous flow capability of approximately 20 pounds–mass per second for a single stream. The air is heated to the desired temperature by means of an 8–inch diameter propane burner system located in the support strut. The maximum allowed temperature was 1960° Rankine.

Fuel for propane burners is stored in a 1500–gallon tank outside the building, where the liquid propane is pumped to 150 psig and then vaporized in a steam–powered heat exchanger. The resulting gaseous propane is piped into the test area through a heated and insulated fuel line to assure that the propane remains gaseous.

As shown in the figures, the simulator has a boundary–layer bleed system. While bleed surfaces are located on both the trailing edge of the nacelle fairing and the uppermost aft portion of the tapered strut, only the nacelle location was used in the present study. The bleed surface is perforated with 1/16–inch holes with staggered centers for a 22.7 % open area. The strut and nacelle fairings form the vacuum plenum.

Prior to the present nozzle testing a study was conducted of the boundary layer profiles produced by this bleed system. As a result of this study it was decided to operate the bleed system at a rate of approximately 4.5 pound–mass per second in order to produce the desired boundary layer profile. No boundary layer bleed was used for tunnel–off testing.

2.3. Force Balance

Force measurements were made using the Boeing E–3 force balance. While this is a 6–component balance the measurement of interest for the present testing was the axial force.

2.4. Acoustic Instrumentation and Data Acquisition

Acoustic data were collected using both near– and far–sideline microphones and an elliptic mirror. The near–sideline data were taken with two microphones mounted on a traversing mechanism, and the far–sideline data were taken with 16 pole–mounted microphones. These installations are shown in the drawing in Figure 1 and the photograph in Figure 2.

The near–sideline microphones were Brüel and Kjær (B&K) 1/4–inch model 4136 microphones with model UA0385 nosecones and were installed parallel to the flow, nosecones facing upstream. The traverse mechanism moved along a 4.7–foot sideline relative to the model jet and covered an angular range of 50 to 165 degrees. These two microphones were thus in the free–jet flow when the tunnel was operating. The traverse mechanism moved at 1 degree/second and data were integrated over a two–second period to acquire 1/3 octave band data from 200 to 80,000 Hertz.

The far–sideline microphones were B&K 1/4–inch model 4135 microphones without gridcaps. The 16 microphones were located along a 20–foot sideline relative to the model jet and covered an angular range of 60 to 150 degrees. These measurements were thus made out of the free–jet flow. The microphones were "pointed" toward the model nozzle, i.e., with the diaphragms normal to a line from the nozzle. An eight–second integration time was used to acquire 1/3 octave band data from 200 to 80,000 Hertz. In addition, narrowband data were acquired for the nominal 60–, 90–, and 120–degree microphones.

The elliptic mirror had a diameter of 1.5 meters and its focal points were about 3.1 meters apart. The mirror was mounted outside of the flow on a traverse mechanism. Its far focal point was postioned on the model–jet axis, and a microphone was mounted at its near focal point. While traversing parallel to the model–jet axis, the mirror focal points were aligned at some constant look angle ranging from 60 degrees (relative to the upstream jet axis) to 132 degrees. The elliptic mirror microphone was a B&K 1/4–inch model 4136 microphone without gridcap. The traverse mechanism moved at 1 inch/second and data were integrated over a two–second period to acquire 1/3 octave band data from 200 to 80,000 Hertz.

All microphones were calibrated with a 124 dB, 250 Hertz pistonphone (corrected for barometric pressure) before and after each day's testing. All noise data were processed on–line, using the Boeing ADP–1 system. Corrections for frequency response and incidence angle were made at this time. B&K 2133 analyzers were used for the 1/3 octave band data, and HP3562 analyzers were used for the narrowband data. The acoustic and aerothermal data were transmitted to an Apollo computer system for further analysis.

2.5. Aerothermal Instrumentation

Aerothermal performance data were collected with the Aerothermal Data System (ATDAS). These data included temperatures and pressures measured in the test chamber, in the wind tunnel, in the air flowmeter, in the fuel flowmeter, and in the charging station. In addition the model nozzle was extensively instrumented with both total and static pressure taps. The accompanying volume of this report provides details of the aerothermal performance aspects of the test, including instrumentation, data reduction, and results.

3. Description of Nozzles and Test Conditions

3.1. Round Convergent Nozzle

The round convergent (RC) nozzle provided a set of reference data for the mixer–nozzle data and also served as a means of checking various aspects of the model jet simulator operation and instrumentation. The RC nozzle had an exit area of 13.2 square inches, and is shown installed on the model jet simulator in Figure 5.

3.2. Axisymmetric Coannular Ejector Nozzle

The Axisymmetric Coannular Ejector (ACE) nozzle was an axisymmetric plug nozzle with an ejector cowl designed to aspirate 20% of the primary flow at takeoff conditions. Figure 6 is a schematic drawing of the nozzle and Figure 7 is a photograph of the nozzle, with and without the ejector installed. The principle of an ejector nozzle is that the high–velocity primary flow is mixed (to some degree depending on the shroud length) with an aspirated flow before being exhausted into the lower velocity ambient flow. This reduces the higher velocity gradients, and stronger noise sources, associated with the direct mixing of the primary and the ambient flows. The model consisted of several parts including: a primary nozzle ring; a centerbody plug; an ejector inlet and mixing duct closeout ring assembly. The primary ring formed a convergent divergent nozzle with the plug surface. This nozzle was designed for a nozzle pressure ratio of 2.5. The primary nozzle throat area was 20 square inches with an area ratio of 1.03. The suppressor area ratio (SAR) was 1.2. The aspirated flow passage was formed by attaching the ejector inlet ring to the primary ring with eight struts.

The overall length of the model was 62 inches and the external diameter was 10.48 inches. In general, the high temperature parts (plug adapter duct, primary ring) were manufactured from Inconel 625. The plug was made from Haynes Alloy 230, and parts under less heat stress (duct aerodynamic skins, closeout nozzles, etc.) were manufactured from 316 stainless steel. Aerothermal instrumentation included six aspiration inlet boundary layer total pressure rakes, two mixing duct exit profile total pressure rakes, and a myriad of static pressures. Further design and fabrication details of the ACE nozzle are given in the accompanying volume of this report.

Four interchangeable primary rings and two interchangeable closeout rings were tested. The nozzle was also tested without an ejector shroud. The primary rings and the closeout rings were configured with various mixing enhancers and were tested in various combinations as shown in Figure 8. They are described in the following sections.

3.2.1. Primary Nozzles

Baseline: The baseline primary ring had no mixing enhancers.

Delta Tabs: Thirty–six triangular shaped delta tabs were equally spaced around the trailing edge of a primary ring and protruded 0.095 inches into the primary stream. This is about 1.1 times the computed boundary layer thickness at that location. Figure 9 shows a close–up photograph and the design details of the delta tabs on the primary ring.

Tone Injection Rods: These rods are round plugs that were welded into the trailing edge of a primary ring. The rods are 0.281 inches in diameter and were set back 0.625 inches from the primary ring trailing edge. Thirty–six of these mixing devices were placed on the outside of the primary ring, therefore protruding into the aspiration stream. Figure 10 shows a close–up photograph and the design details of the tone injection rods on the primary ring.

Wheeler Ramps: Three hundred sixty wheeler ramps were attached to the outer edge of one of the primary rings. The wheeler ramps were equally space around the primary ring at 0.060 inches from the trailing edge and protrude into the aspiration stream. Figure 11 shows a close–up photograph and the design details of the wheeler ramps on the primary ring.

3.2.2. Closeout Nozzles

Baseline: The baseline closeout ring had no mixing enhancers.

Delta Tabs: The delta tabs used on the closeout ring were the same shape as the delta tabs used on the primary ring; however, the closeout ring delta tabs were somewhat smaller, protruding only 0.083 inches into the mixed exit stream. The delta tabs were equally spaced around the trailing edge of the closeout ring with 36 delta tabs used overall. Figure 12 shows a close–up photograph and the design details of the delta tabs on the closeout ring.

3.3. Test Conditions

The RC and ACE nozzles were tested along the General Electric GE21/F15–A17 0.62 bypass ratio throttle line, shown in Figure 13. The nozzles were tested at a tunnel Mach number of 0.245. Additionally, a couple selected configurations were tested without the wind tunnel operating, as shown in Figure 8.

4. Extrapolation Procedure

In order to determine the noise that a given nozzle configuration would be expected to produce if installed on an airplane, a procedure is required to project the measured model–scale data to actual flight conditions. A computer program which does this extrapolation for supersonic jet noise measured in the LSAF was developed for a previous test program and was used in the present study with some modifications.

4.1. Extrapolation Program

The major elements of the extrapolation program are shown in Figure 14. Certain of these are described in the following sections.

4.1.1. Noise Floor Subtraction

The facility noise floor consists of noise not associated with the model being tested. It can include: wind tunnel noise; noise generated by flow over the jet simulator; noise generated by flow over the microphones; and noise produced by the jet simulator bleed system. For the present study the noise floors were measured by operating the model jet at a temperature and velocity to match the tunnel flow, and operating the bleed system at the rate that was used throughout the study. The noise floors were subtracted (for the tunnel–on case) from the measured signals. The noise floors are shown in Figure 15 for the 20–ft sideline microphones and in Figure 16 for the 4.7–ft sideline microphones. Also shown in these figures are the ACE nozzle measured levels for two pressure ratios, 1.5 (the lowest power point tested) and 2.5 (near the power setting for the sideline noise certification measurement). The indicated frequency range of interest is based on a full–scale frequency range of 50 Hertz to 10 kiloHertz and an approximate model scale factor of 10. Although the noise floor, in some cases, comes close to the measured signal, the results of the noise floor subtraction showed no obvious anomalies or indications of noise floor contamination.

4.1.2. Noise Component Separation

The measured spectra are separated into four components, as shown in Figure 14, specifically, tones, shock–associated noise, low–frequency jet noise, and high–frequency jet noise. An example of the result of this component separation is shown in Figure 17. There are two primary reasons for the component separation: 1) to achieve a more accurate extrapolation by being able to use different source locations for the different components; and 2) to be able to eliminate a particular component from the spectra. This latter process can be used, for instance, to eliminate a tone that is known not to be associated with the model, or to examine the effect of being able to reduce a particular component, e.g. shock–associated noise.

4.1.3. Noise Source Distributions

The extrapolation program used a distributed noise source model, illustrated in Figure 18. For each of the four components, and for each one third octave band, this sort of distribution is used. From the desired extrapolation sideline and angle, the acoustic ray is traced back to determine the microphone from which to project the data.

4.1.4. Free–jet Shear–layer Corrections

The data measured outside the tunnel flow were corrected for propagation through the free–jet shear layer using the method developed by Amiet (Reference 8).

4.2. Extrapolation Conditions

4.2.1. Flight Geometry and Conditions

The Round Convergent nozzle and the Axisymmetric Coannular Ejector nozzle data were extrapolated to full–scale flight conditions chosen to be representative of the General Electric GE21/F15–A17 0.62 bypass ratio engine with the ACE nozzle, on the Boeing 1080–926 airplane. The specific conditions were as follows:

condition	altitude (feet)	engine pitch (degrees)	flight angle (degrees)	airspeed (knots)	mic sideline (feet)	nozzle pressure ratio	est'd. un–installed thrust (lbf)	stage 3 limit (EPNdB)
sideline	689	14.6	7.1	266.8	1476	2.7	52,000	102.6
cutback	835	9.8	2.3	267.4	0	1.8	28,000	105.5

4.2.2. Scaling Factor

The appropriate scale factors for the RC and ACE nozzle extrapolations were chosen by using the following procedure:

1. For a series of test points taken along the throttle line, the measured model mass flow was plotted versus the measured model jet velocity. A second order curve fit was put through these data. This was done for both the RC and the ACE nozzles, and the results are shown in Figure 19.
2. For the sideline and cutback points the full–scale engine air mass flow and jet velocity were determined.
3. At the full–scale sideline and cutback jet velocities, the ratios of the full–scale to the model–scale mass flows were calculated. The square roots of these ratios are the scale factors.

The scale factors differed slightly for the sideline and cutback conditions, being about 10.8 and 11.2 for the RC nozzle, and about 8.9 and 9.2 for the ACE nozzle, for the sideline and cutback conditions, respectively. It was decided to use the sideline values of 10.8 and 8.9 for the RC and ACE nozzles, respectively, since this was considered the more critical noise certification point.

4.3. Relative Velocity Adjustments

The tunnel Mach of 0.245 that the nozzles were tested at was less than the actual airplane Mach number for the noise certification points, as indicated above. An empirical correction was derived to account for this relative velocity effect and adjust the Effective Perceived Noise Level (EPNL) data to the certification airspeed.

The test conditions were defined by three independent variables: nozzle pressure ratio and temperature, and tunnel speed. However, the empirical correction was modeled on three independent variables that are more consistent with theories of jet noise. The noise intensity was assumed to behave as follows:

$$I \propto \left(V_{jet} \right)^{m} \left(V_{jet} - V_{ambient} \right)^{n} \left(T_{jet} \right)^{p}$$

Therefore

$$EPNL = 10 \left[m \log (V_{jet}) + n \log (V_{jet} - V_{ambient}) + p \log (T_{jet}) \right] + \text{constant}$$

and the EPNL adjustment can be derived to behave as follows:

$$\Delta \text{ EPNL} = \left.\frac{\partial \text{ EPNL}}{\partial \log(V_{jet})}\right|_{\text{const } V_{rel}, T_{jet}} \Delta \log(V_{jet}) + \left.\frac{\partial \text{ EPNL}}{\partial \log(V_{rel})}\right|_{\text{const } V_{jet}, T_{jet}} \Delta \log(V_{rel})$$

$$+ \left.\frac{\partial \text{ EPNL}}{\partial \log(T_{jet})}\right|_{\text{const } V_{jet}, V_{rel}} \Delta \log(T_{jet})$$

where the partial derivatives are the 10 m, 10 n, and 10 p terms, respectively.

Since the target throttle line was achieved, i.e., the temperatures and primary jet velocities were correctly duplicated, only the relative velocity terms are needed to adjust the data. A least squares routine was used with RC nozzle data and with data from selected ACE nozzle configurations to solve for this partial derivatives. The resulting values were:

nozzle	V_{rel} term
RC	59
ACE	56

This indicates that although the relative velocity effects will change the absolute EPNLs for the two nozzles the suppression levels for the ACE nozzle relative to the RC nozzle will not be significantly affected.

Additionally, an empirical thrust correction was derived to account for the increased ram drag that would exist on the ACE nozzle at the higher tunnel Mach number. This correction was derived by a least squares fit to tunnel–off and tunnel–on data. The correction was small, amounting to a reduction in thrust of less than 1 percent when adjusting the data from an ambient velocity of 276 to 450 feet per second.

The results of the relative velocity and ram drag corrections are shown in Figure 20. This figure shows the corrected and uncorrected thrusts and sideline EPNLs for the RC nozzle and a selected ACE nozzle configuration.

4.4. Data Accuracy and Selection

As described in previous sections data were taken both with the wind tunnel not operating and operating at a tunnel Mach number of 0.245, and data were taken on two different sidelines. The various data sets for any given nozzle configuration are illustrated in Figure 21, which indicates potential sources of inaccuracies in these data. By projecting data from different "boxes" in this figure to some common conditions and comparing the results, it is possible to get an indication of the seriousness of these sources of error. For instance, Figures 22 and 23 show a comparisons of tunnel–on data from the two different measurement sidelines (i. e., boxes C and D) projected to a full–scale flight condition. Figure 22 shows the directivity pattern for the three noise components for their respective peak frequencies. The agreement, which reflects the effects of the source locations, near–field effects, and shear–layer correction, is considered reasonable. Figure 23 shows the in–flow and out–of–flow data to agree to within less than 1 EPNdB, and generally within a few

tenths of an EPNdB. Particular effects could be better isolated by comparing data from different data sets, for example from boxes A and B to examine the source location effects. These comparisons could be used to adjust the source location distributions until satisfactory agreement is achieved.

In this report wind tunnel–on, out–of–flow microphone data are presented. The tunnel–on data better account for the relative velocity effect, i.e., the empirical relative velocity effects are smaller. The out–of–flow (20–foot sideline) data are less sensitive to source location assumptions, are unlikely to have near–field effects, and have a better signal–to–noise ratio. Based on the present test and previous LSAF tests the Amiet shear layer correction is felt to be quite accurate.

5. Discussion of Test Results

The following sections discuss the test results. Noise from various sources are discussed, including: facility noise, screech tones, broadband shock–associated noise, and turbulent jet–mixing noise.

5.1. Facility Noise

A facility–related tone was present at 630 Hertz (or about 63 Hertz when converted to full–scale frequencies) in certain cases. The most probably cause of this tone is the burner unit of the jet simulator. This tone is not included in the noise floor and, although the capability exists to remove the tone in the data reduction procedure, this was not done. The tone was never large and had no impact on EPNLs.

5.2. Screech Tones

The use of delta tabs to eliminate or reduce screech tones associated with supersonic jet flows has been demonstrated by several researchers (References 2 through 7). The ACE nozzle, however, did not show screech tones even with the baseline (i.e., no mixing enhancer) configuration. The absence of screech tones may be due the presence of the plug.

5.3. Broadband Shock–associated Noise

5.3.1. Spectral Analysis

A theory of broadband shock–associated noise has been developed by Tam and Tanna (References 9 through 11). In their model the shock–associated noise is postulated to be generated by the interaction between the large turbulence structures from the shear–layer instability and the quasi–periodic shock–cell structures. As described in a previous section, the component separation procedure produces a shock–associated noise spectrum. The broadband shock–associated noise is seen for the ACE nozzle for nozzle pressure ratios of 3.0 and above. Examples of these spectra are shown in Figures 24 through 31. This spectral shape matches closely that predicted by Tam and Tanna's theory. The figures show the characteristic trends of shock–associated noise: to peak at higher frequencies at higher angles; to peak at higher frequencies at lower jet velocities; and to be most evident at forward and mid angles.

Some researchers have reported reductions of broadband shock–associated noise on simple (i.e., non–ejector) circular nozzles by the use of delta tabs (References 4 and 6). Comparisons of Figures 28 and 29 to Figures 30 and 31 show that for the ACE nozzle without ejector the delta tabs on the primary reduce the shock–associated noise at npr 3.0 and eliminate it at npr 4.0. Similar comparisons of Figures 24 through 27 show that with the ACE ejector shroud installed the tabs do not reduce the shock–associated noise. None of the other mixing enhancer configurations showed any effect on the shock–associated noise.

5.3.2. Effective Perceived Noise Level Impact

The impact of the broadband shock–associated noise on the EPNL can by determined by using the component separation procedure to eliminate the shock–associated noise before calculating the EPNL. Figures 32 and 33 show the results of this analysis for several nozzle configurations. These figures show that, at the most, the shock–associated noise causes about a half an EPNdB increase. At the power settings of interest for noise certification regulations there is no impact. These figures also show that the reductions of broadband

shock–associated noise due to the delta tabs that were noted above in the model–scale spectra did not have any significant impact on the EPNL.

5.4. Jet–mixing Noise

5.4.1. Spectral Analysis

This report, in an attempt to provide a fairly complete set of data covering the range of ACE nozzle configurations and conditions tested, presents model–scale spectral results in Figures 34 through 63. Any given figure presents the nozzle configurations from either a row or a column of the Figure 8 configuration matrix for one throttle condition. For example, Figure 42 shows the effect of the various different primary nozzle configurations with the baseline ejector shroud installed at an npr 2.5 throttle condition. Three angles are shown – 90, 120, and 140 degrees – as representative of the different characteristic spectral shapes that were observed. No forward angles are shown since, in general, the spectra in the forward arc were similar in shape to the 90° spectra. In addition, some representative directivity plots are shown in Figures 64 and 65.

Several researchers have reported reductions in the broadband jet mixing noise, particularly at lower frequencies, due to delta tabs on simple circular nozzles (References 2 through 6). In some cases an accompanying increase in the higher frequency noise levels was observed (References 3 and 6). These same trends (with a few exceptions) were seen in the present study, as typified by Figure 48 and discussed below.

Low– to Mid–frequency Noise

The delta tabs on the primary nozzle generally reduce the low– to mid–frequency (about 500 to 10 kHz) jet–mixing noise relative to the other three primary nozzle configurations (i.e., baseline nozzle, tone–injection rods, and wheeler ramps), which all give almost identical results. This reduction is typically 2 to 4 dB, and is seen for all three ejector shroud configurations (i.e., no ejector, baseline ejector, and ejector with tabs). Figure 48 shows an example of this trend at the npr of 2.5, a power setting near the sideline certification setting.

An exception to this trend occurs for the configuration of baseline ejector and rods on the primary at high angles. Although the rods generally do not show any reduction of noise, they do for these conditions. Figure 42 shows this configuration giving over 5 dB greater suppression than the more general trend.

Another exception is at an npr of 1.5 where there are not as pronounced differences among the various nozzle configurations.

High–frequency Noise

The delta tabs on the primary nozzle generally increase the high frequency (over 10 kHz) jet–mixing noise at low to mid angles and for power settings up to 3.0, relative to the other three primary nozzle configurations (i.e., baseline nozzle, tone–injection rods, and wheeler ramps), which all give almost identical results. This increase is typically 5 dB or more, and is seen for all three ejector shroud configurations (i.e., no ejector, baseline ejector, and ejector with tabs). This high–frequency noise increase is not seen for the highest power settings (npr's 3.5 and 4.0) or the highest angles (e.g., 140°). Figure 48 shows an example of this trend at the npr of 2.5, a power setting near the sideline certification setting. As this figure shows, an increase of high–frequency noise does not occur at high angles when an ejector shroud is installed. For these high angles the primary tabs show noise reduction across the entire spectrum.

Exceptions for "No–ejector" Configurations

The ACE nozzle configurations with no ejector shroud (essentially large–plug nozzles) behave a little differently from the above trends. The noise reduction benefit of the primary delta tabs is generally not achieved. Figure 60 shows that some mid– and high–frequency levels are higher when an ejector is not installed. In a few instances at higher powers, however, the noise levels are lower without the ejector, as shown in Figure 57.

5.4.2. Effective Perceived Noise Levels

Effective Perceived Noise Levels were calculated for the RC nozzle and and the various ACE nozzle configurations as described in a previous section. These results can be plotted as functions of npr, of jet velocity, or of thrust, as shown in Figures 66 and 67, for selected configurations at the sideline and cutback conditions, respectively. Plotting versus thrust allows for any thrust loss associated with particular configurations to be accounted for.

Figures 66 and 67 show that the EPNLs for the various ACE nozzle configurations are all fairly close. The primary delta tabs with ejector shroud configurations generally have the lowest levels, while the baseline primary generally has the highest levels. As noted in the discussion of spectra, the "large plug" configuration has the lowest levels at the npr 4.0 setting.

5.4.3. Effective Perceived Noise Level Attenuations

The attenuation levels of the various ACE configurations relative to the RC nozzle are shown in Figures 68 through 81. As in the case of the model–scale spectra plots, a fairly complete set of data covering the range of ACE nozzle configurations and conditions tested are presented in this report. Similarly, any given attenuation plot presents the nozzle configurations from either a row or a column of the Figure 8 configuration matrix.

The greatest attenuation levels were achieved for the configuration of delta tabs on the primary nozzle with an ejector shroud installed – either the baseline or the tabbed ejector. Figures 70 and 71 show that with the primary tabs there is little difference between the baseline or the tabbed ejector, except at the highest power setting where a slight advantage is seen for the tabbed ejector. Without an ejector attenuations were a half to one EPNdB less at the cutback and sideline nozzle pressure ratios. However, these figures also show that the lower thrust loss of large plug nozzle relative to an ejector nozzle results in very similar attenuation levels when these levels are plotted versus thrust.

Figures 78 to 81 show that, with either of the two ejector configurations, there is up to two EPNdB more attenuation with the primary delta tabs relative to the other three primary nozzle configurations (i.e., baseline nozzle, tone–injection rods, and wheeler ramps) when compared on an npr basis. The exact benefit depends on the extrapolation condition and the power setting. The other three primary configurations give attenuation levels within an EPNdB of each other. Which of these other primary configurations gives the greatest attenuation depends on the shroud configuration, the extrapolation condition, and the power setting.

Figures 82 and 83 summarize the noise reductions achieved by the various ACE nozzle configurations, relative to the RC nozzle, at the sideline and cutback flight conditions and power settings. Figure 82 shows that for sideline delta tabs on the primary nozzle, with either ejector installed, give the greatest attenuation, 5.3 EPNdB when compared on an npr

basis. Without an ejector the primary tabs gave 4.7 EPNdB attenuation. The various other configurations (i.e., all those without primary tabs, including the baseline primary nozzle, the tone–injection rods, and the wheeler ramps performed fairly similarly, achieving between 3.5 and 4.2 EPNdB attenuation. The effect of comparing ACE and RC nozzles on a thrust basis, i.e., accounting for the reduced thrust of the ACE nozzle relative to the RC at the same gas conditions, is to reduce the attenuation levels by between 1 and 1 $^1/_2$ EPNdB. Figure 83 shows that for cutback all the configurations tested performed fairly similarly, giving between 0.6 and 1.6 EPNdB attenuation. This reflects the fact that at the low power setting of cutback the ACE nozzle is not very effective. The effect of comparing ACE and RC nozzles cutback levels on a thrust basis is to reduce the attenuation levels by about half an EPNdB.

6. Conclusions

As stated in the Introduction, the main acoustic objectives of this test were to: 1) evaluate the EPNL attenuation attainable from the ACE nozzle; and 2) evaluate the effectiveness of a number of different mixing enhancer designs. Each of these objectives is addressed here.

EPNL Attenuation

For sideline flight conditions and power settings delta tabs on the primary nozzle, with either ejector installed, give the greatest attenuation, 5.3 EPNdB relative to the RC nozzle when compared on an npr basis (Figure 82). Without an ejector the primary tabs gave 4.7 EPNdB attenuation. The various other configurations (i.e., all those without primary tabs, including the baseline primary nozzle, the tone–injection rods, and the wheeler ramps) performed fairly similarly, achieving between 3.5 and 4.2 EPNdB attenuation. For cutback flight conditions and power settings all the configurations tested performed fairly similarly, giving between 0.6 and 1.6 EPNdB attenuation relative to the RC nozzle when compared on an npr basis (Figure 83).

Mixing Enhancer Effectiveness

Broadband shock–associated noise is seen for the ACE nozzle for nozzle pressure ratios of 3.0 and above. For the ACE nozzle without ejector the delta tabs on the primary reduced this shock–associated noise at npr 3.0 and eliminated it at npr 4.0 (Figures 28 through 31). None of the other mixing enhancer configurations, either with or without ejectors, showed any effect on the shock–associated noise. However, the contribution of the broadband shock–associated noise to the EPNL was small, at most half an EPNdB, and the reductions that were achieved did not have any significant impact on the EPNL.

The effect of the mixing enhancers on jet–mixing noise tend to follow certain characteristic trends, as shown in Figure 48 and described as follows: The delta tabs on the primary nozzle generally reduce the low– to mid–frequency (about 500 to 10 kHz model–scale) jet–mixing noise by 2 to 4 dB, and increase the high frequency (over 10 kHz) jet–mixing noise by 5 dB or more, relative to the other three primary nozzle configurations (i.e., the baseline nozzle, the tone–injection rods, and the wheeler ramps), which all give almost identical results. The high–frequency noise increase is not seen for the highest power settings (npr's 3.5 and 4.0) or the highest angles (e.g., 140°). These trends are seen for all three ejector shroud configurations (i.e., no ejector, baseline ejector, and ejector with tabs), although some exceptions were observed as noted in preceding sections.

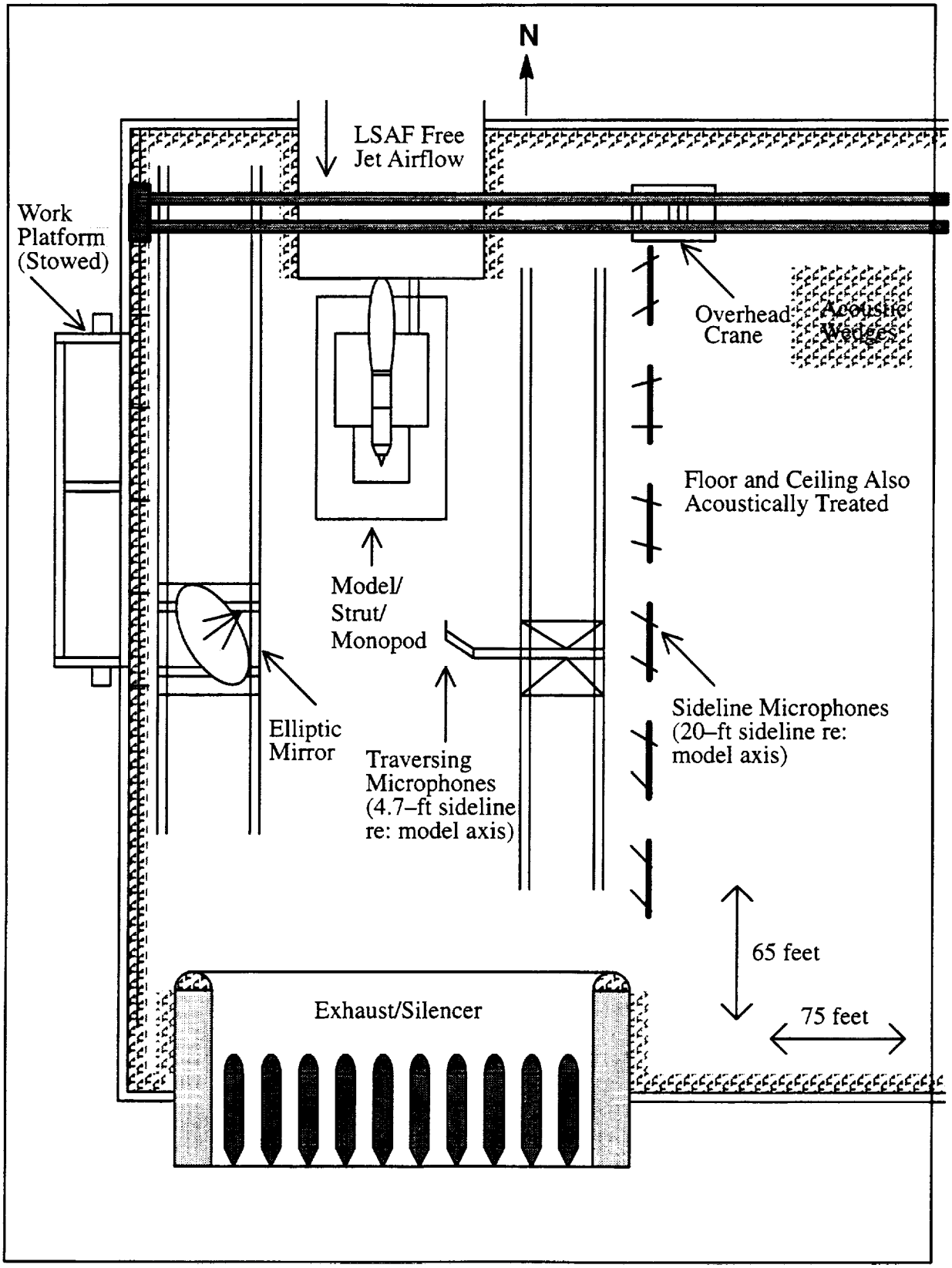

Figure 1. Drawing of the LSAF

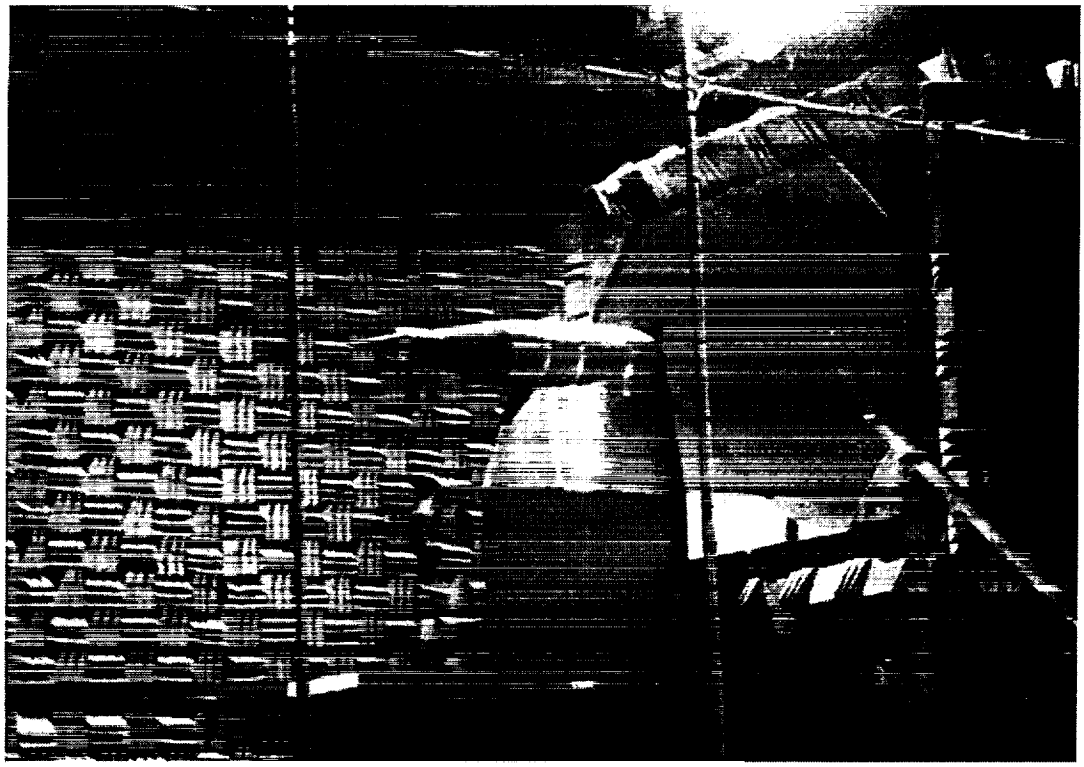

Figure 2. Photograph of the ACE Nozzle Installed in the LSAF

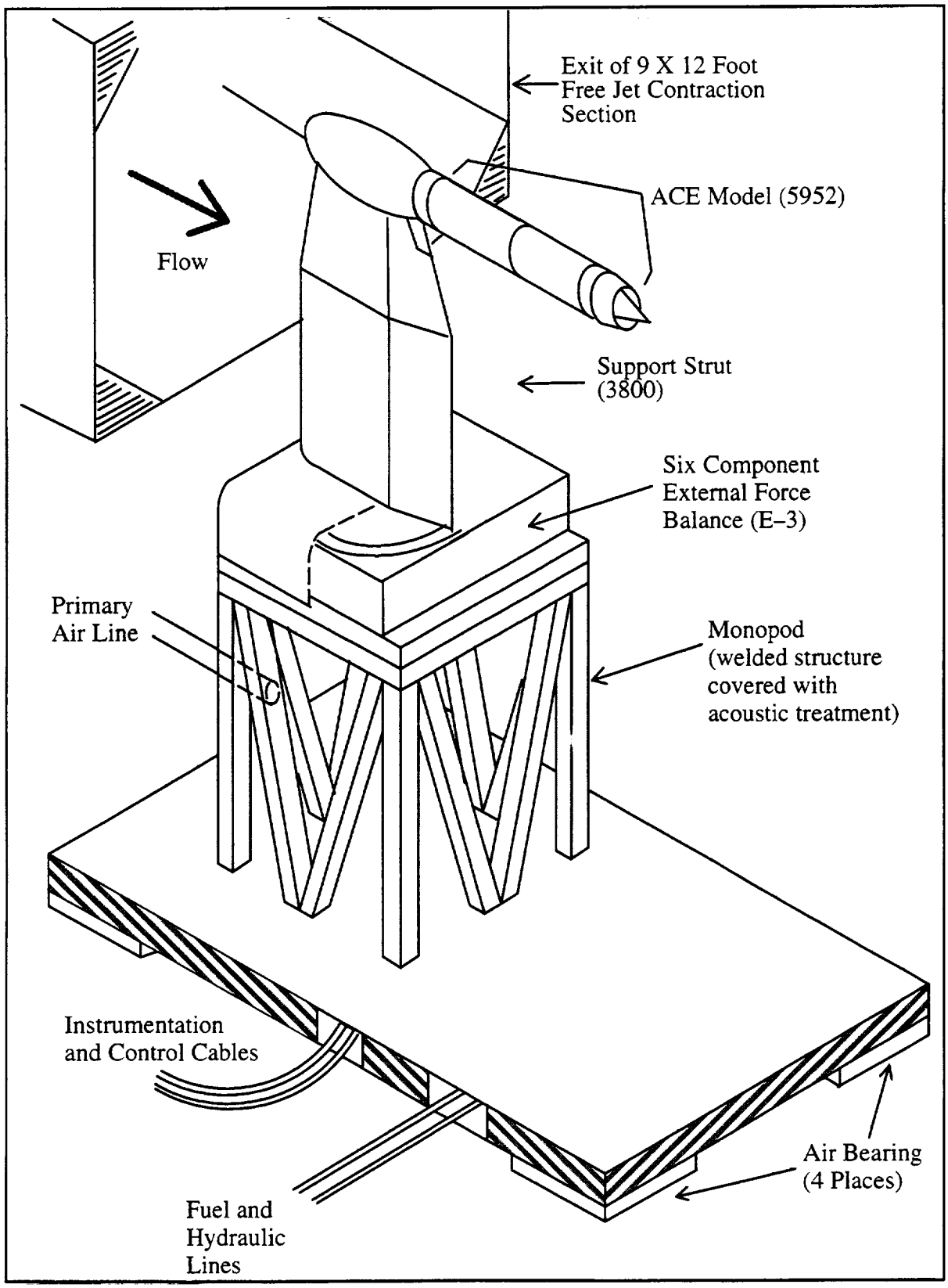

Figure 3. Drawing of the Model Installation

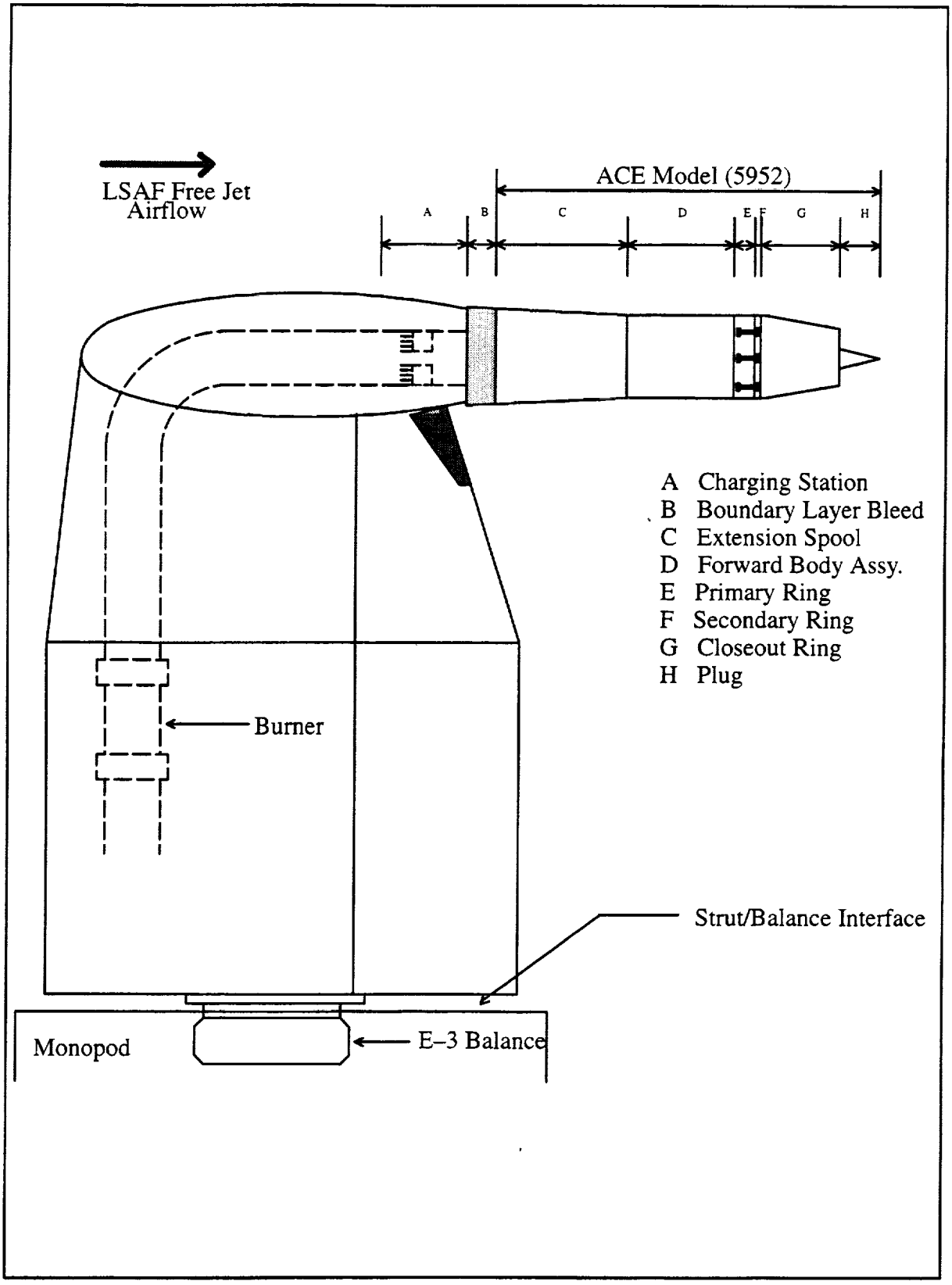

Figure 4. Drawing of the Model–jet Simulator

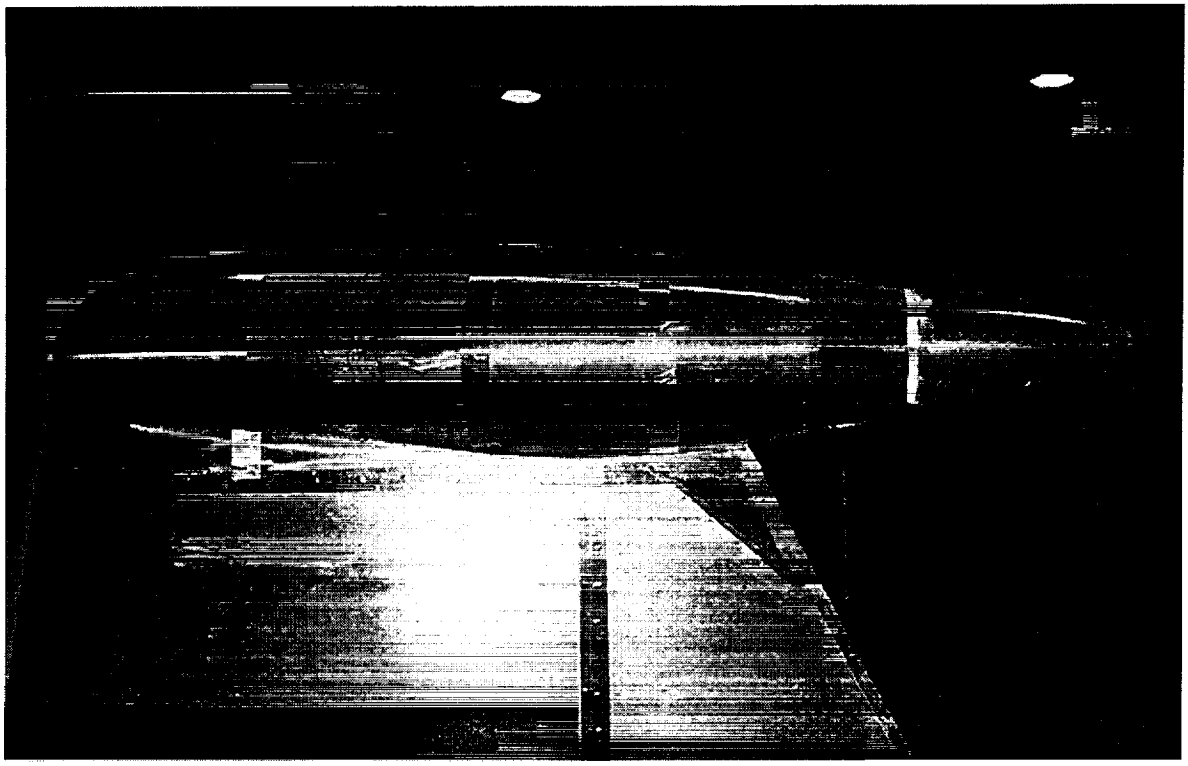

Figure 5. Photograph of the RC Nozzle Installed on the Flow Simulator

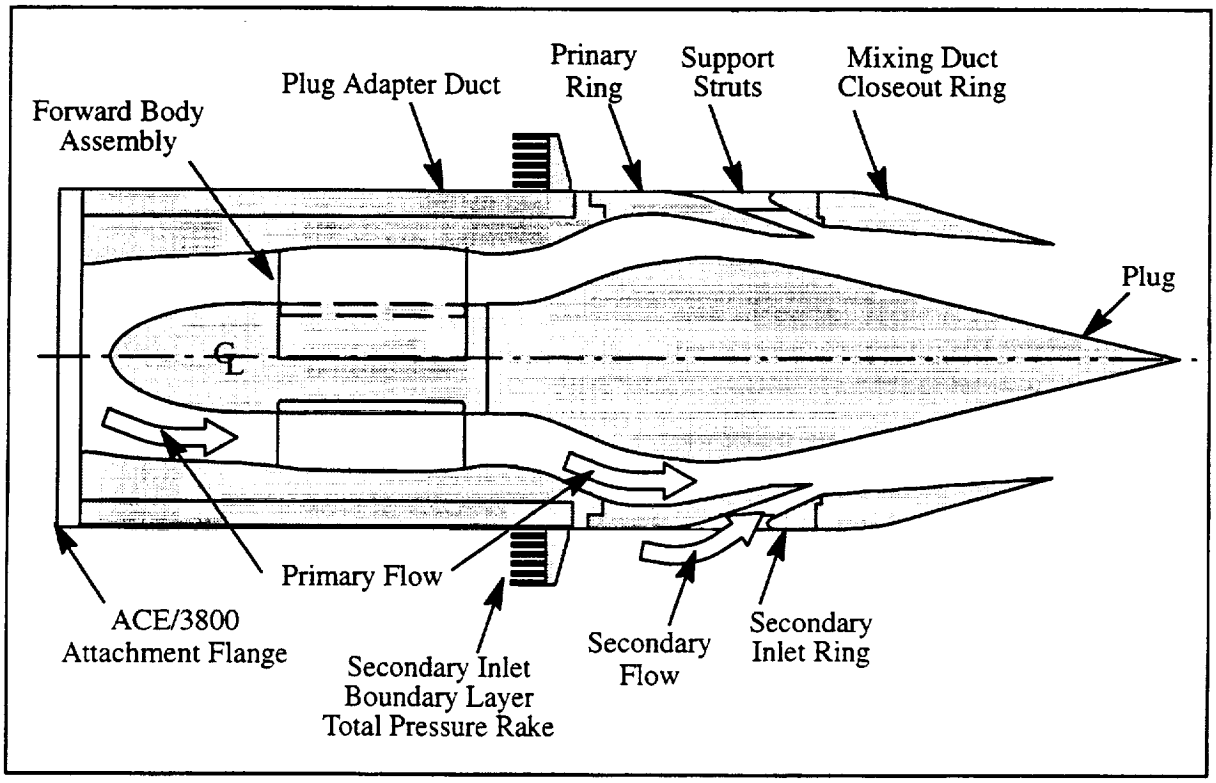

Figure 6. Schematic Diagram of the ACE Nozzle

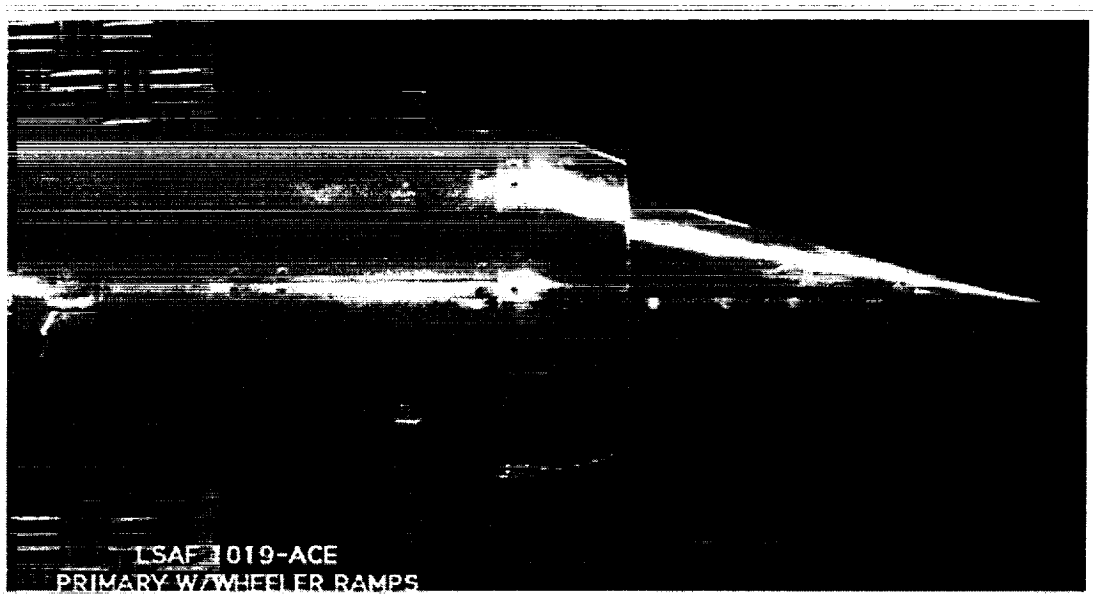

ACE Nozzle without Ejector

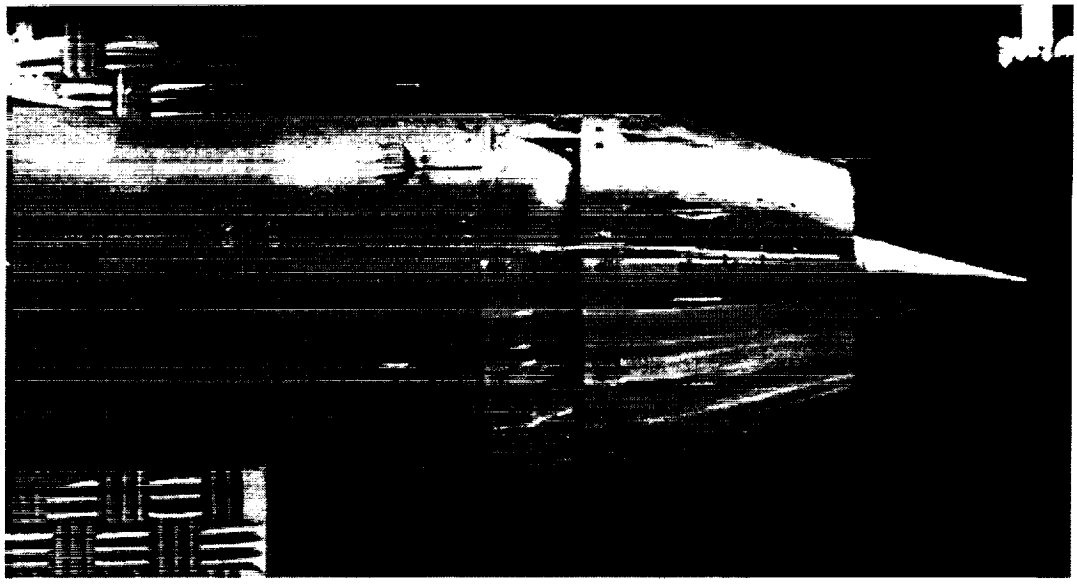

ACE Nozzle with Ejector

Figure 7. Photographs of the ACE Nozzle

Ejector Shroud	Primary Nozzle: baseline	tabs	rods	wheeler ramps
none	tunnel off and on config'n. 510	tunnel on config'n. 520	(not tested) config'n. 530	tunnel on config'n. 540
baseline	tunnel off and on config'n. 511	tunnel on config'n. 521	tunnel on config'n. 531	tunnel on config'n. 541
tabs	tunnel on config'n. 512	tunnel on config'n. 522	tunnel on config'n. 532	tunnel on config'n. 542

Figure 8. Test Matrix: Nozzle Configurations and Tunnel Conditions

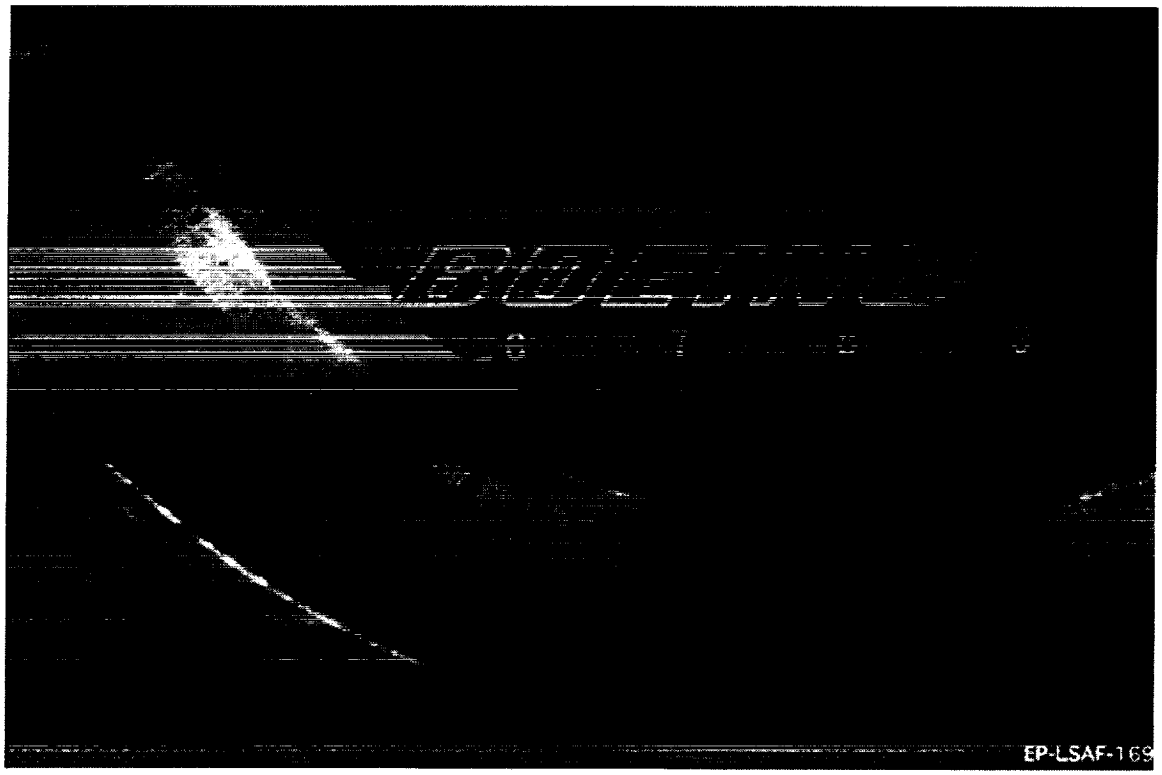

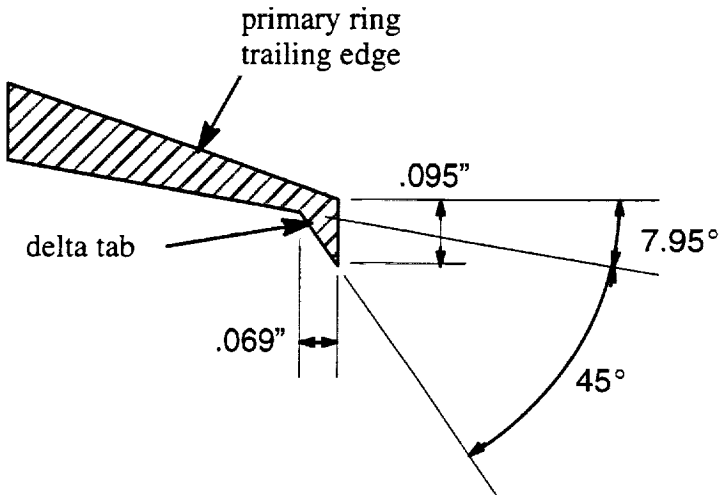

Figure 9. Primary Ring with Delta Tabs

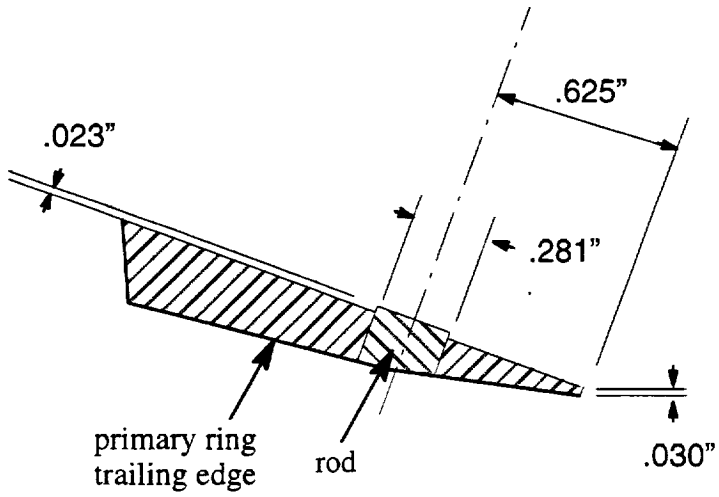

Figure 10. Primary Ring with Tone Injection Rods

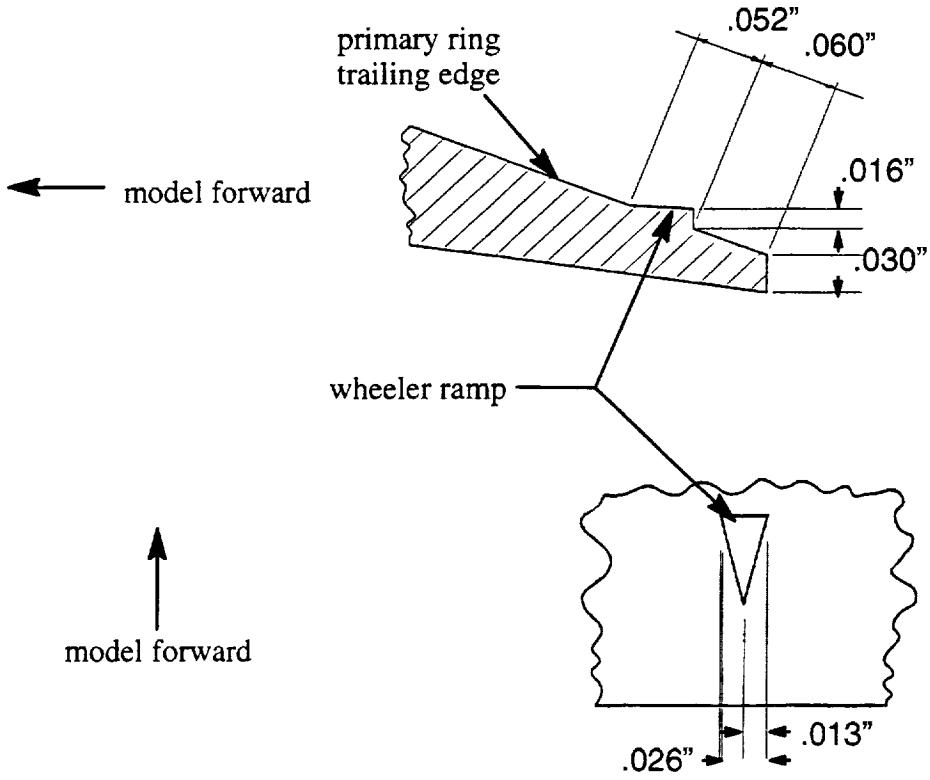

Figure 11. Primary Ring with Wheeler Ramps

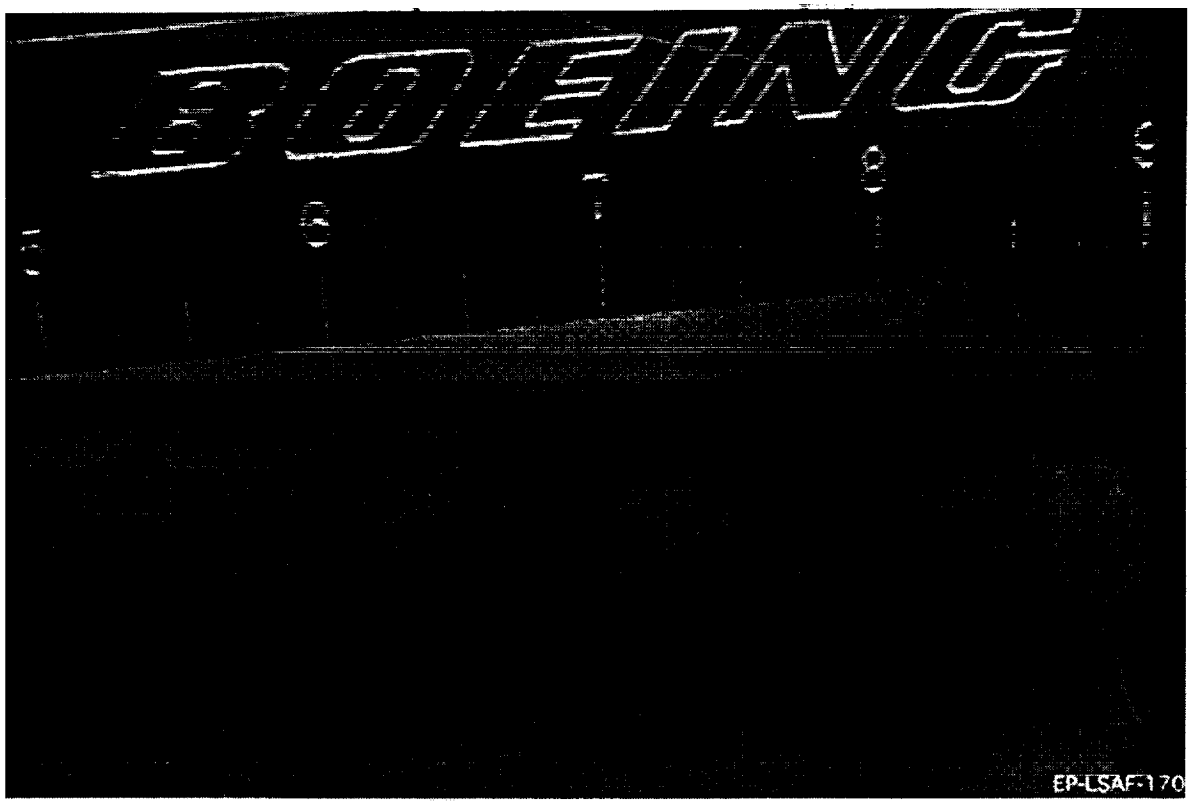

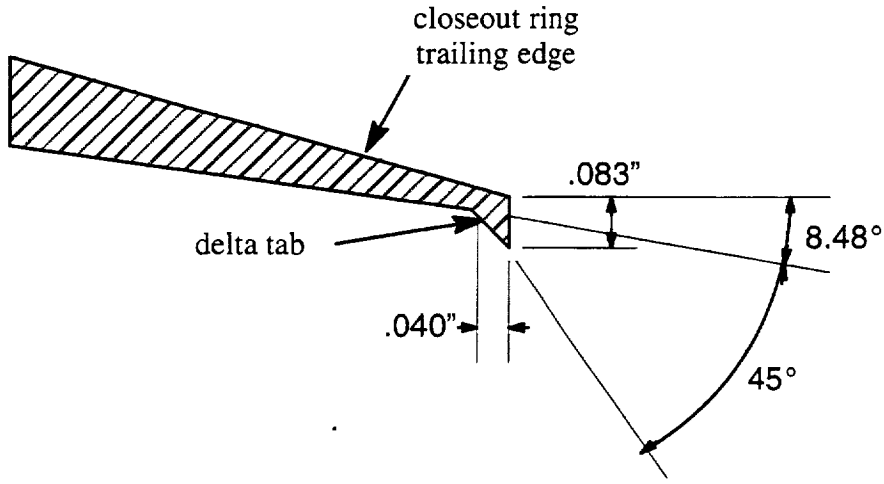

Figure 12. Closeout Ring with Delta Tabs

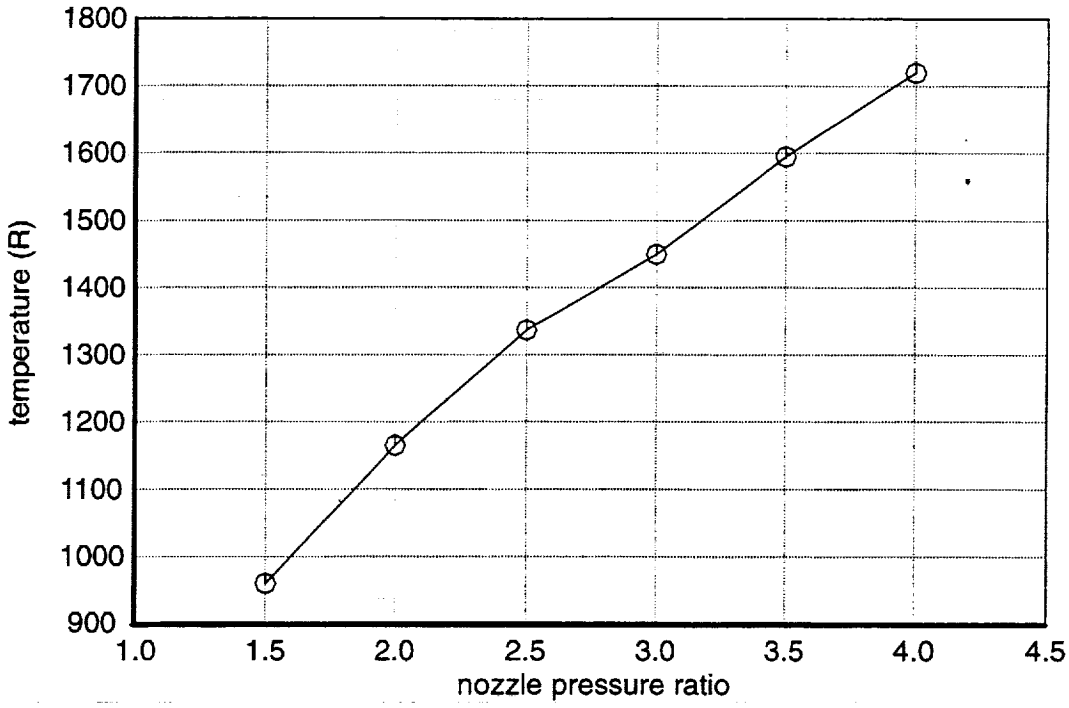

Figure 13. Throttle Line

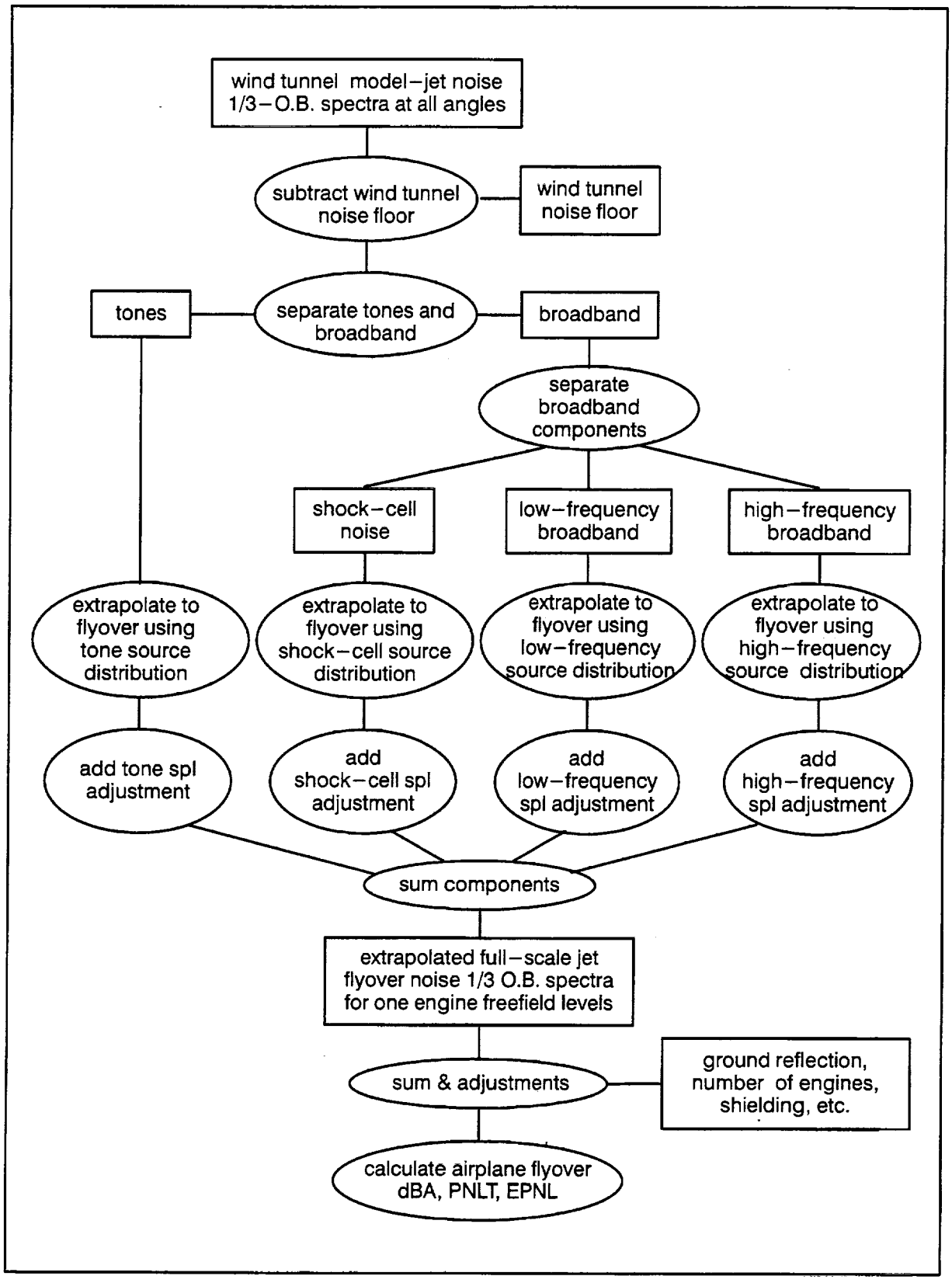

Figure 14. Flow Diagram of the Extrapolation Program

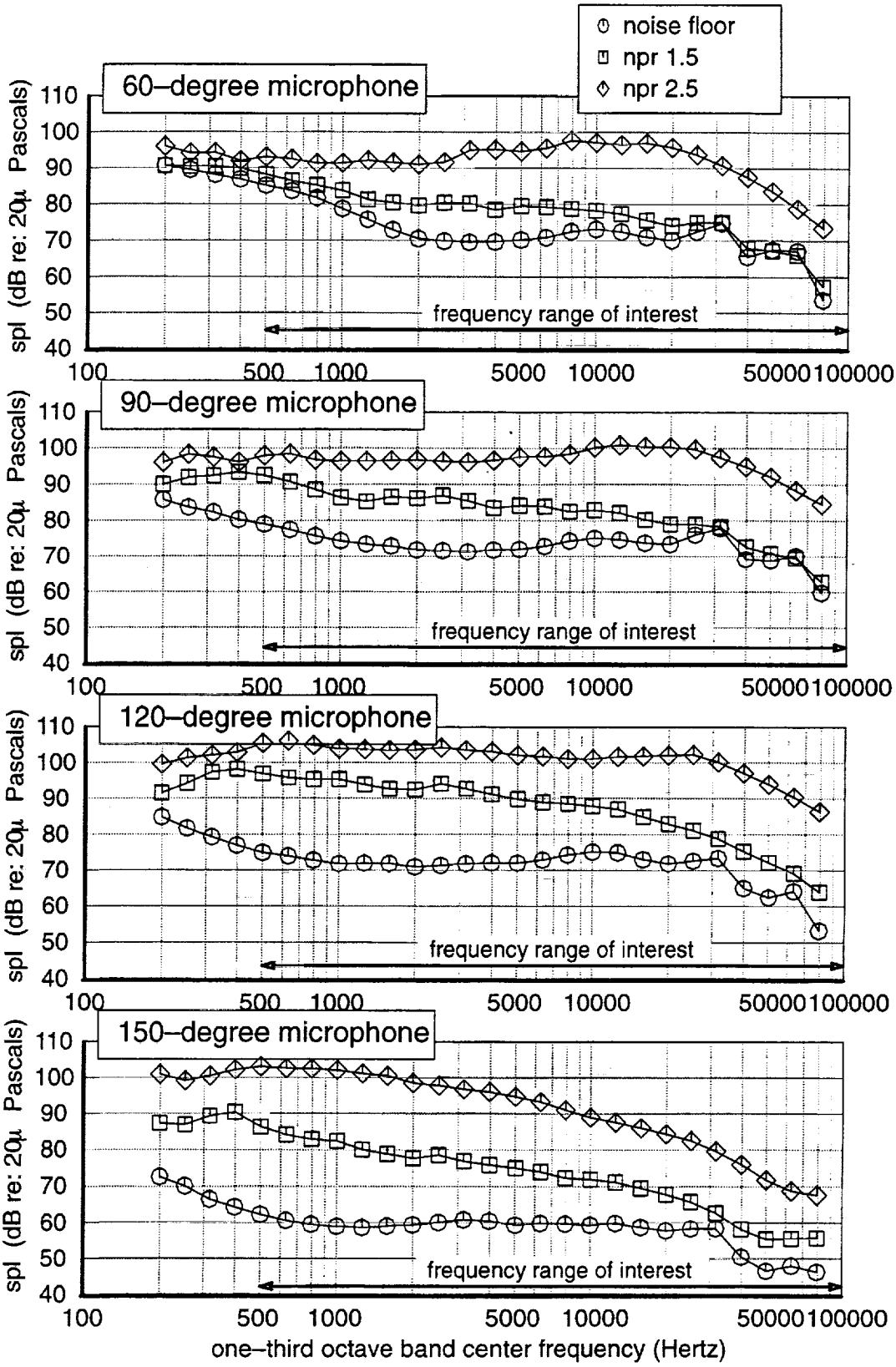

Figure 15. Noise Floors for 20–ft Out–of–flow Microphone Sideline tunnel Mach number of 0.245, ACE nozzle

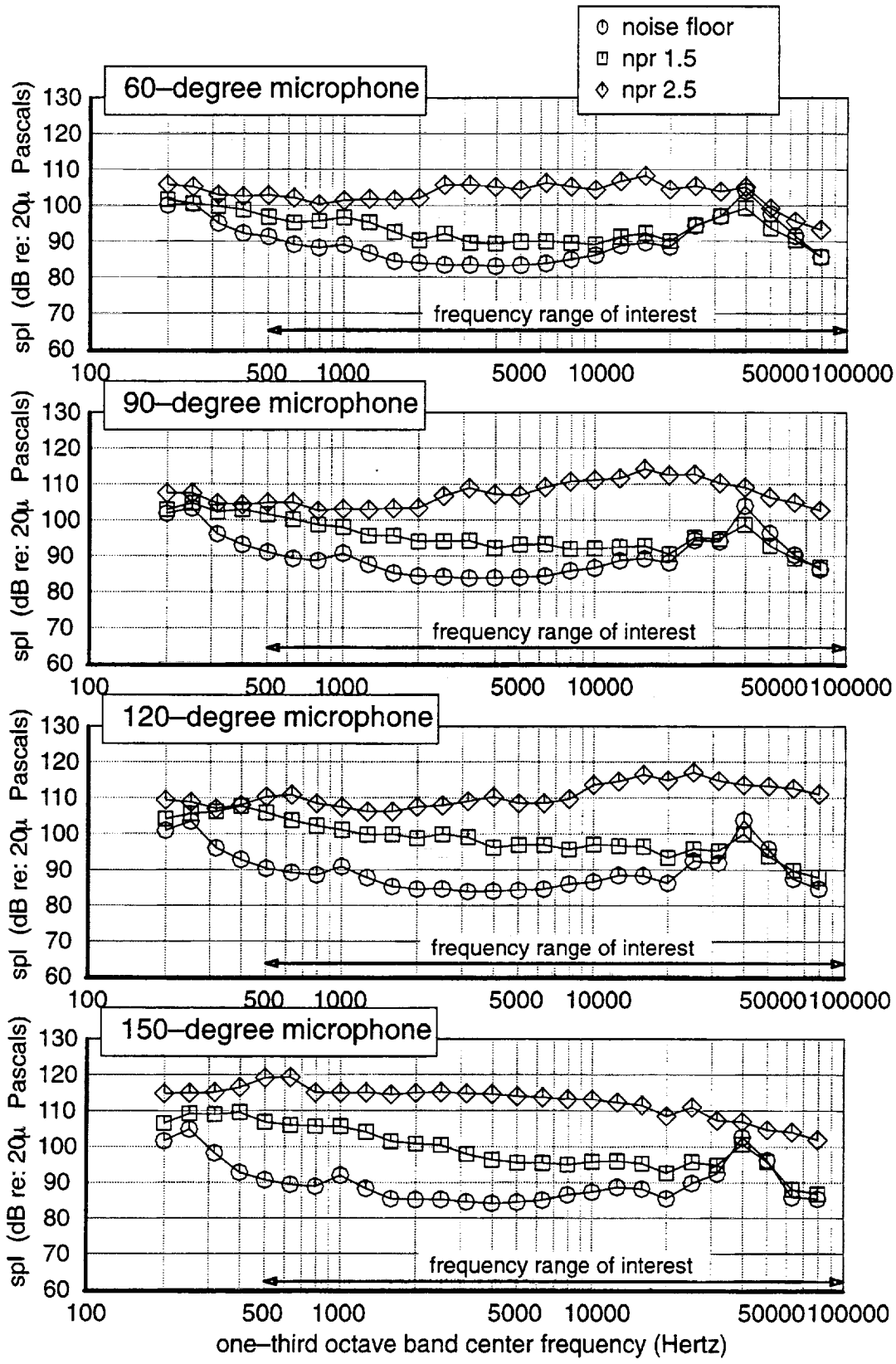

Figure 16. Noise Floors for 4.7–ft In–flow Microphone Sideline
tunnel Mach number of 0.245, ACE nozzle

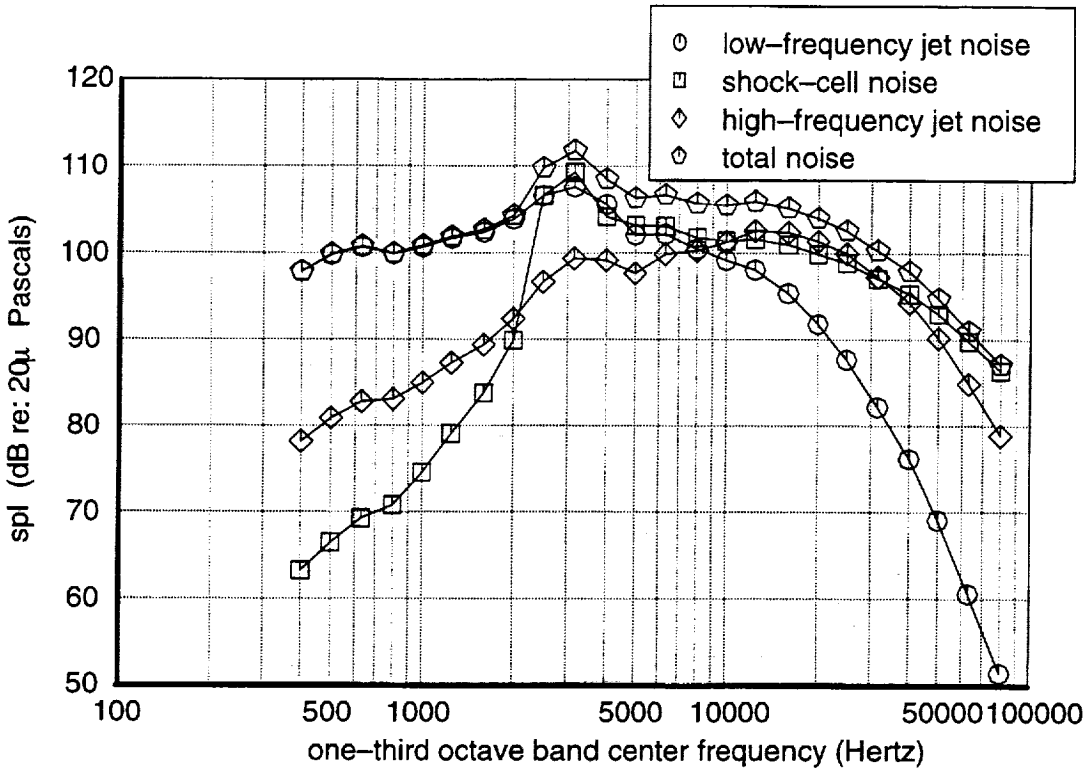

Figure 17. ACE Nozzle Component Separation
model scale, tunnel Mach 0.245, npr 3.0, 20–ft sideline mics, 90–degree mic, tabs on primary and on ejector

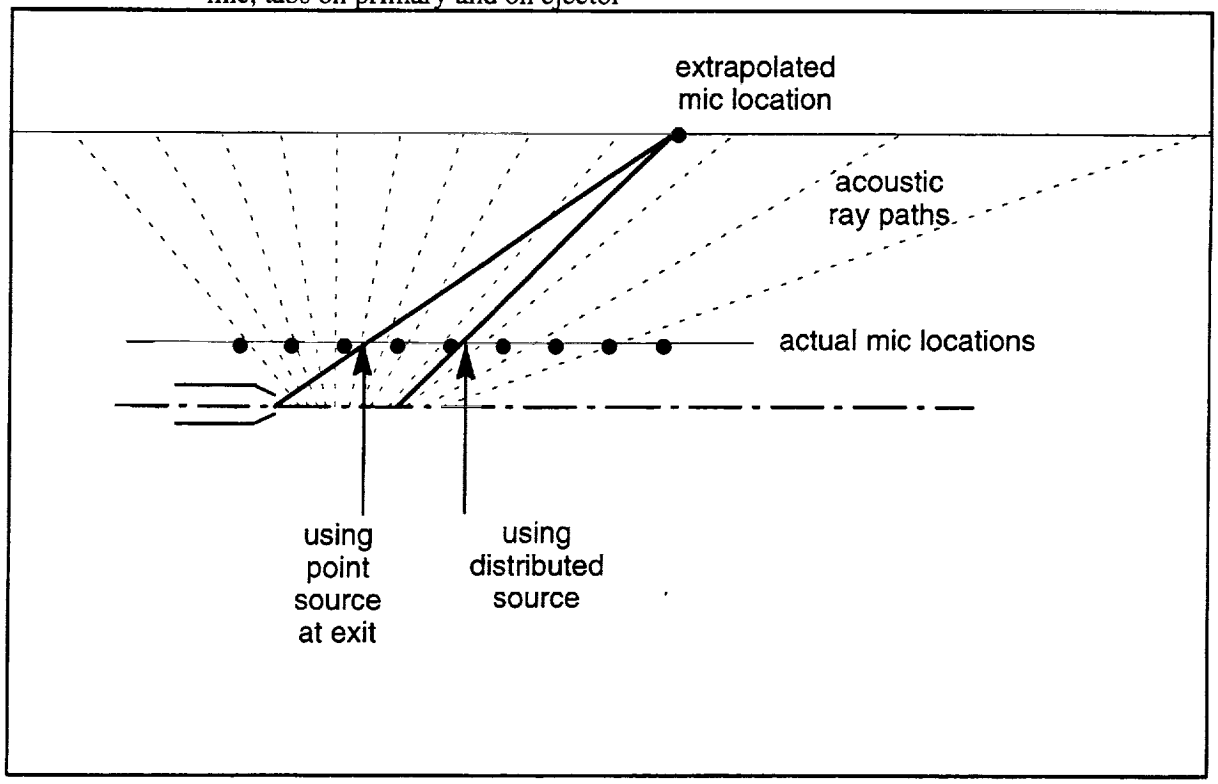

Figure 18. Illustration of Extrapolation Using Distributed Source Locations Situation for One Particular Component at One Particular Frequency

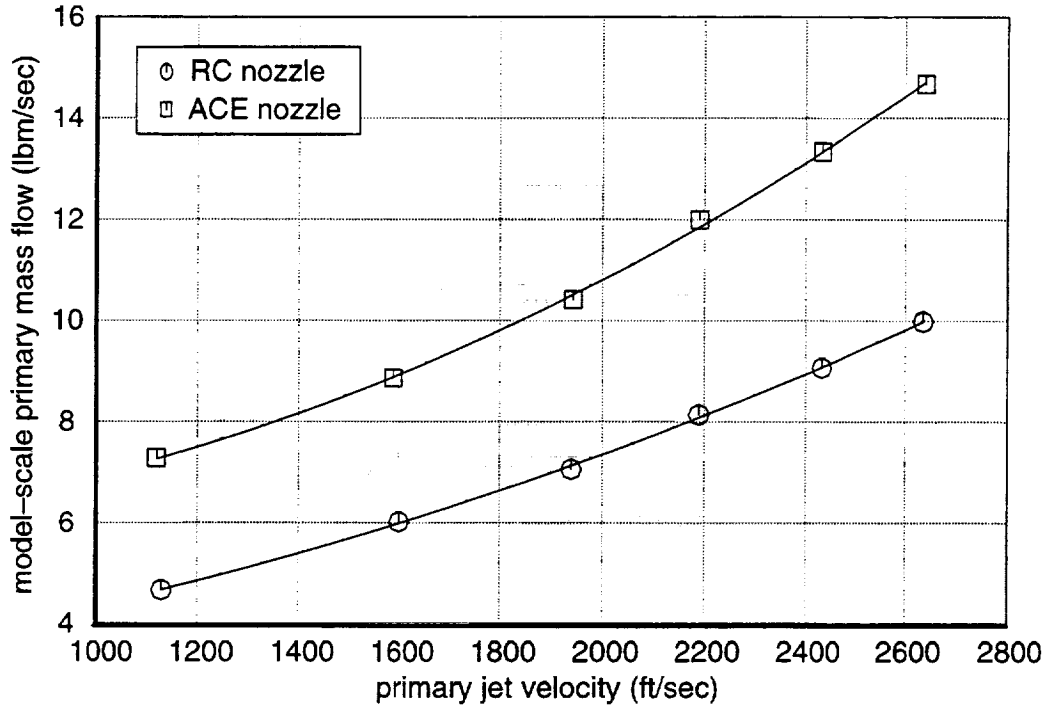

Figure 19. Model–scale Mass Flow versus Jet Velocity

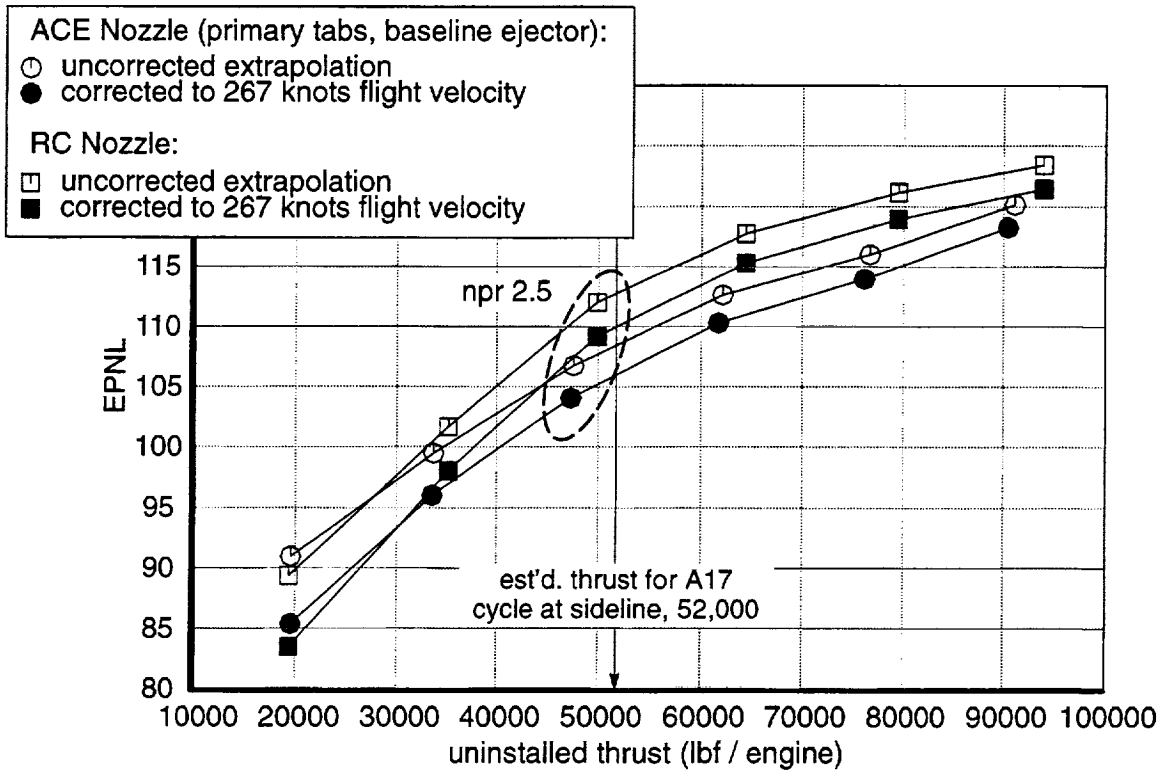

Figure 20. Relative Velocity Corrections
sideline conditions

	4.7–foot sideline data	20–foot sideline data
tunnel–off data	source location (A) near–field effects	(source location)* (B)
tunnel–on data	source location (C) near–field effects noise floor	(source location)* (D) shear–layer correction (noise floor)*

* effect less for the 20–foot sideline data
than for the 4.7–foot sideline data

Figure 21. Potential Sources of Inaccuracies for Various Data Sets

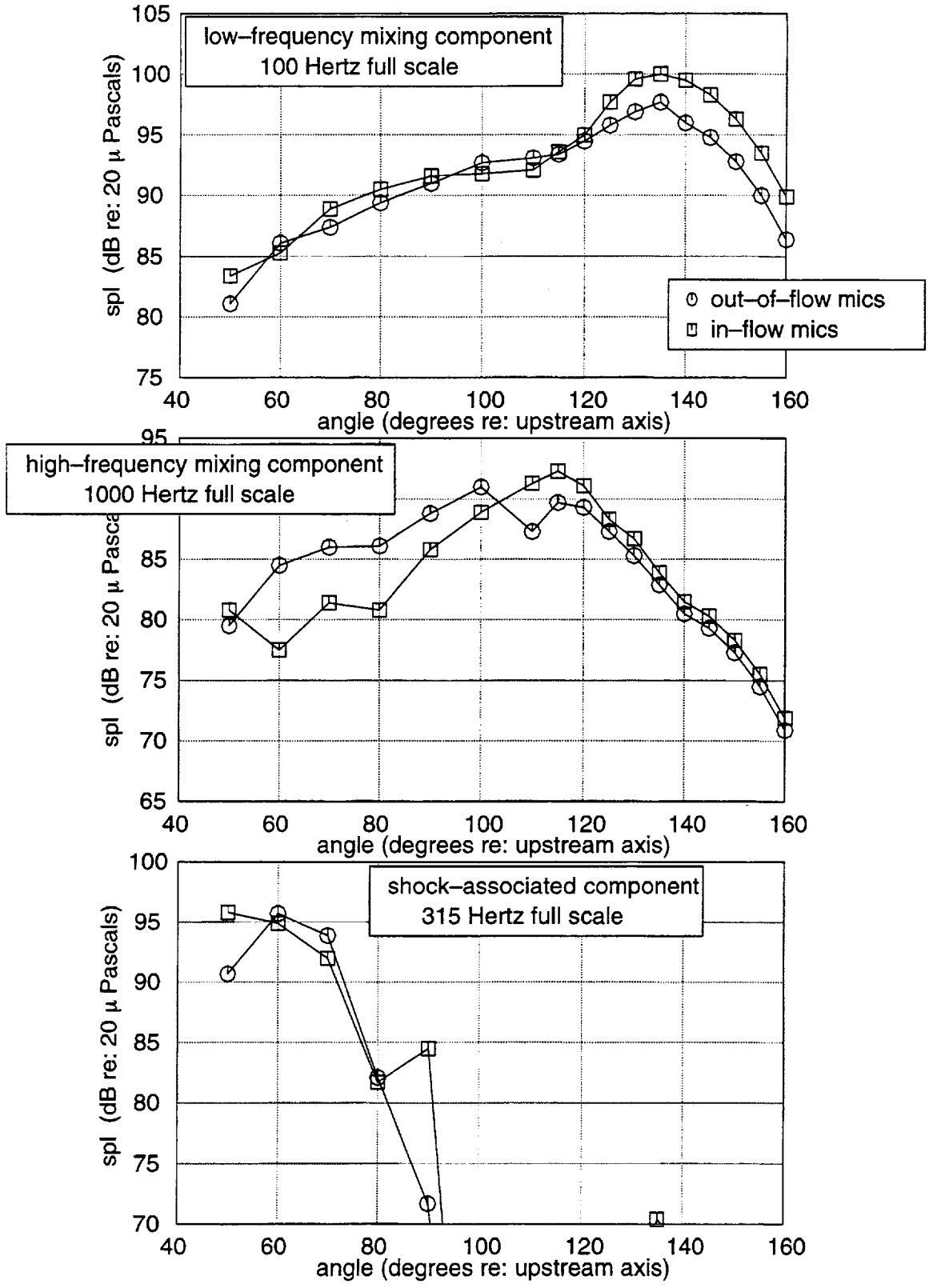

Figure 22. Out–of–flow and In–flow Component Directivity Comparison
tunnel Mach 0.245, sideline conditions (no ground reflection or relative velocity correction), tabs on primary and on ejector

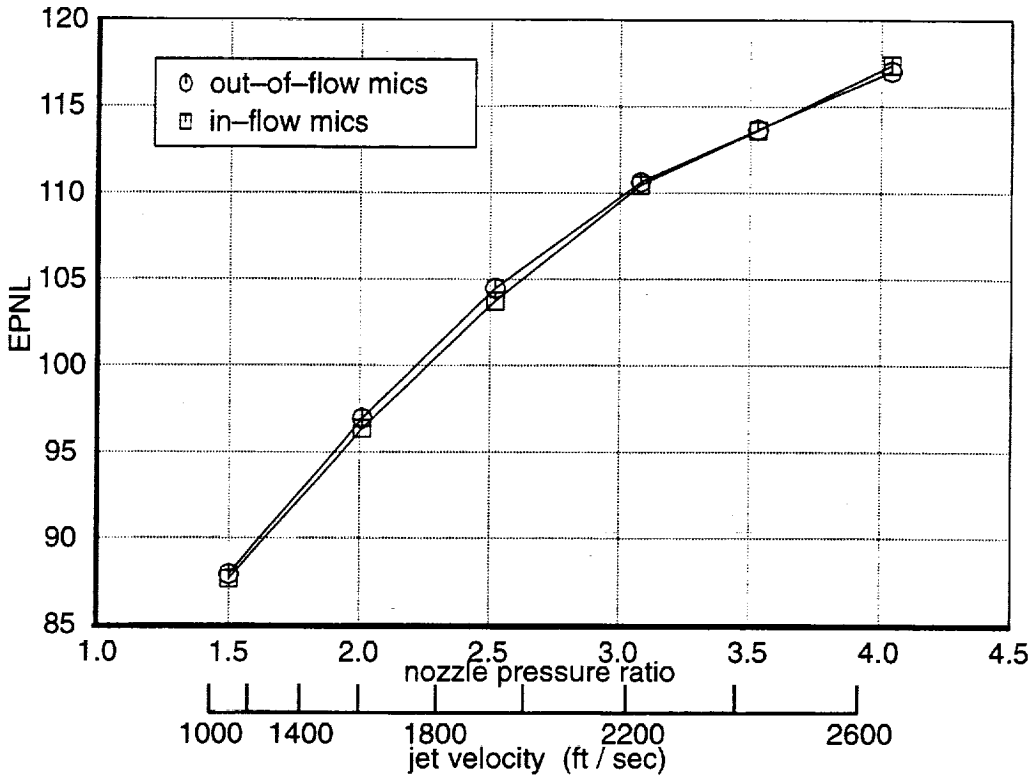

Figure 23. Comparison of Out–of–flow and In–flow Extrapolated EPNLs
tunnel Mach 0.245, sideline conditions (no ground reflection or relative velocity correction), tabs on primary and on ejector

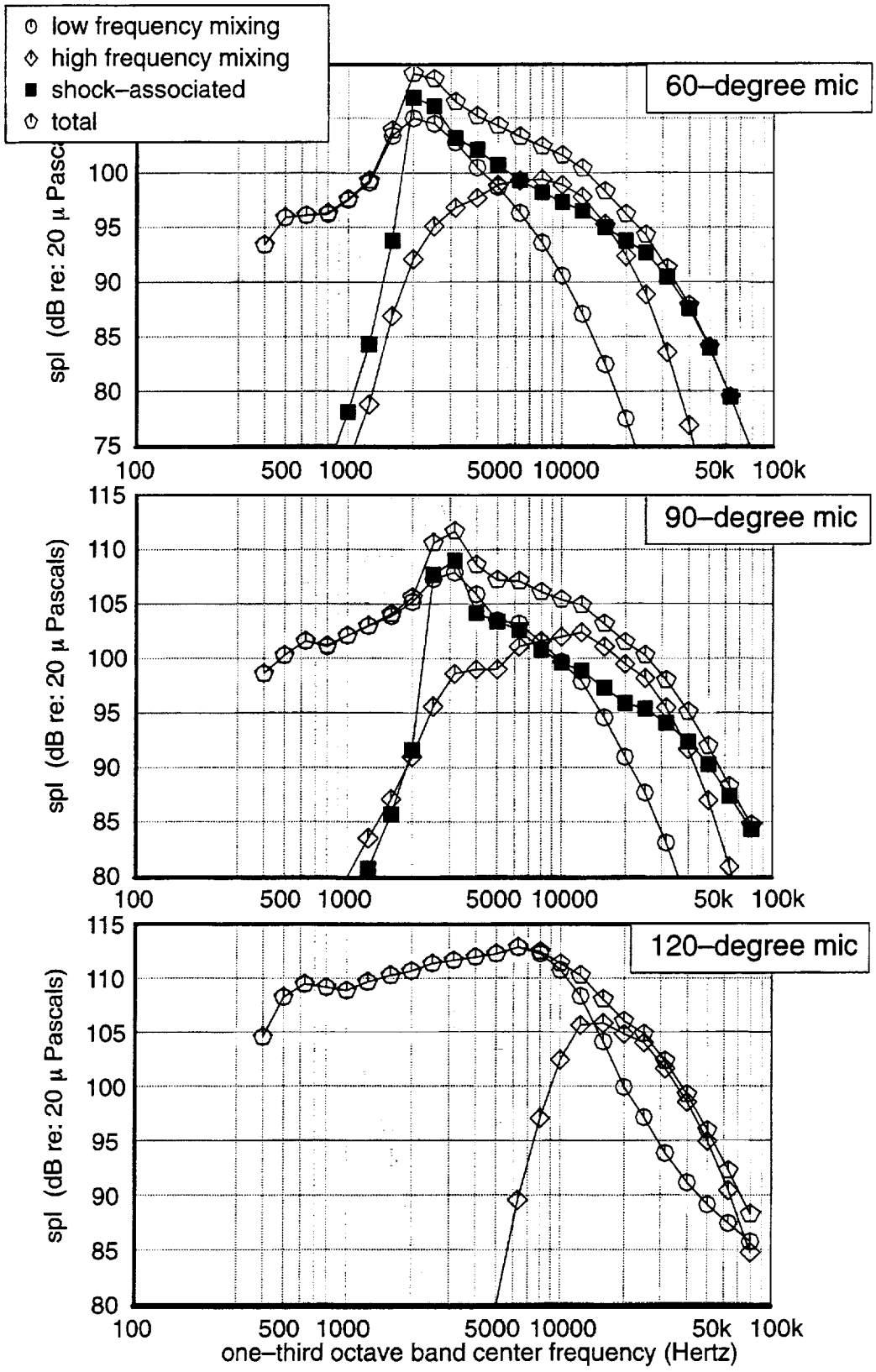

Figure 24. Shock–associated Noise Spectra: npr 3.0, Baseline Primary, Baseline Ejector model scale, tunnel Mach 0.245, 20–ft mics

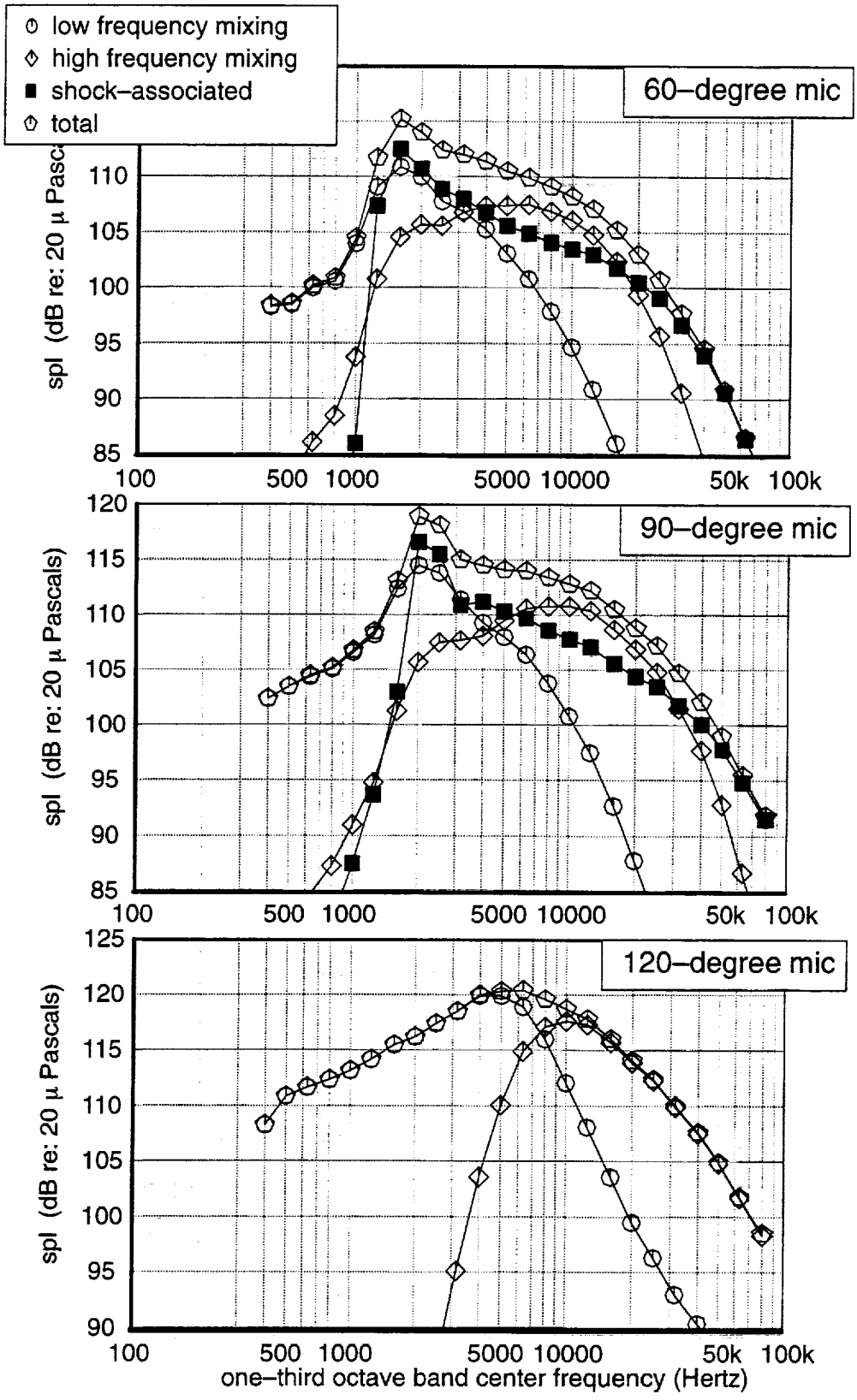

Figure 25. Shock–associated Noise Spectra: npr 4.0, Baseline Primary, Baseline Ejector model scale, tunnel Mach 0.245, 20–ft mics

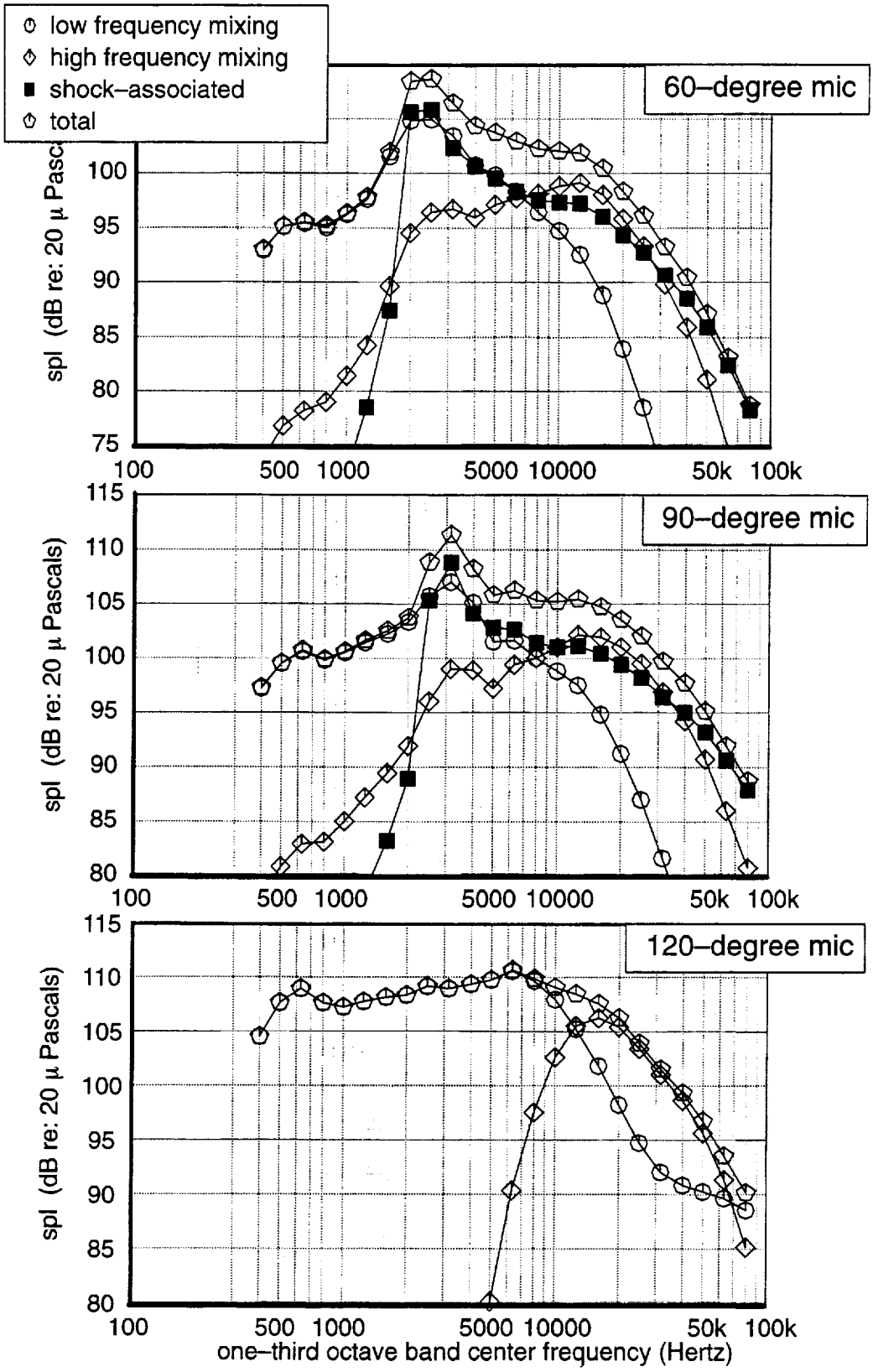

Figure 26. Shock–associated Noise Spectra: npr 3.0, tabbed Primary, Baseline Ejector model scale, tunnel Mach 0.245, 20–ft mics

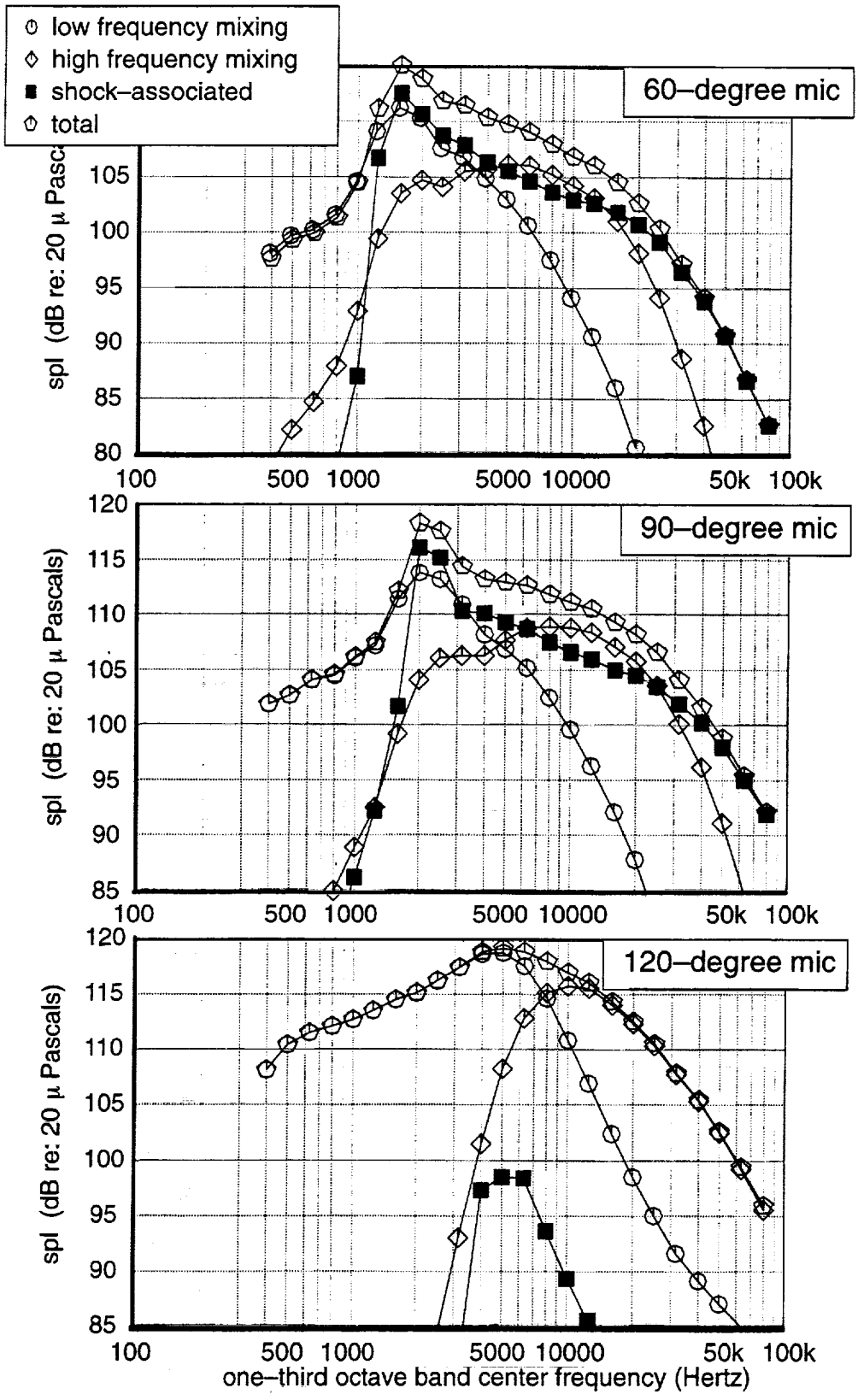

Figure 27. Shock–associated Noise Spectra: npr 4.0, tabbed Primary, Baseline Ejector model scale, tunnel Mach 0.245, 20–ft mics

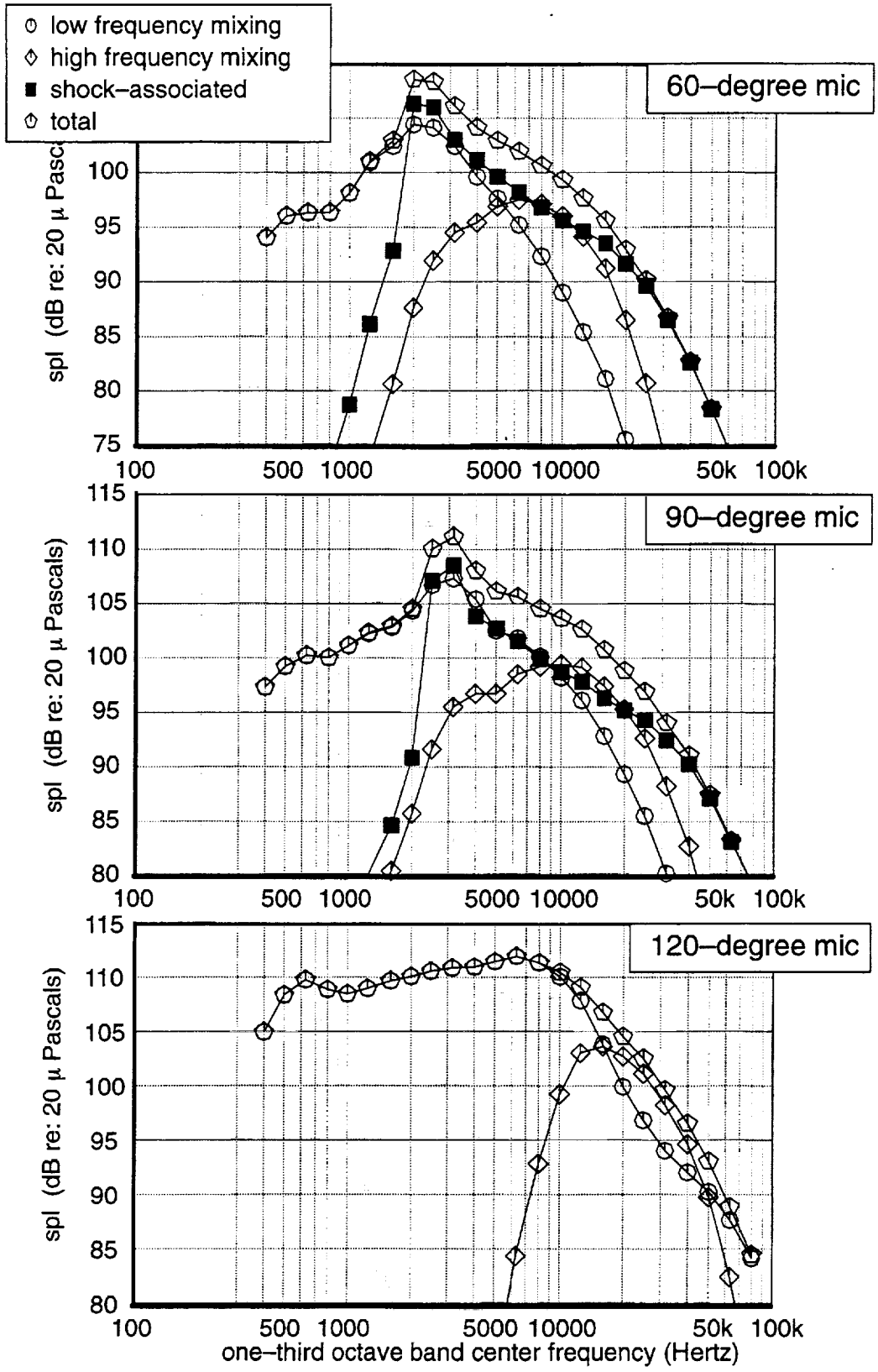

Figure 28. Shock–associated Noise Spectra: npr 3.0, Baseline Primary, no Ejector model scale, tunnel Mach 0.245, 20–ft mics

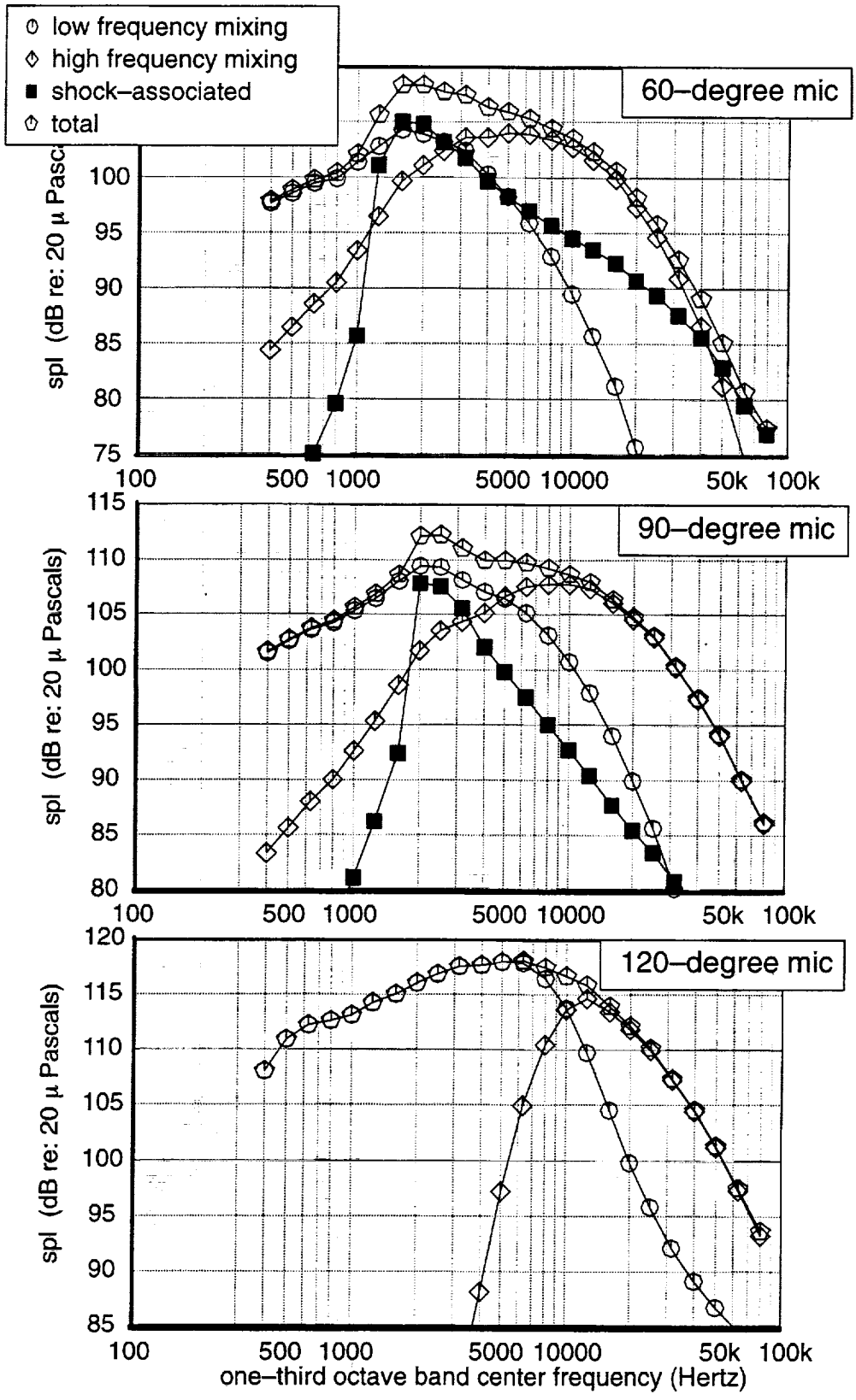

Figure 29. Shock–associated Noise Spectra: npr 4.0, Baseline Primary, no Ejector model scale, tunnel Mach 0.245, 20–ft mics

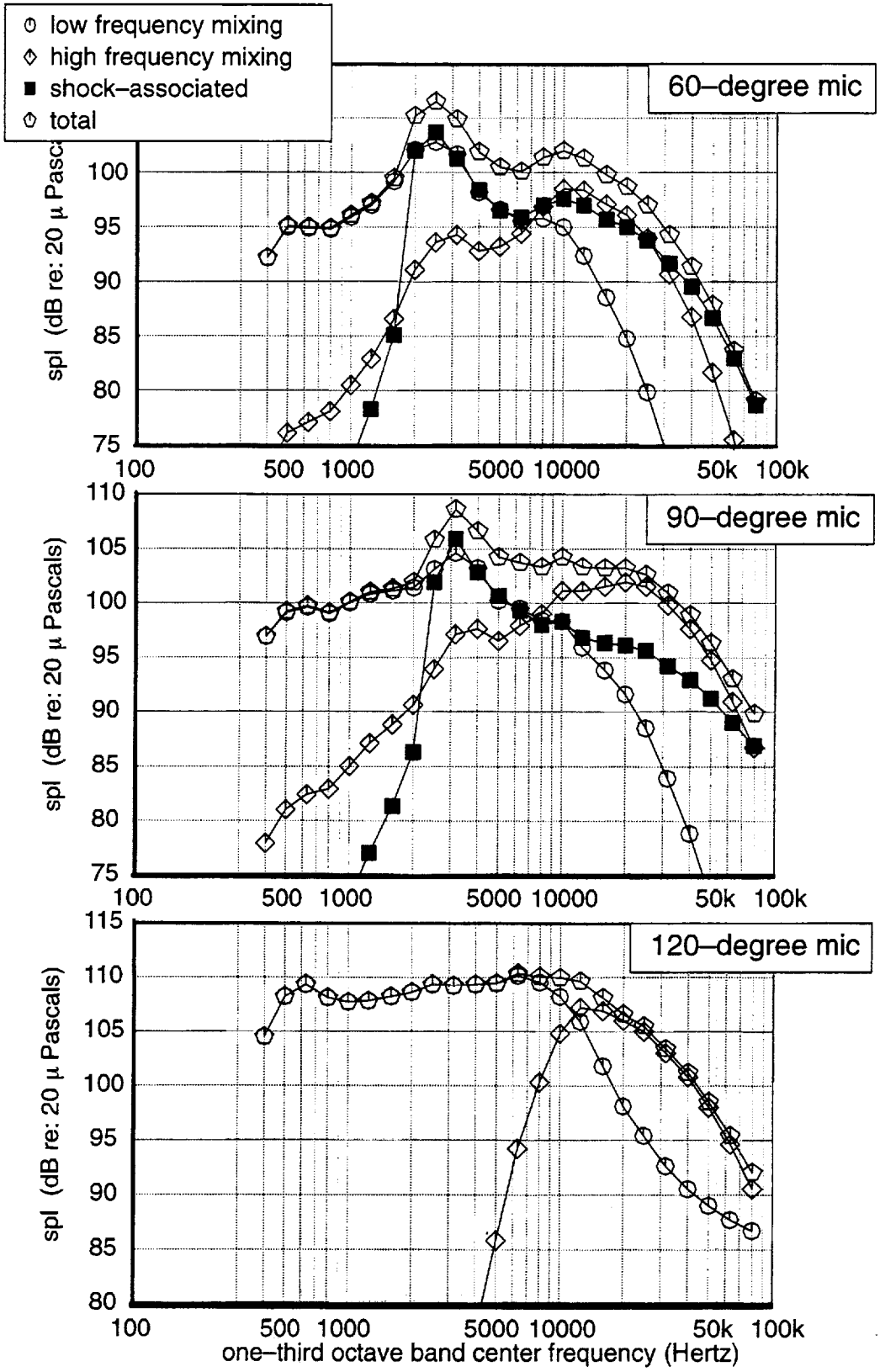

Figure 30. Shock–associated Noise Spectra: npr 3.0, tabbed Primary, no Ejector model scale, tunnel Mach 0.245, 20–ft mics

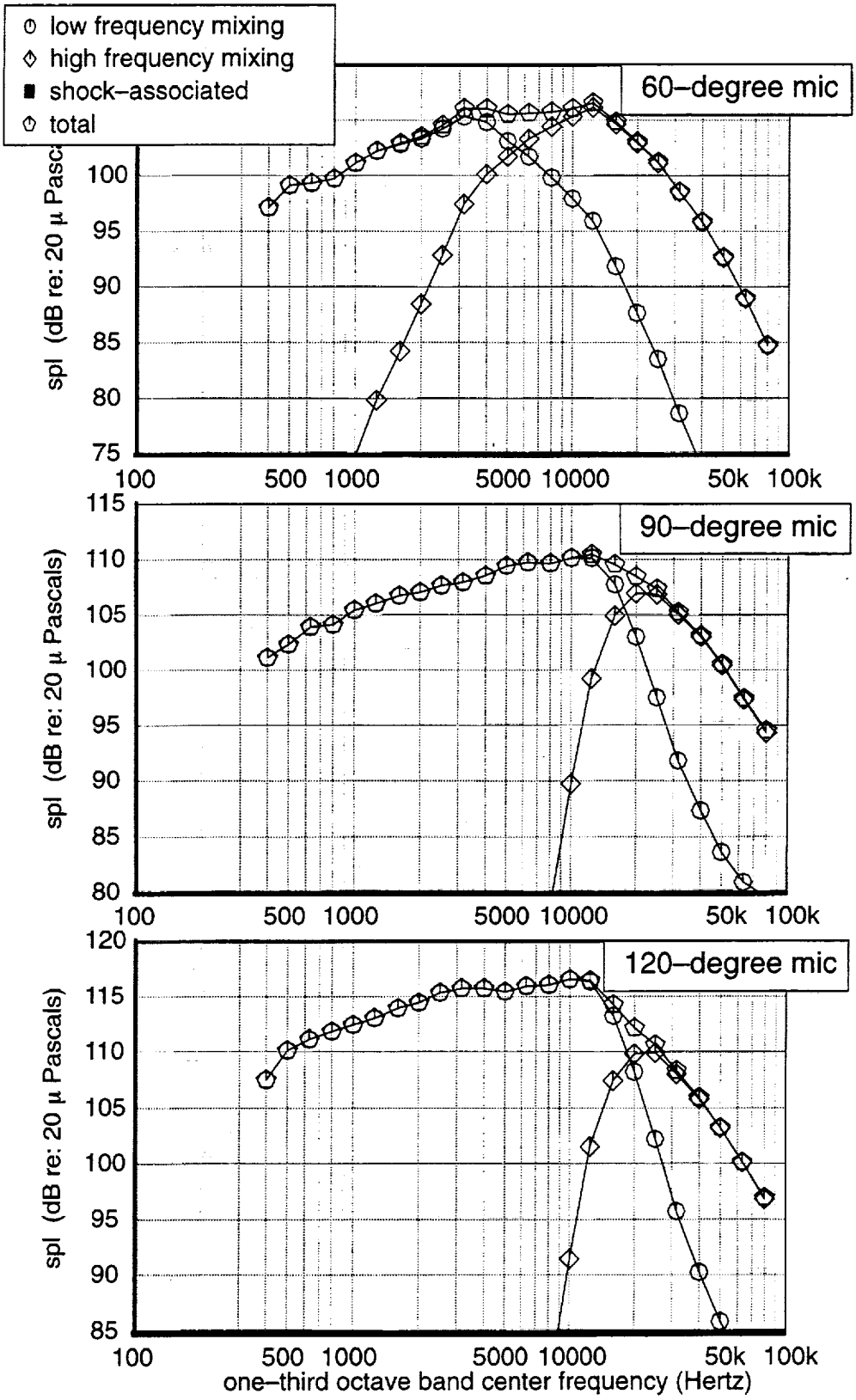

Figure 31. Shock–associated Noise Spectra: npr 4.0, tabbed Primary, no Ejector model scale, tunnel Mach 0.245, 20–ft mics

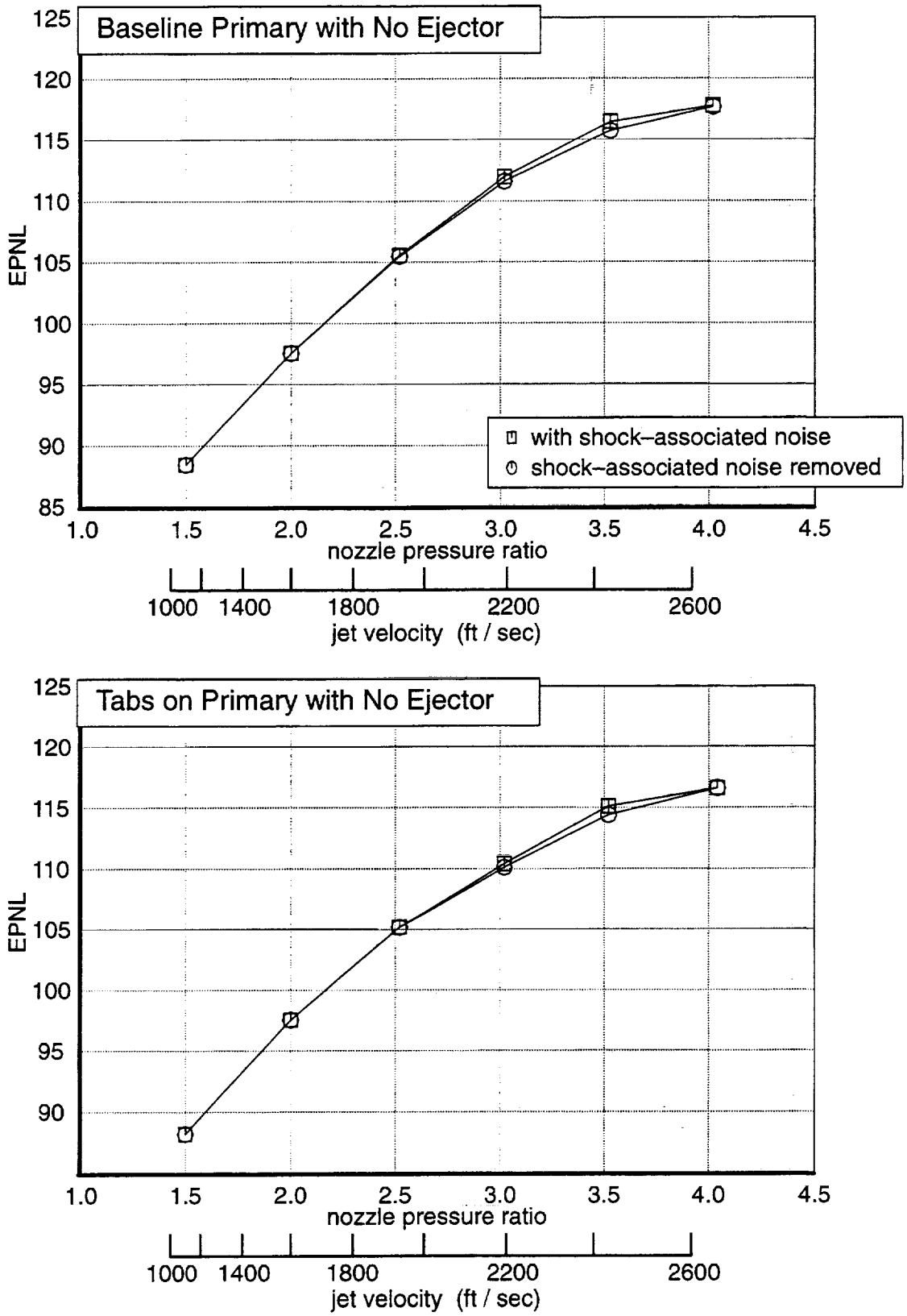

Figure 32. EPNL Effect of Tabs on Shock–associated Noise with No Ejector
tunnel Mach 0.245, 20–ft mics, sideline conditions, no relative velocity adjustment

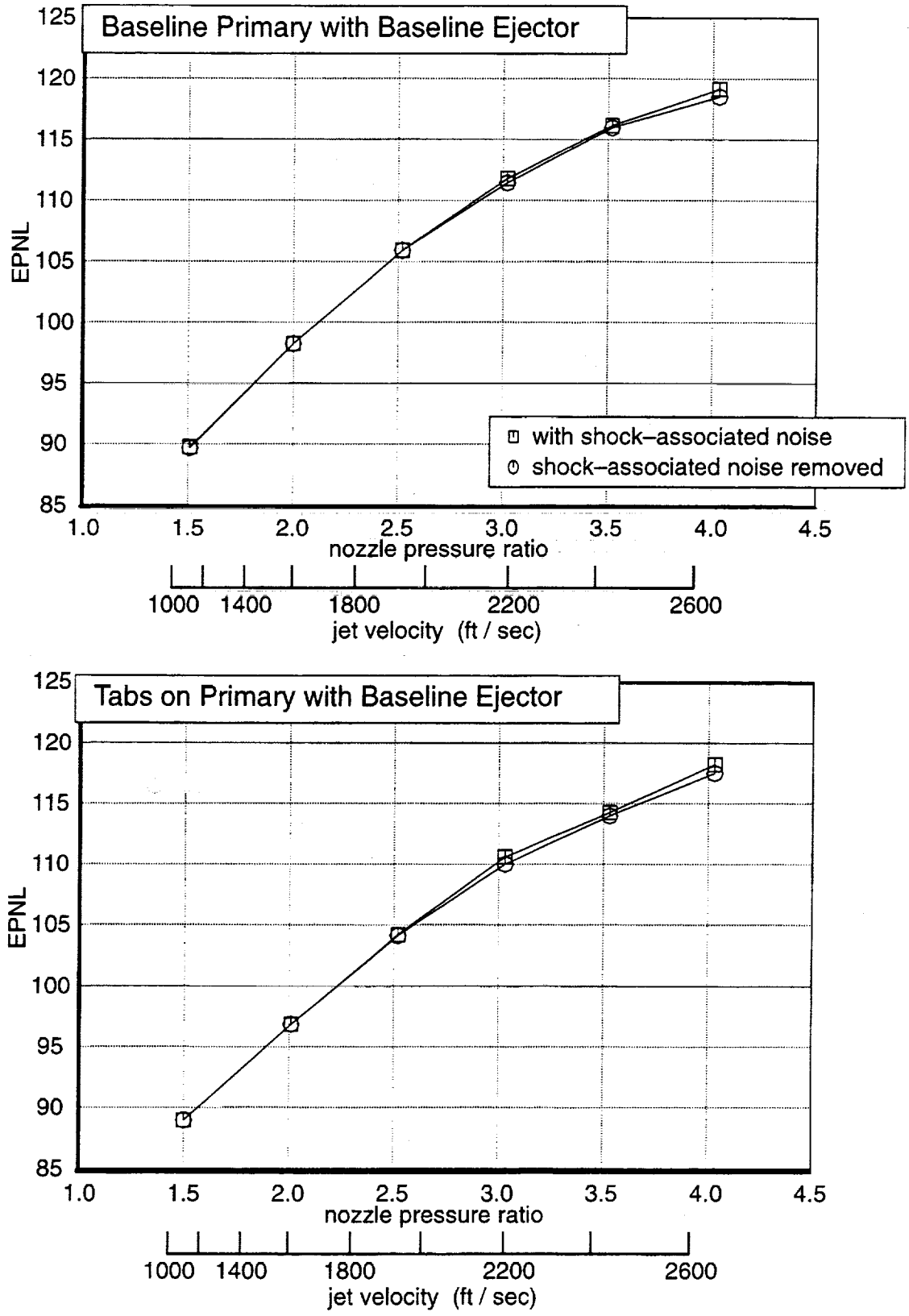

Figure 33. EPNL Effect of Tabs on Shock–associated Noise with Baseline Ejector
tunnel Mach 0.245, 20–ft mics, sideline conditions, no relative velocity adjustment

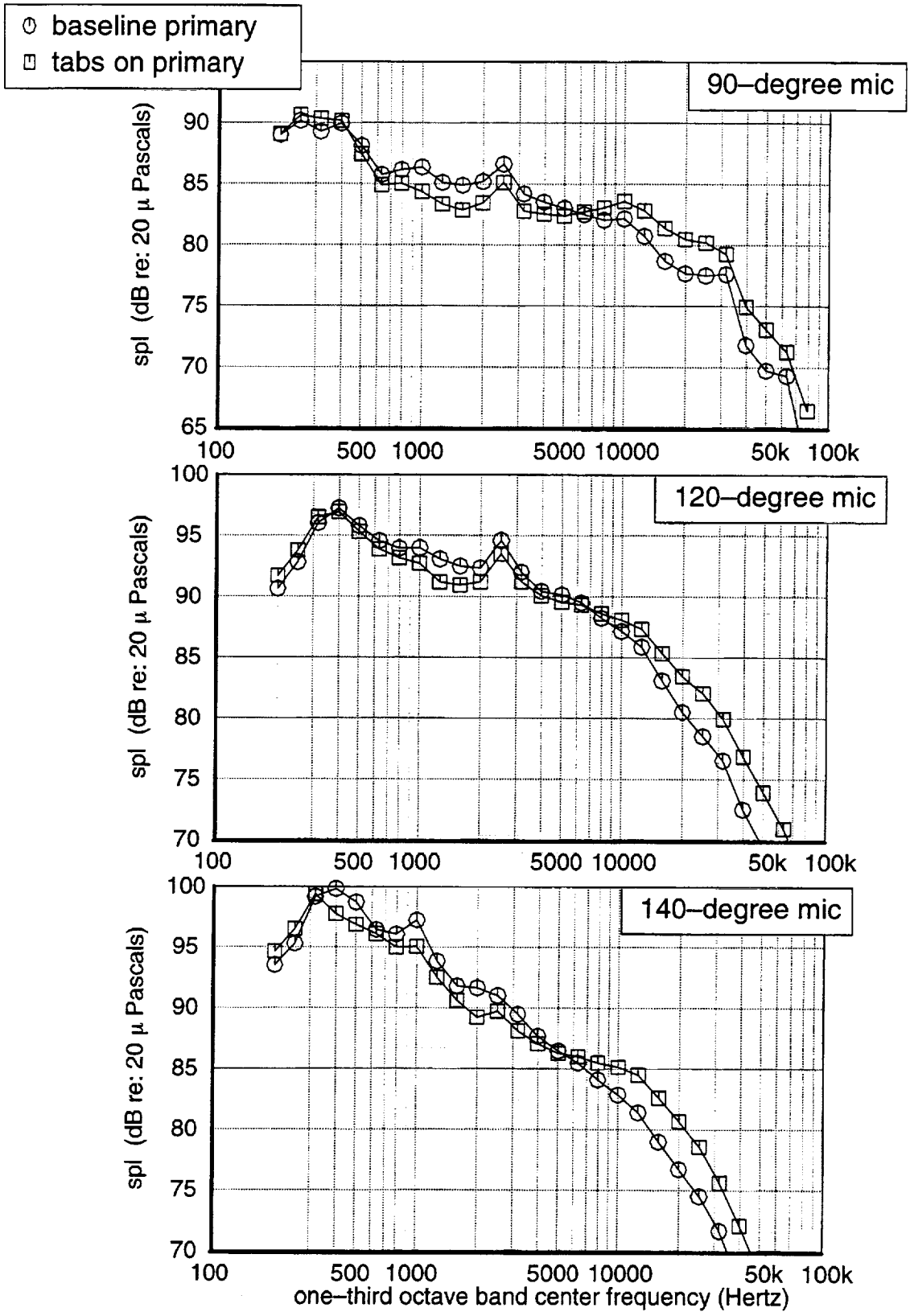

Figure 34. Model–scale Spectra: No Ejector, Various Primaries, NPR 1.5
20–ft sideline mics, tunnel Mach 0.245

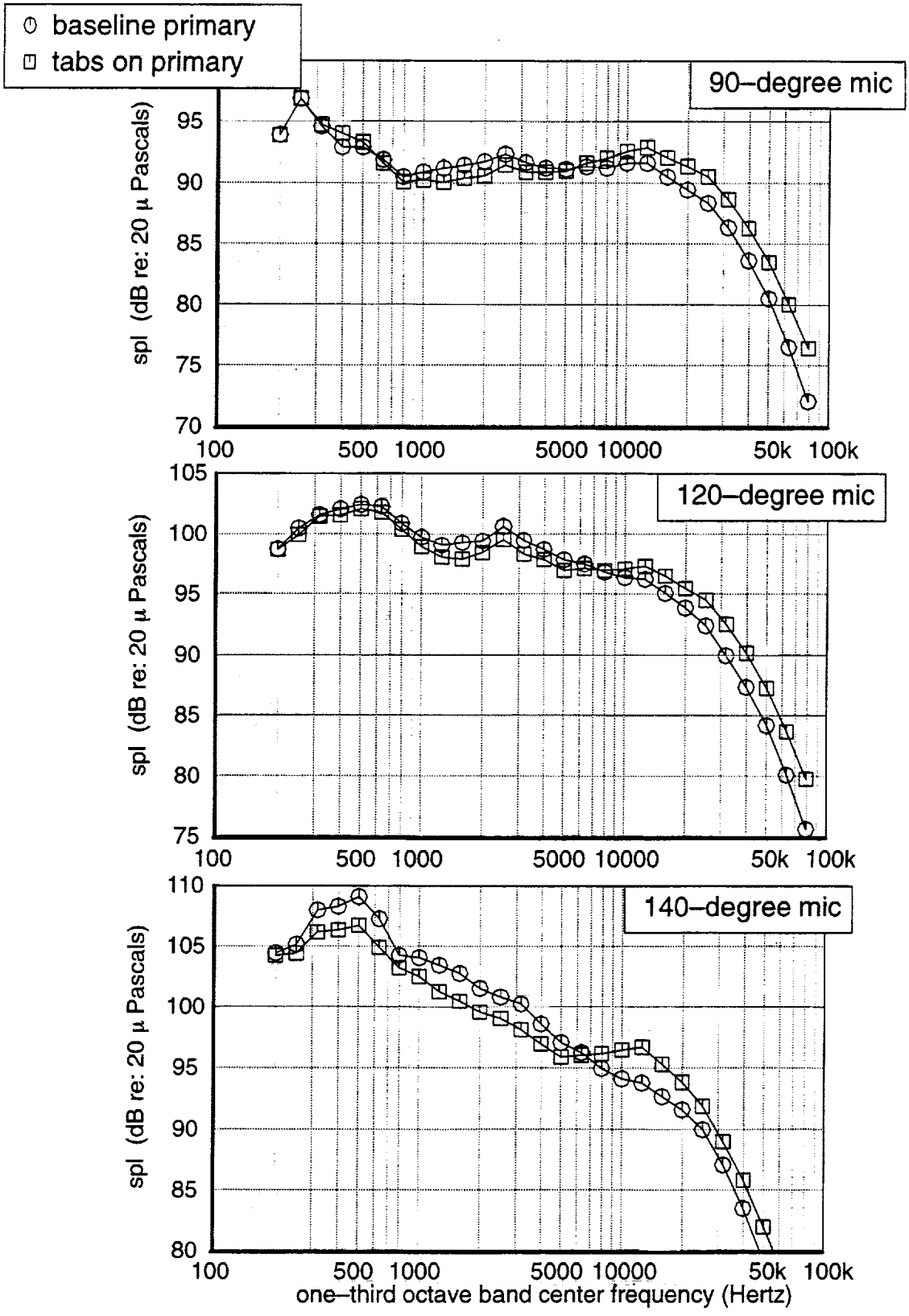

Figure 35. Model–scale Spectra: No Ejector, Various Primaries, NPR 2.0 20–ft sideline mics, tunnel Mach 0.245

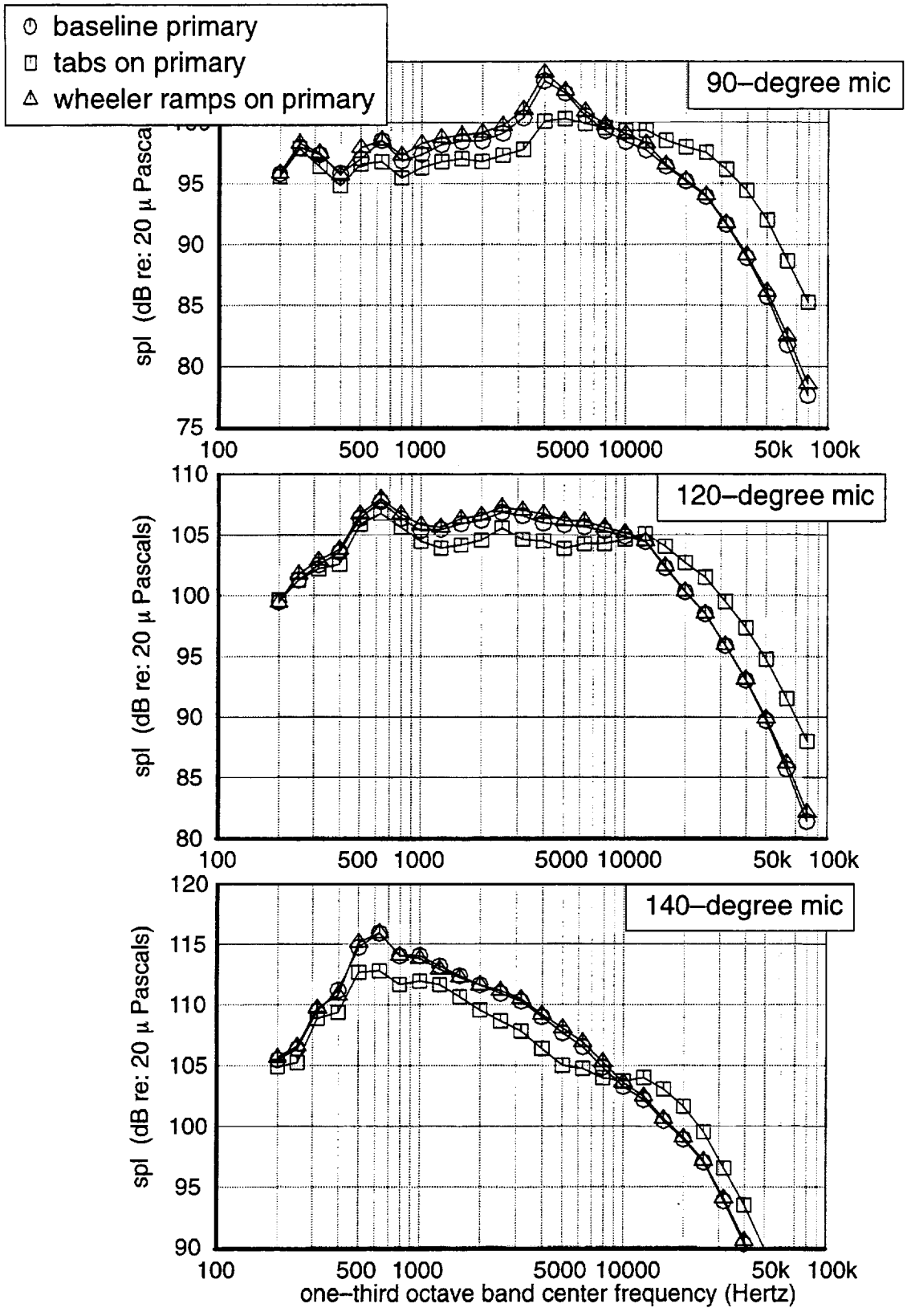

Figure 36. Model–scale Spectra: No Ejector, Various Primaries, NPR 2.5
20–ft sideline mics, tunnel Mach 0.245

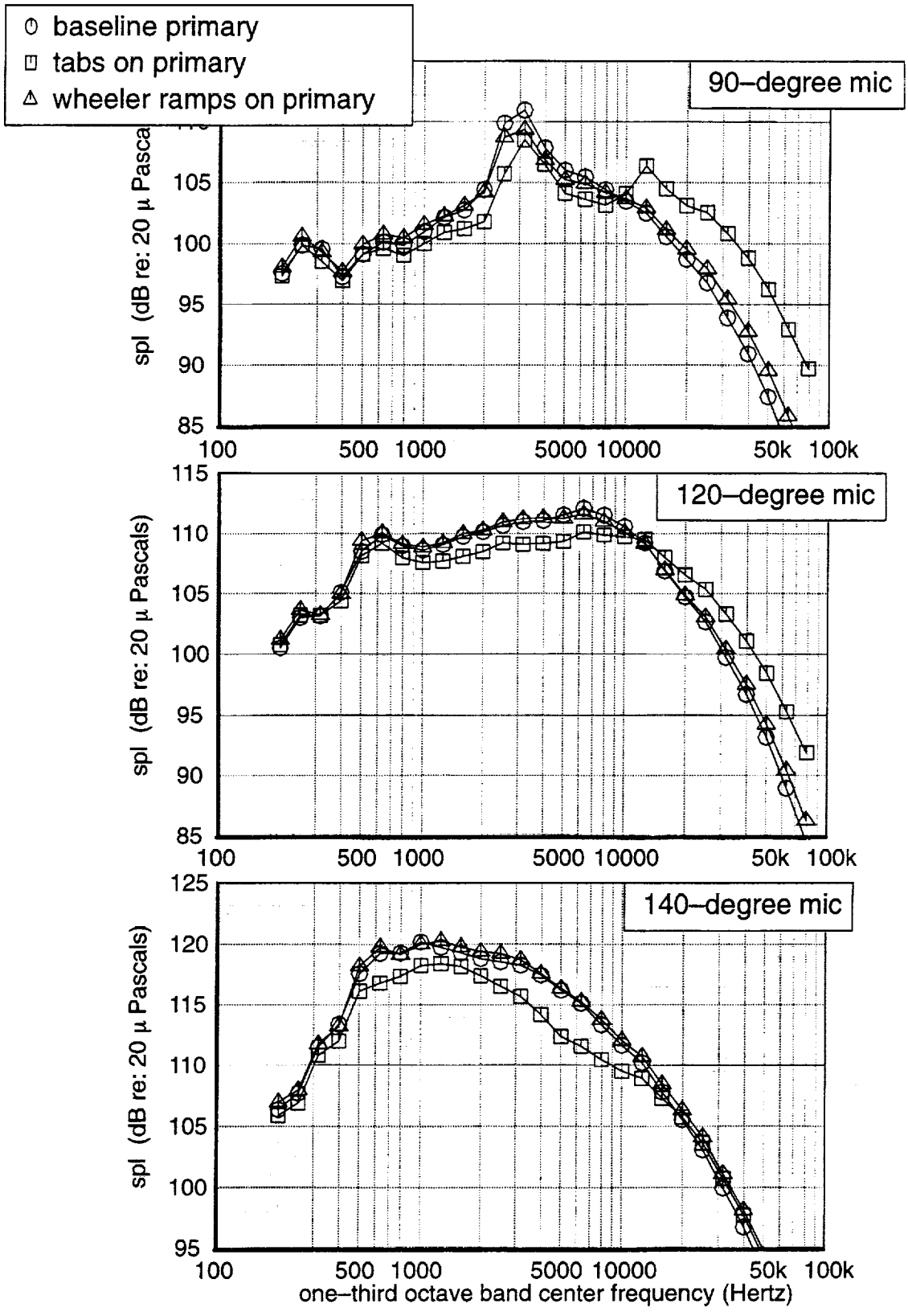

Figure 37. Model–scale Spectra: No Ejector, Various Primaries, NPR 3.0
20–ft sideline mics, tunnel Mach 0.245

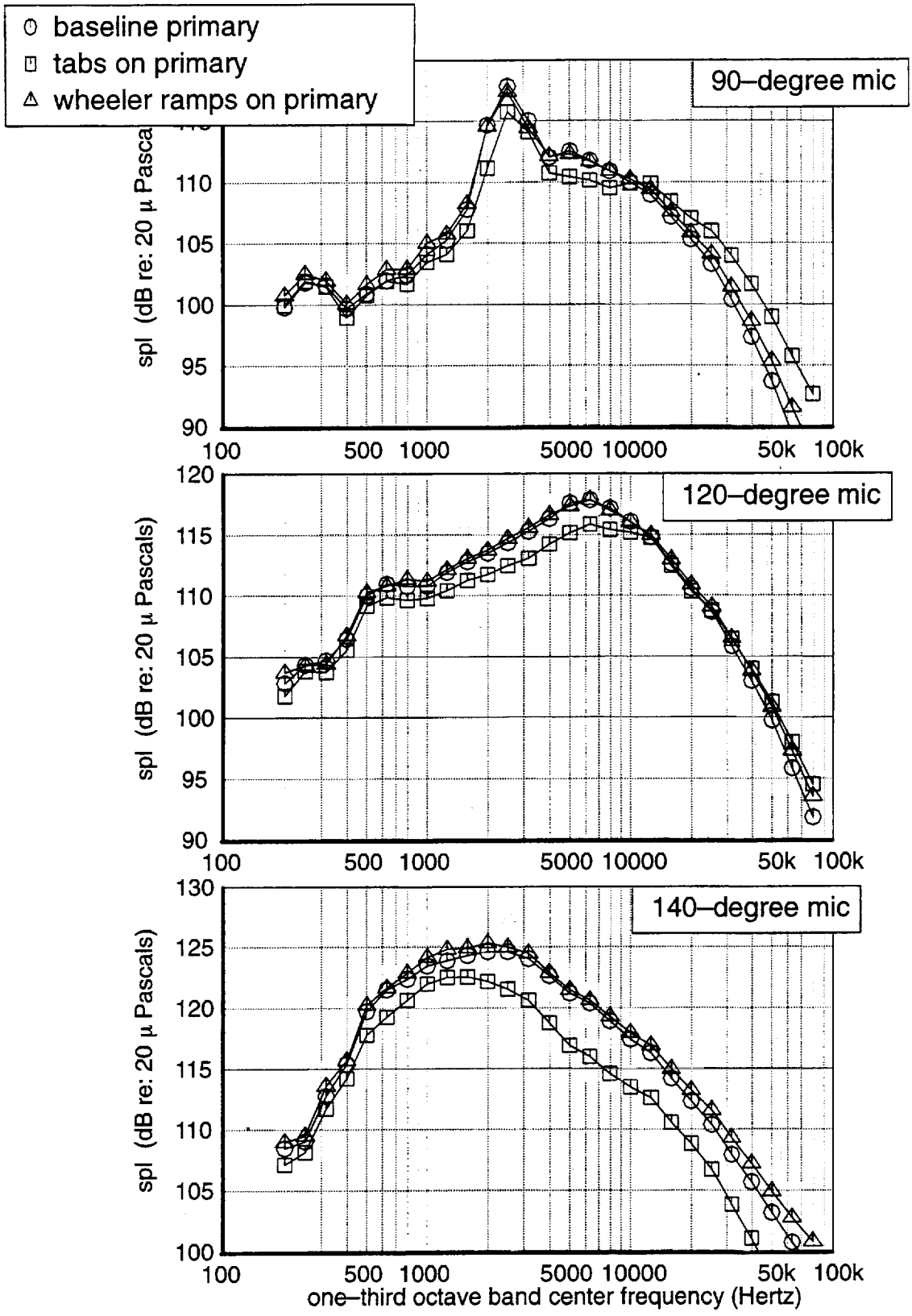

Figure 38. Model–scale Spectra: No Ejector, Various Primaries, NPR 3.5 20–ft sideline mics, tunnel Mach 0.245

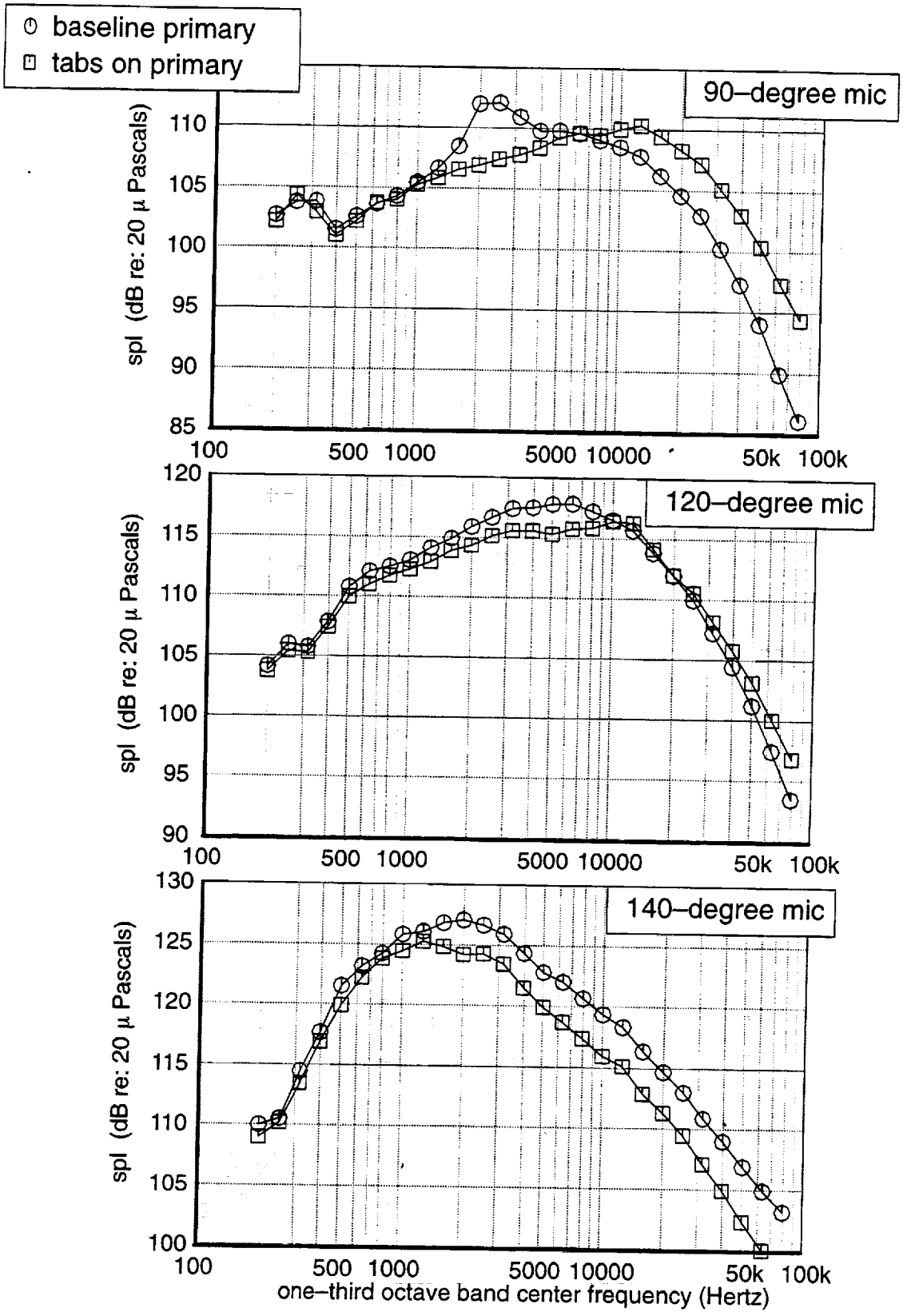

Figure 39. Model–scale Spectra: No Ejector, Various Primaries, NPR 4.0
20–ft sideline mics, tunnel Mach 0.245

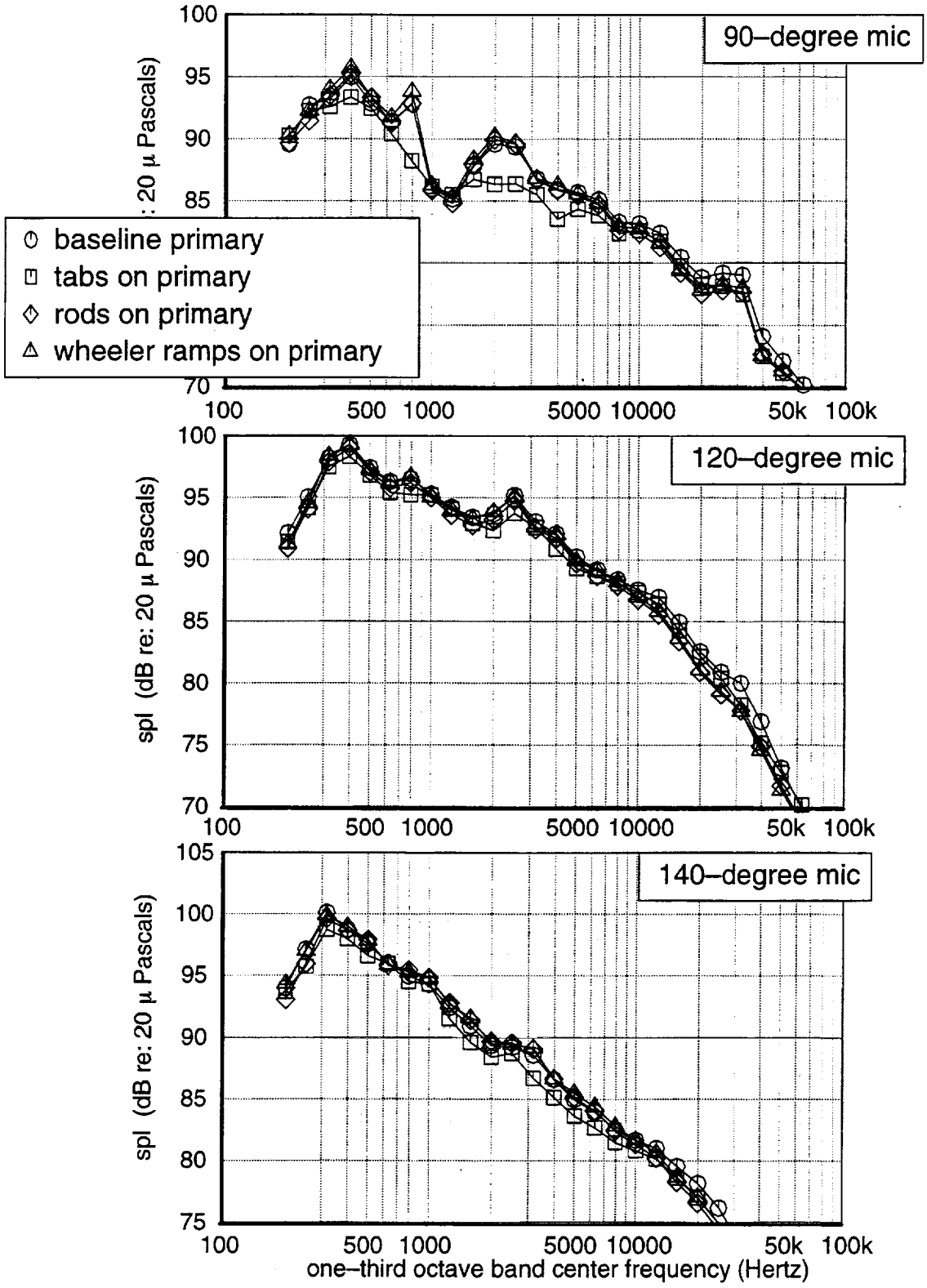

Figure 40. Model–scale Spectra: Baseline Ejector, Various Primaries, NPR 1.5 20–ft sideline mics, tunnel Mach 0.245

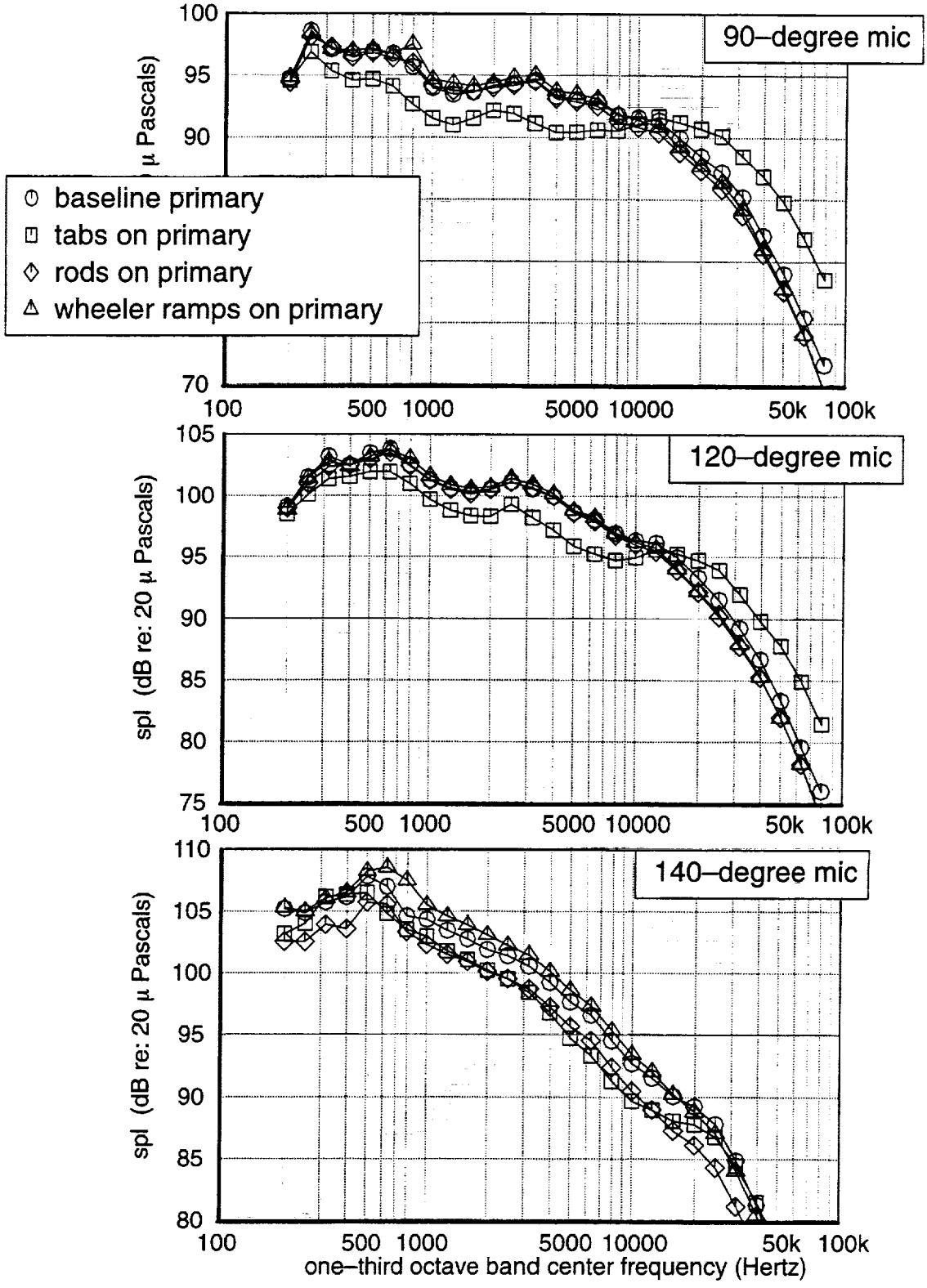

Figure 41. Model–scale Spectra: Baseline Ejector, Various Primaries, NPR 2.0 20–ft sideline mics, tunnel Mach 0.245

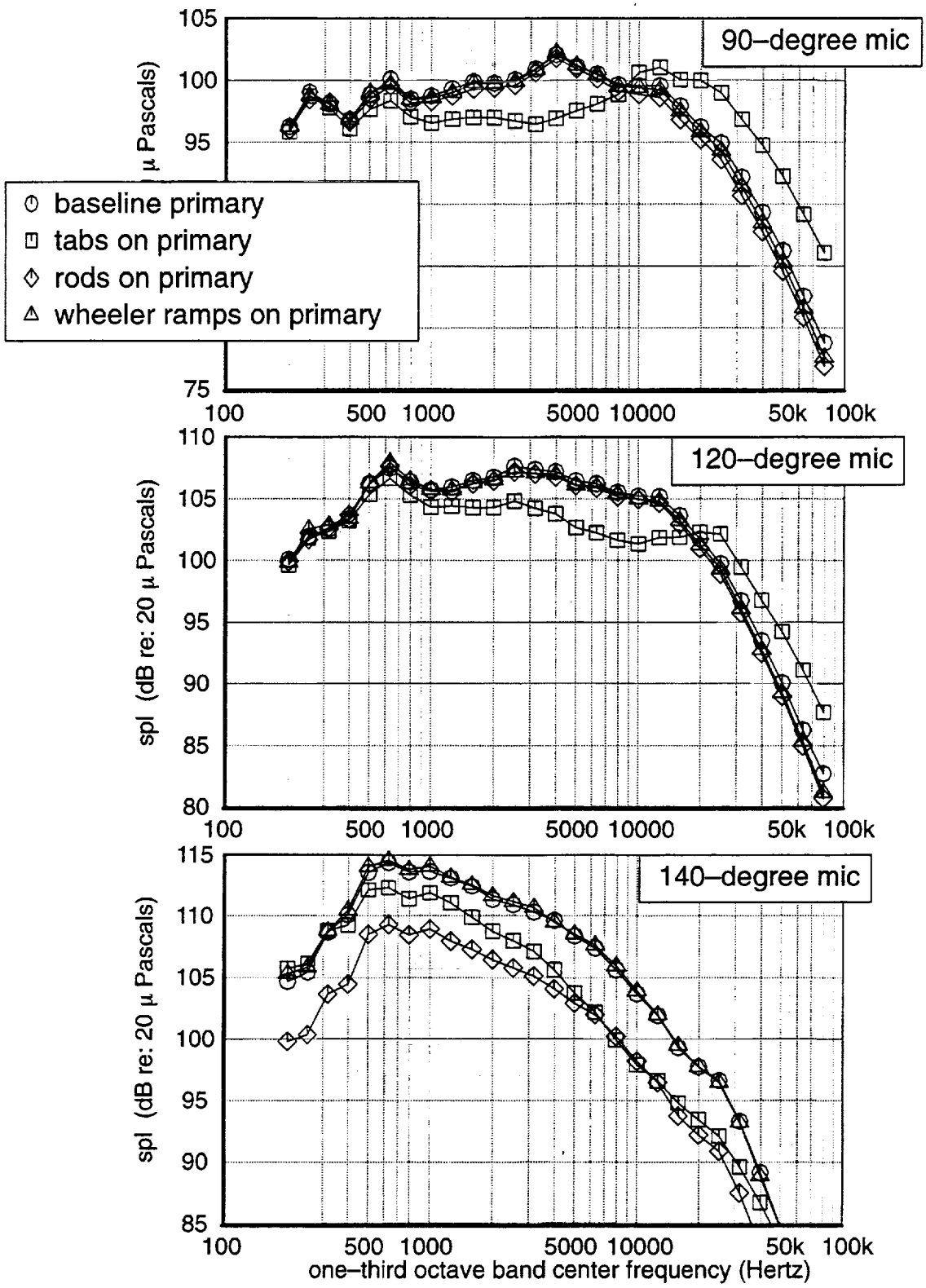

Figure 42. Model–scale Spectra: Baseline Ejector, Various Primaries, NPR 2.5 20–ft sideline mics, tunnel Mach 0.245

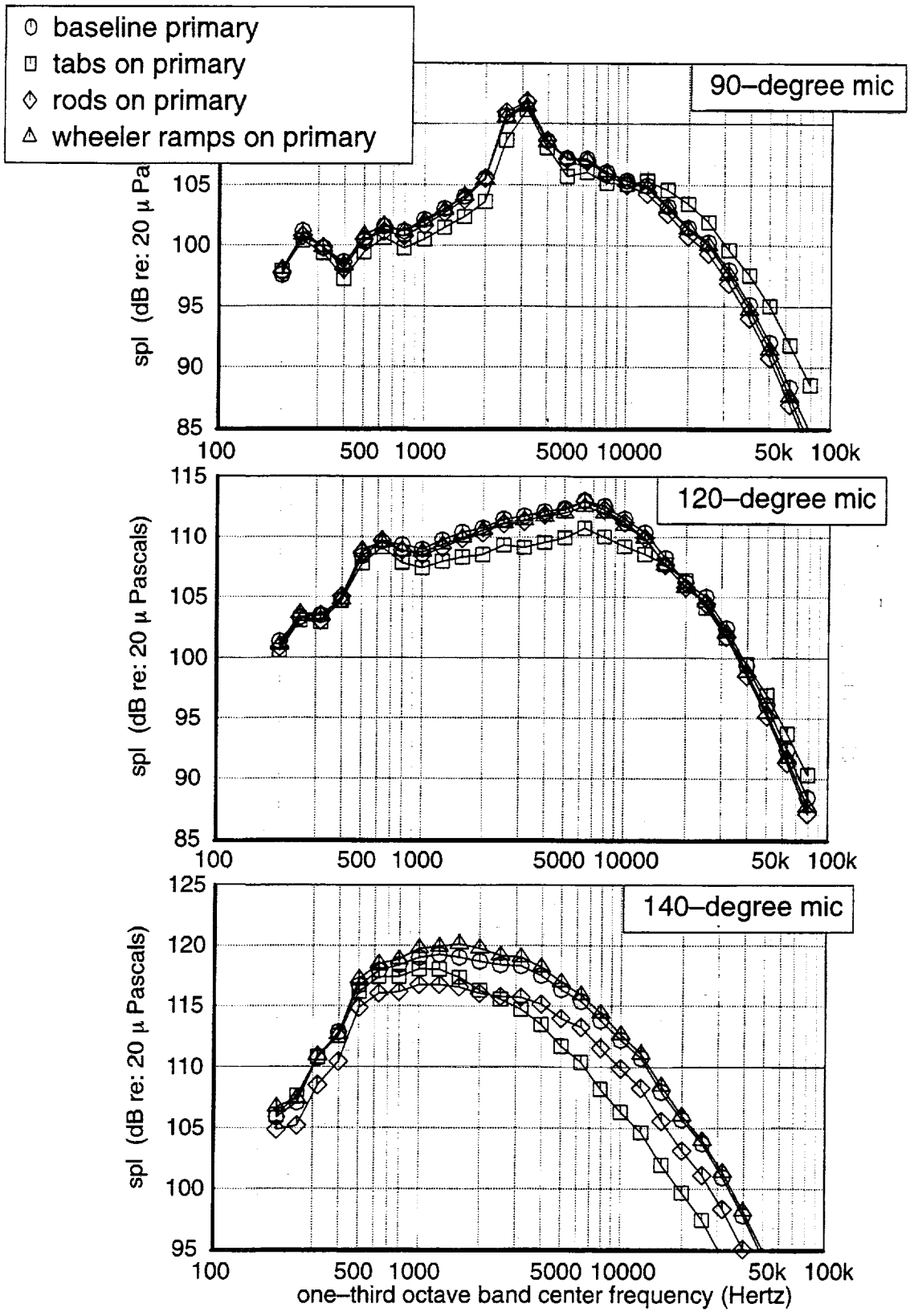

Figure 43. Model–scale Spectra: Baseline Ejector, Various Primaries, NPR 3.0
20–ft sideline mics, tunnel Mach 0.245

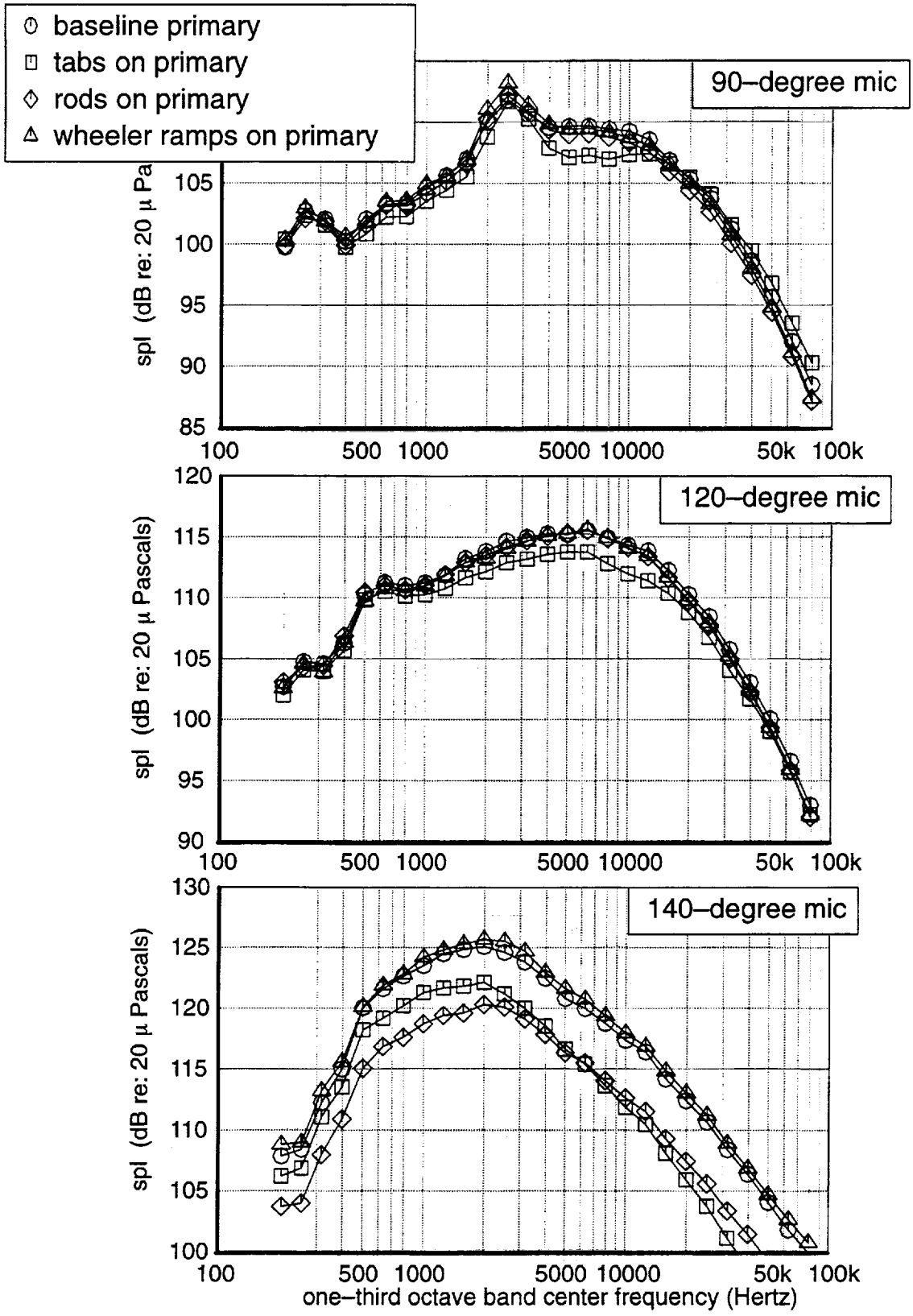

Figure 44. Model–scale Spectra: Baseline Ejector, Various Primaries, NPR 3.5 20–ft sideline mics, tunnel Mach 0.245

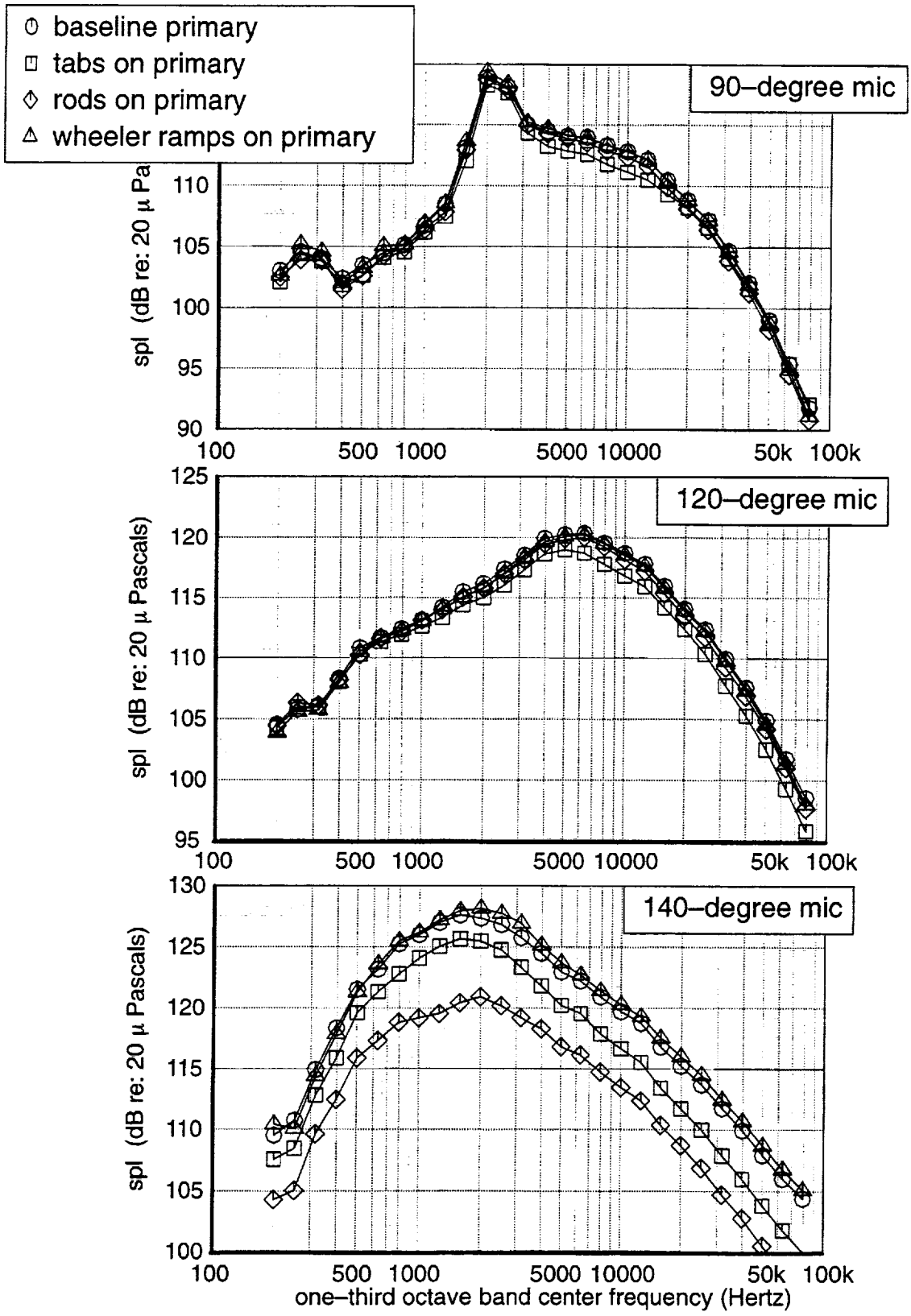

Figure 45. Model–scale Spectra: Baseline Ejector, Various Primaries, NPR 4.0 20–ft sideline mics, tunnel Mach 0.245

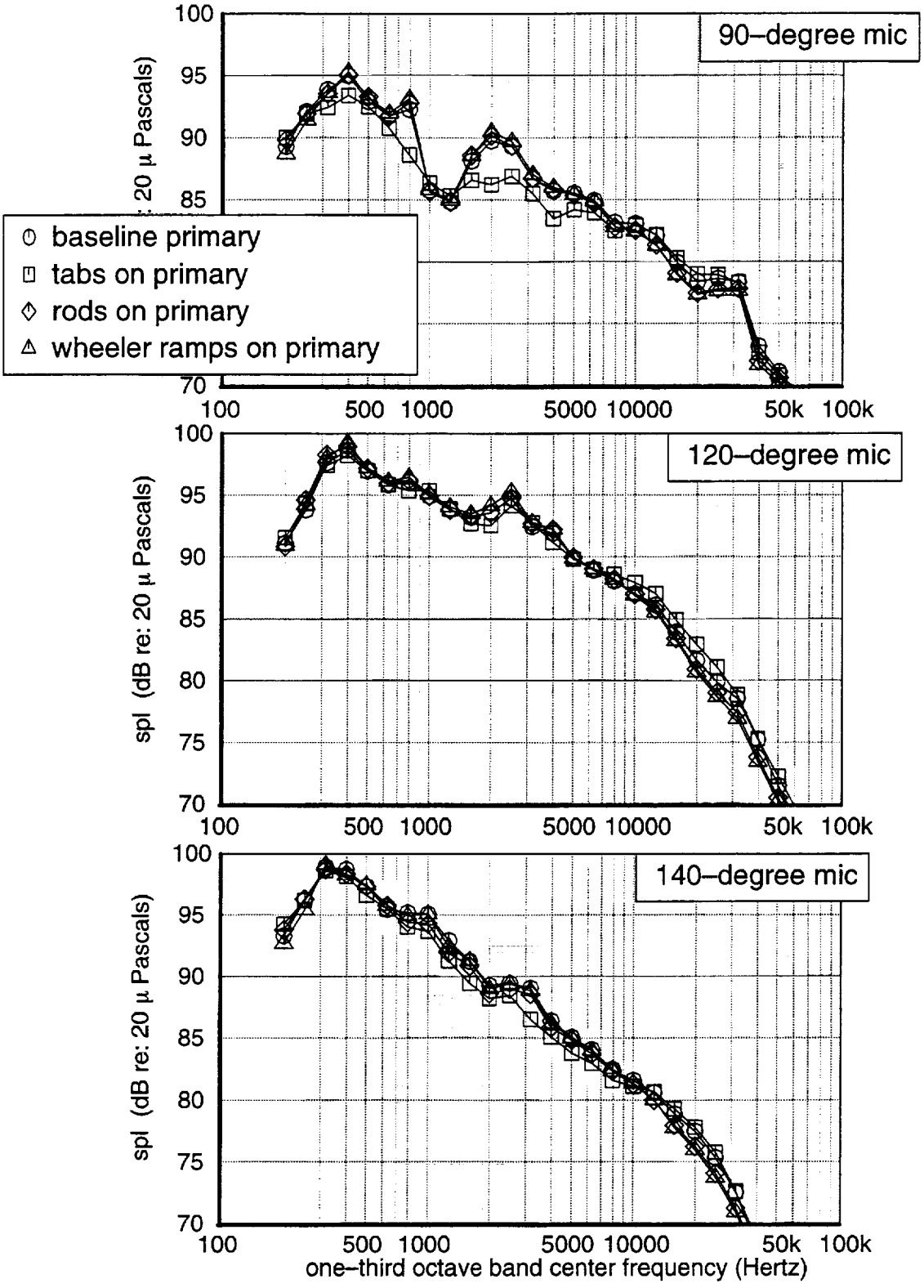

Figure 46. Model–scale Spectra: Tabs on Ejector, Various Primaries, NPR 1.5 20–ft sideline mics, tunnel Mach 0.245

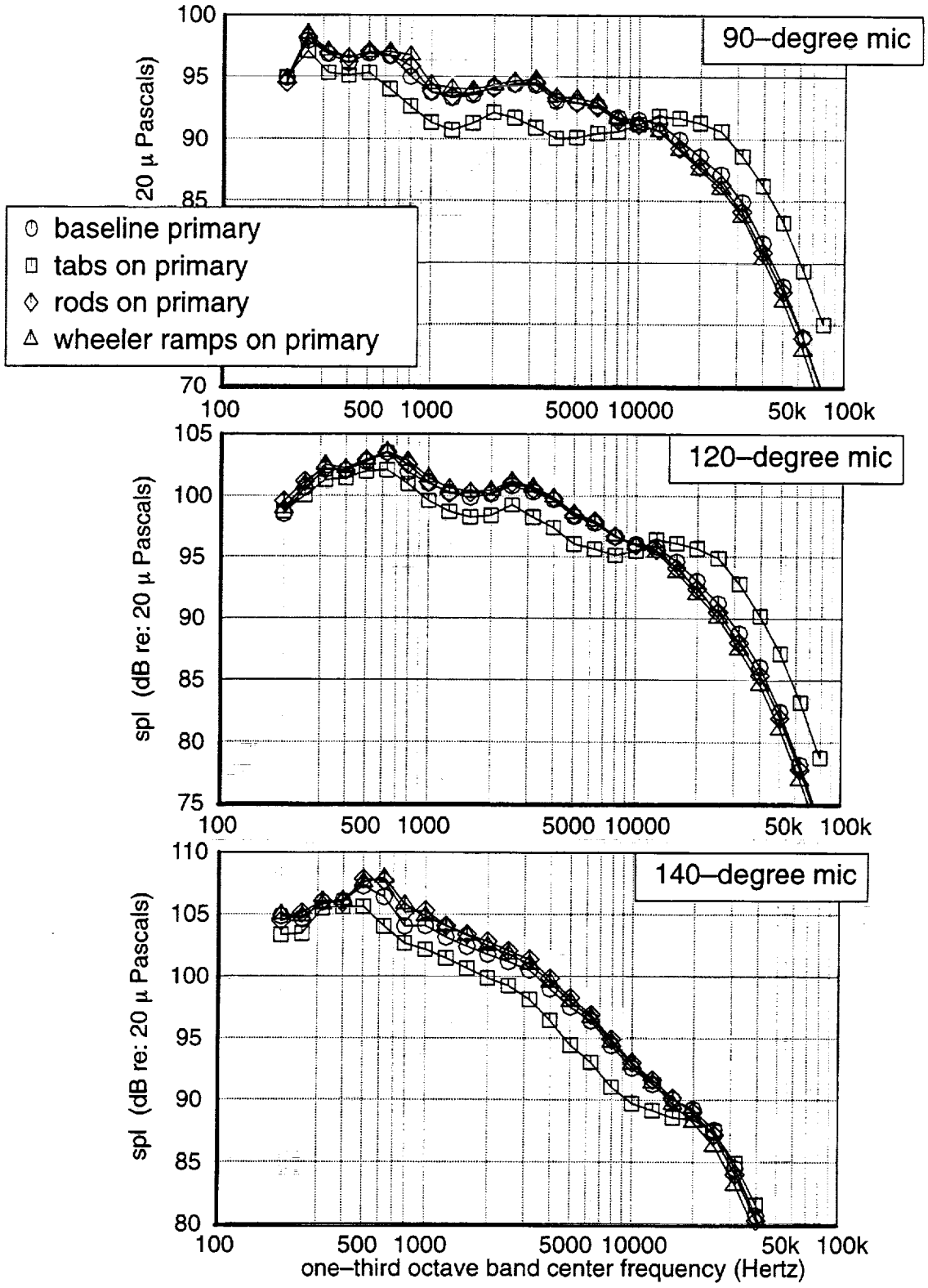

Figure 47. Model–scale Spectra: Tabs on Ejector, Various Primaries, NPR 2.0 20–ft sideline mics, tunnel Mach 0.245

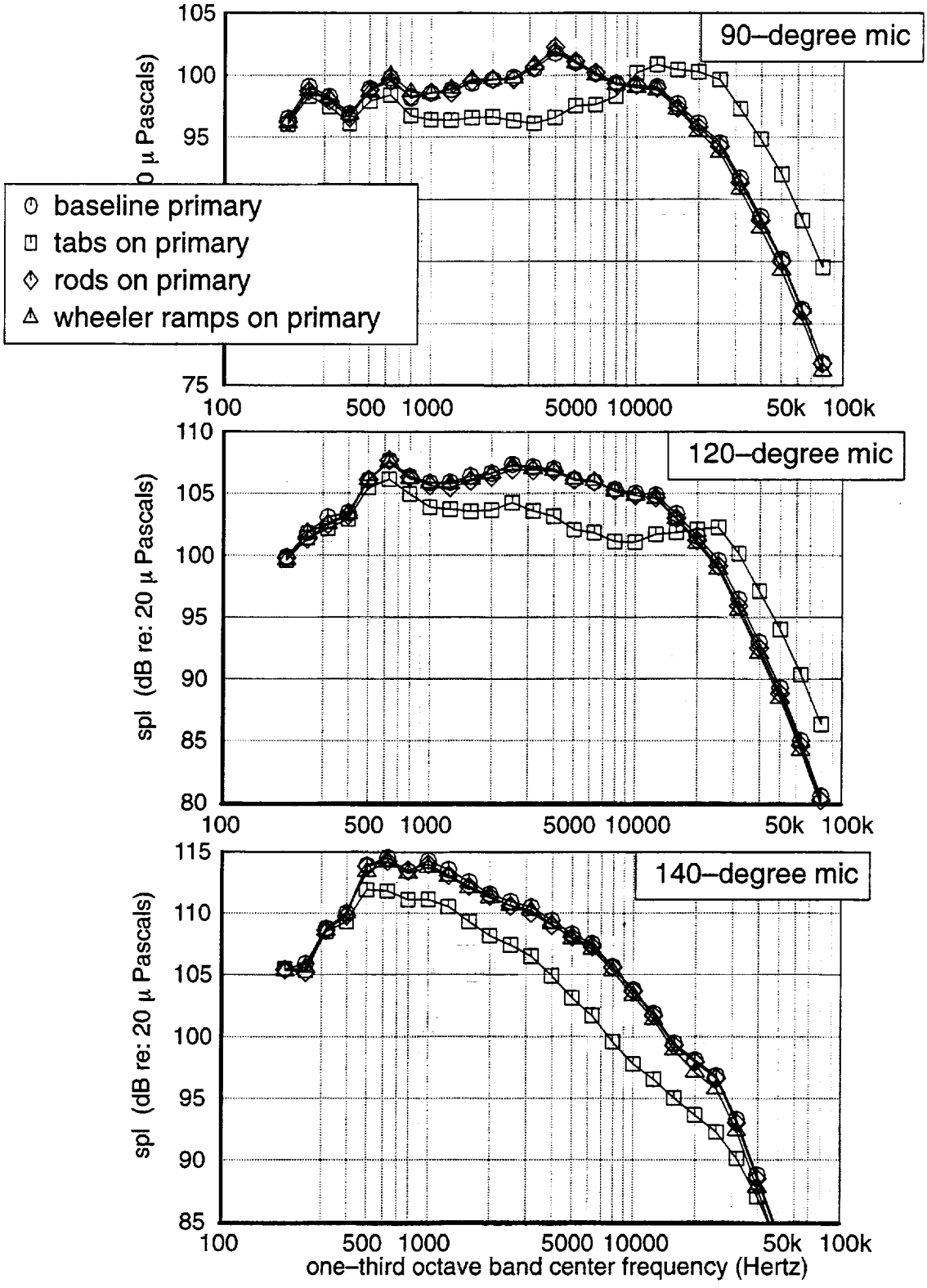

Figure 48. Model–scale Spectra: Tabs on Ejector, Various Primaries, NPR 2.5 20–ft sideline mics, tunnel Mach 0.245

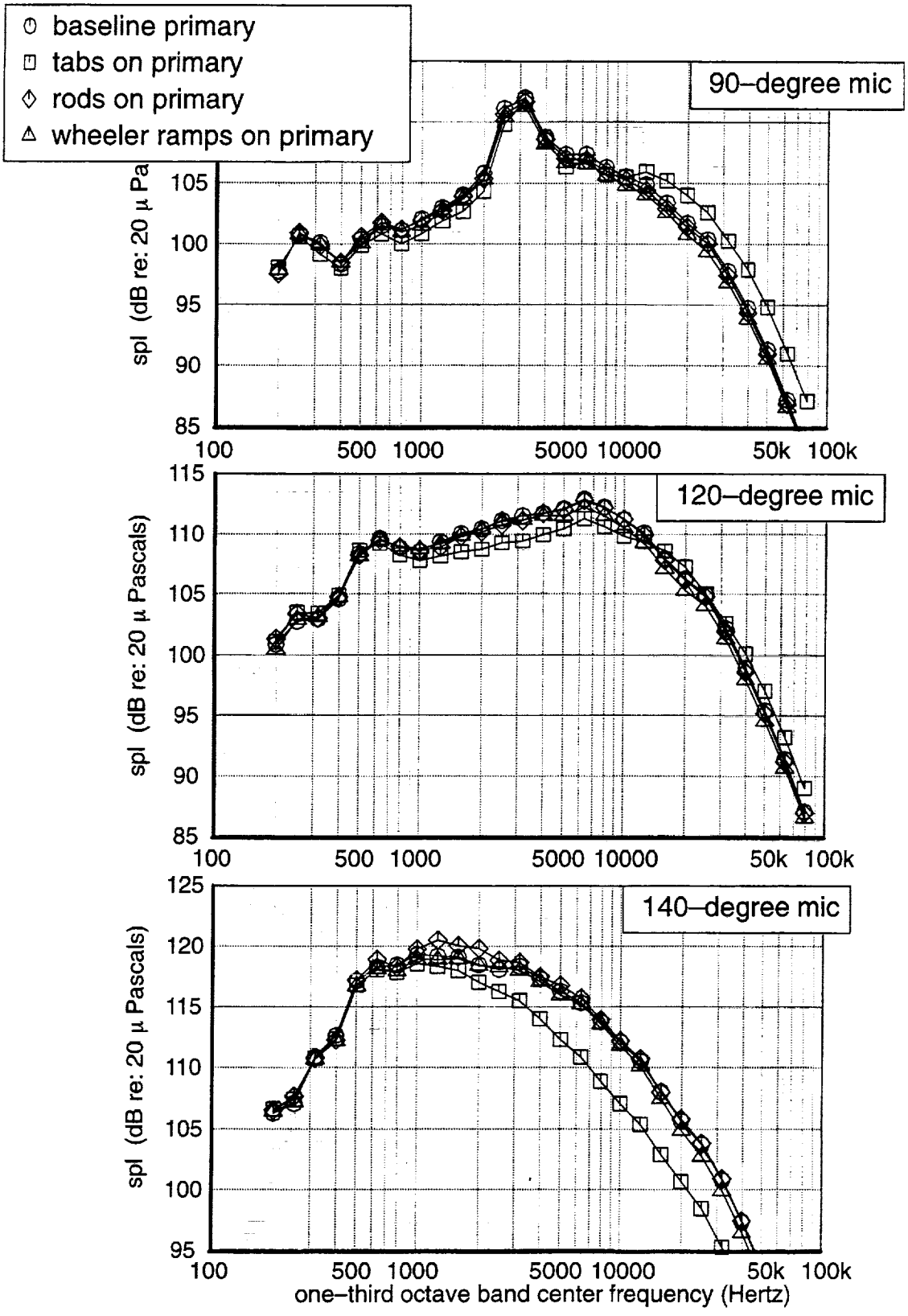

Figure 49. Model–scale Spectra: Tabs on Ejector, Various Primaries, NPR 3.0 20–ft sideline mics, tunnel Mach 0.245

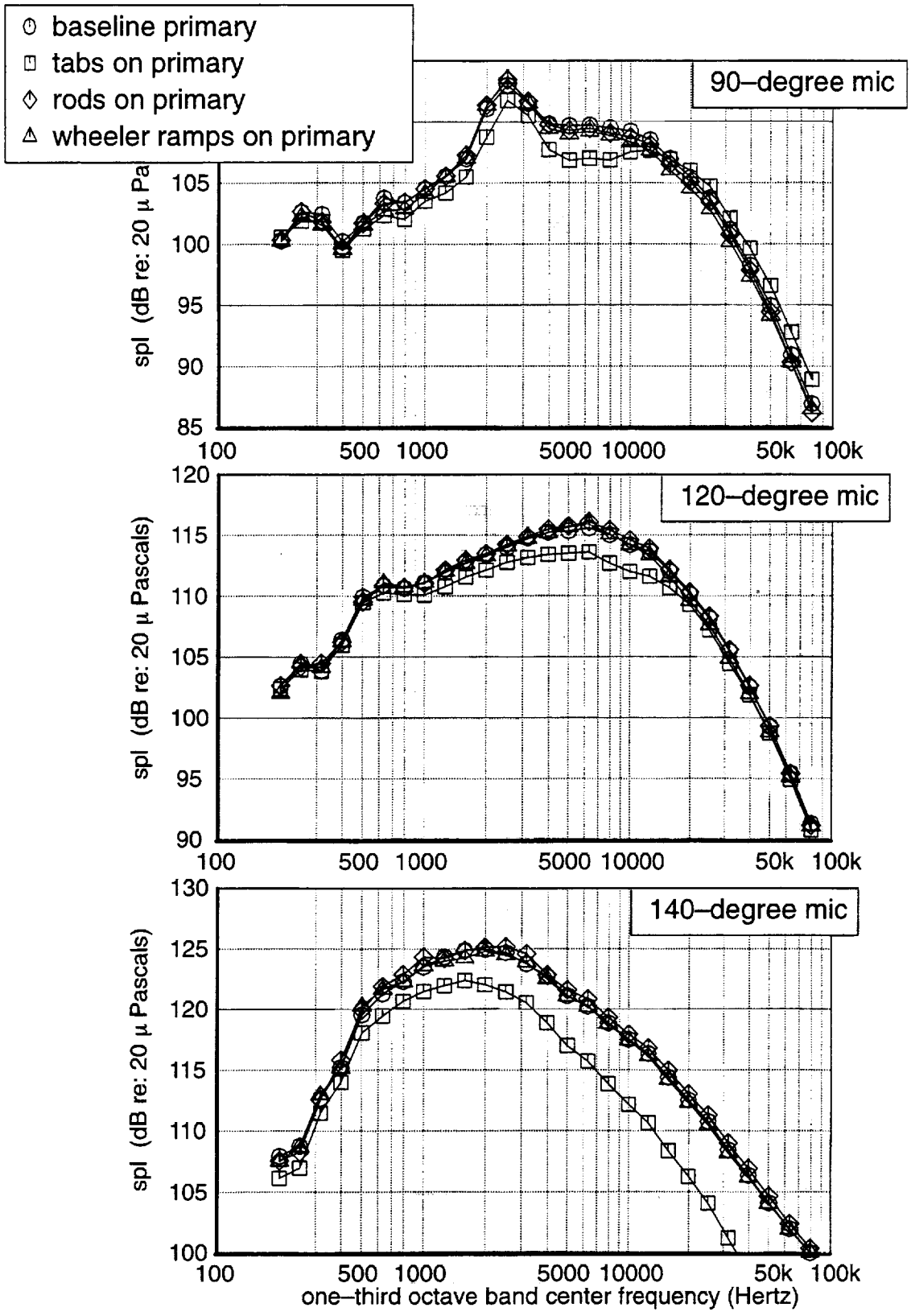

Figure 50. Model–scale Spectra: Tabs on Ejector, Various Primaries, NPR 3.5 20–ft sideline mics, tunnel Mach 0.245

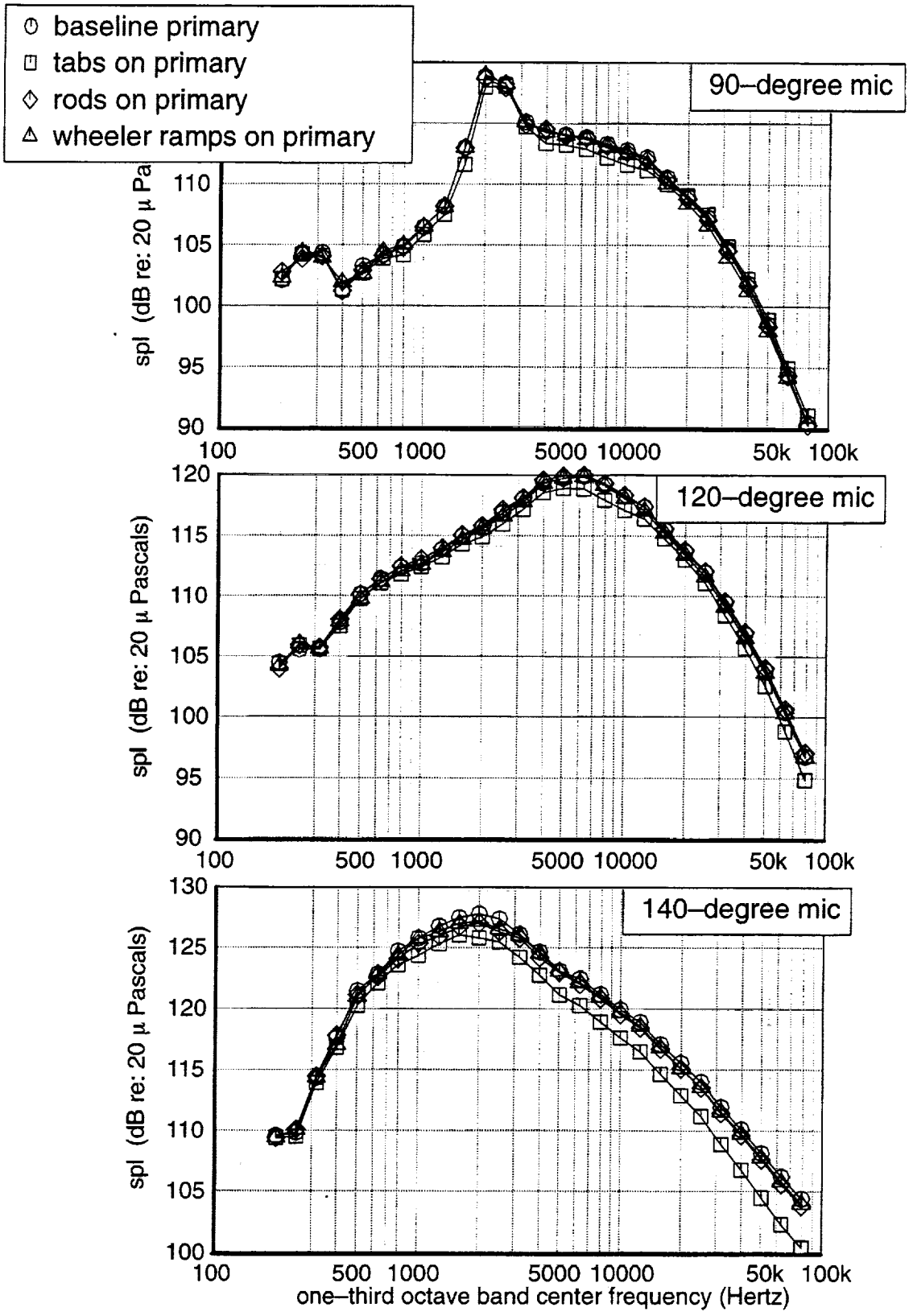

Figure 51. Model–scale Spectra: Tabs on Ejector, Various Primaries, NPR 4.0 20–ft sideline mics, tunnel Mach 0.245

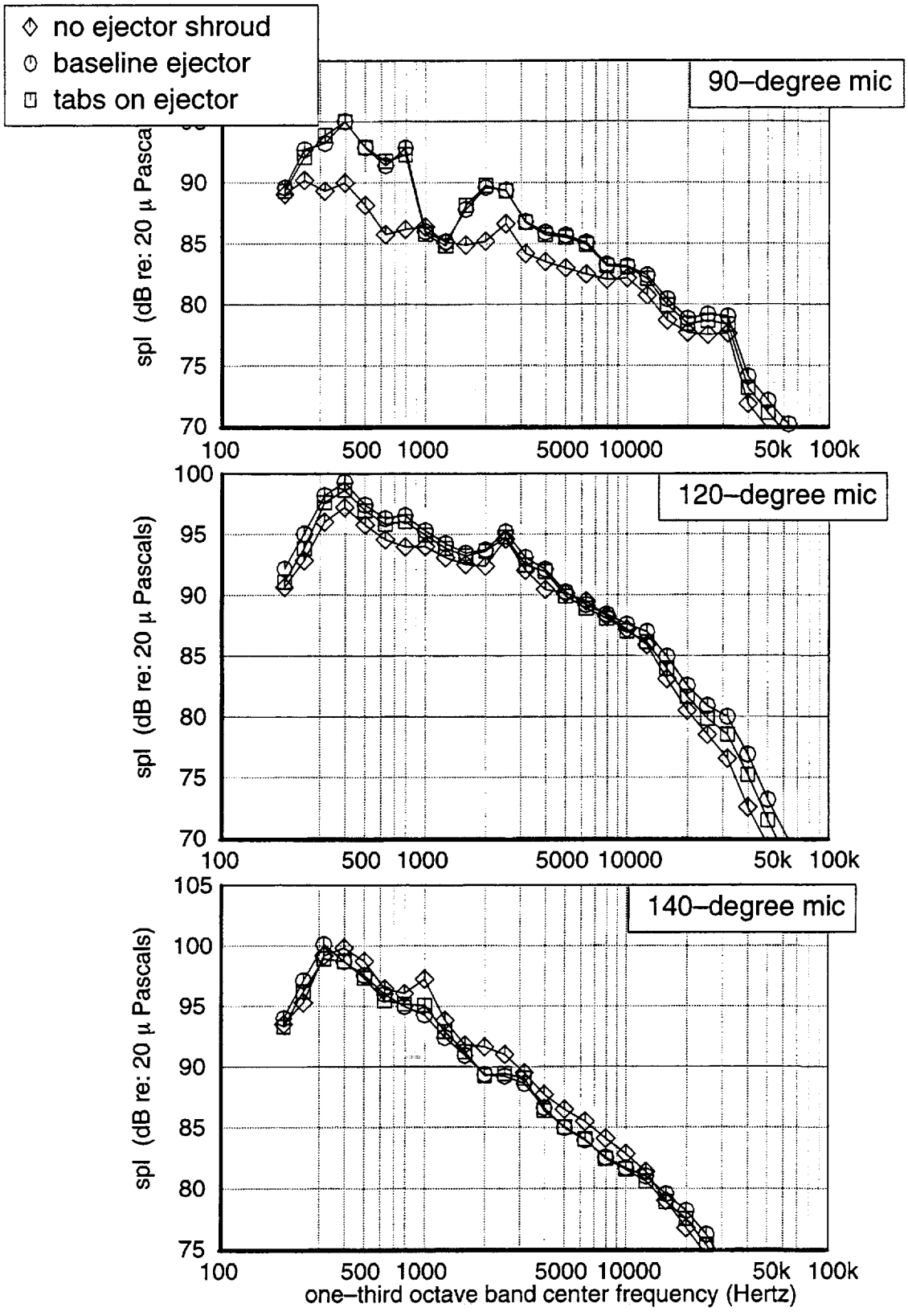

Figure 52. Model–scale Spectra: Baseline Primary, Various Ejectors, NPR 1.5 20–ft sideline mics, tunnel mach 0.245

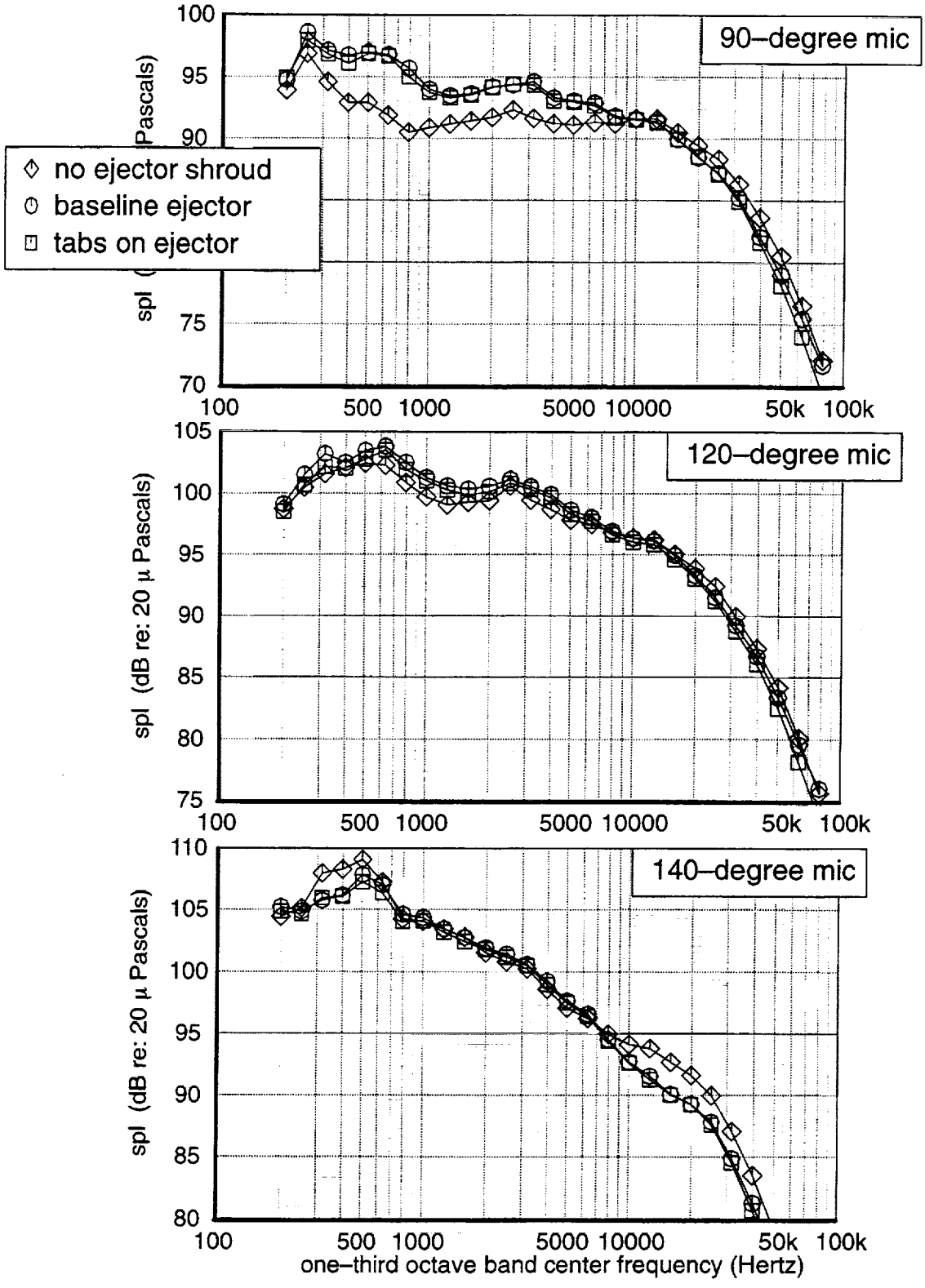

Figure 53. Model–scale Spectra: Baseline Primary, Various Ejectors, NPR 2.0 20–ft sideline mics, tunnel Mach 0.245

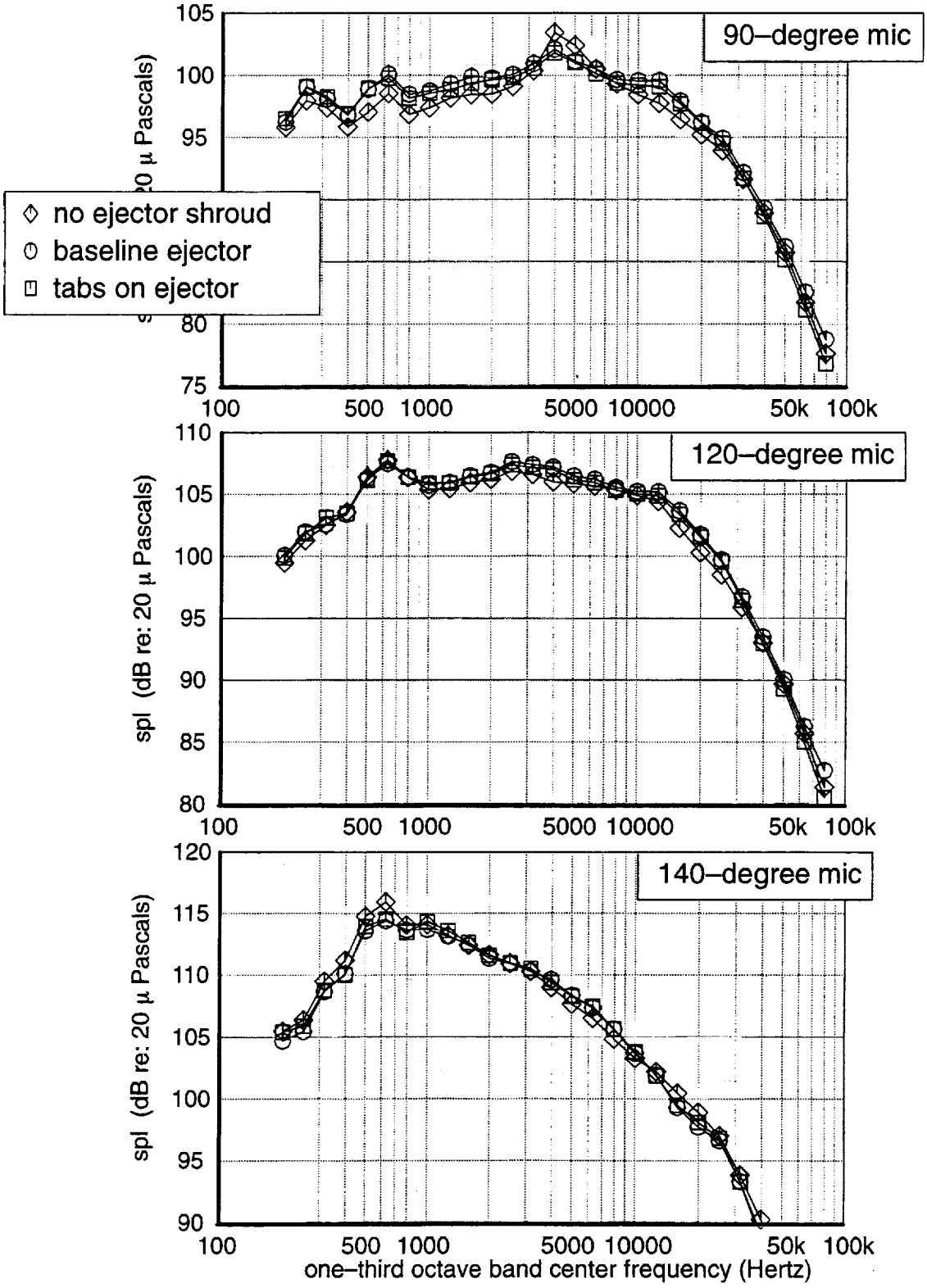

Figure 54. Model–scale Spectra: Baseline Primary, Various Ejectors, NPR 2.5 20–ft sideline mics, tunnel Mach 0.245

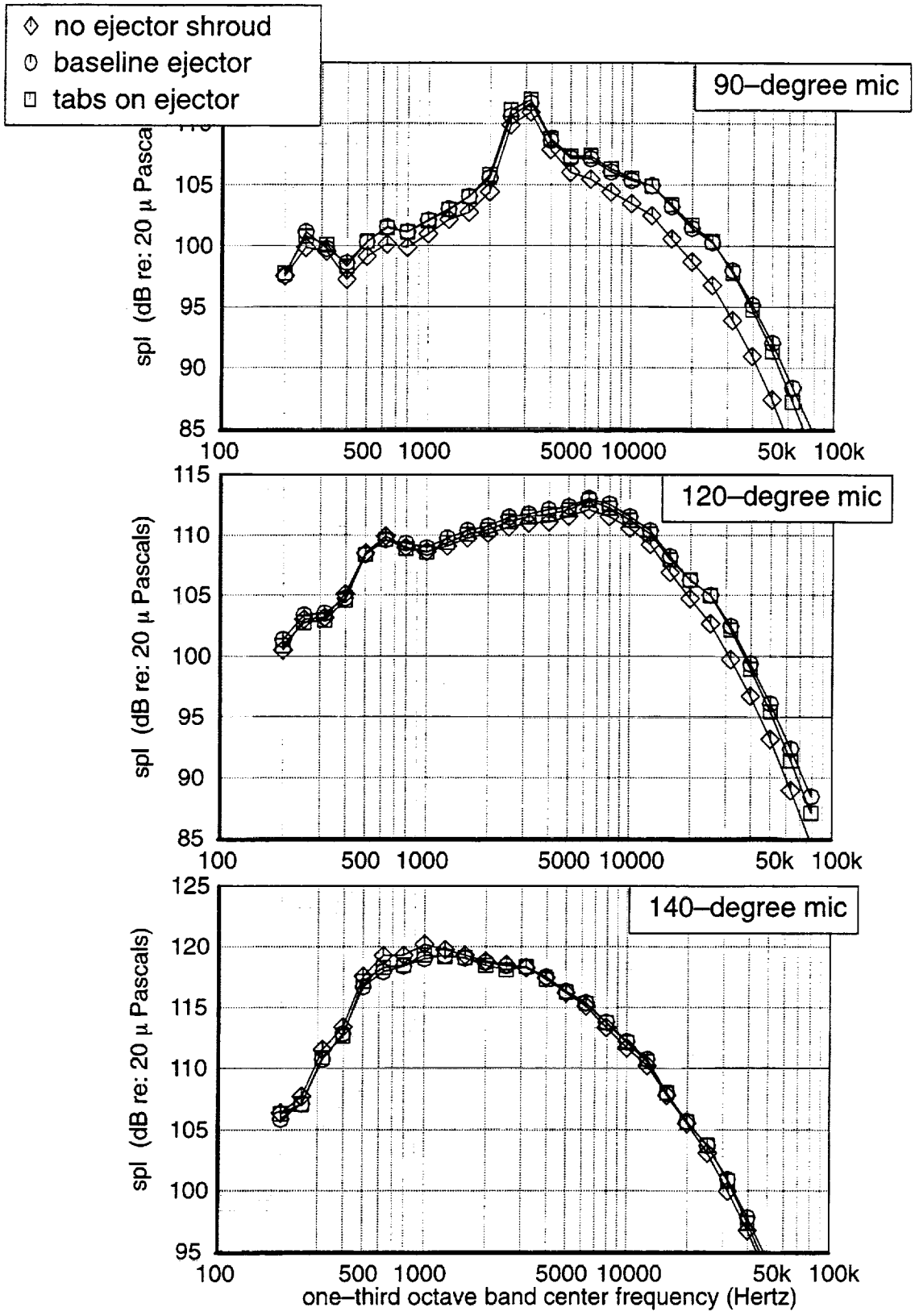

Figure 55. Model–scale Spectra: Baseline Primary, Various Ejectors, NPR 3.0 20–ft sideline mics, tunnel Mach 0.245

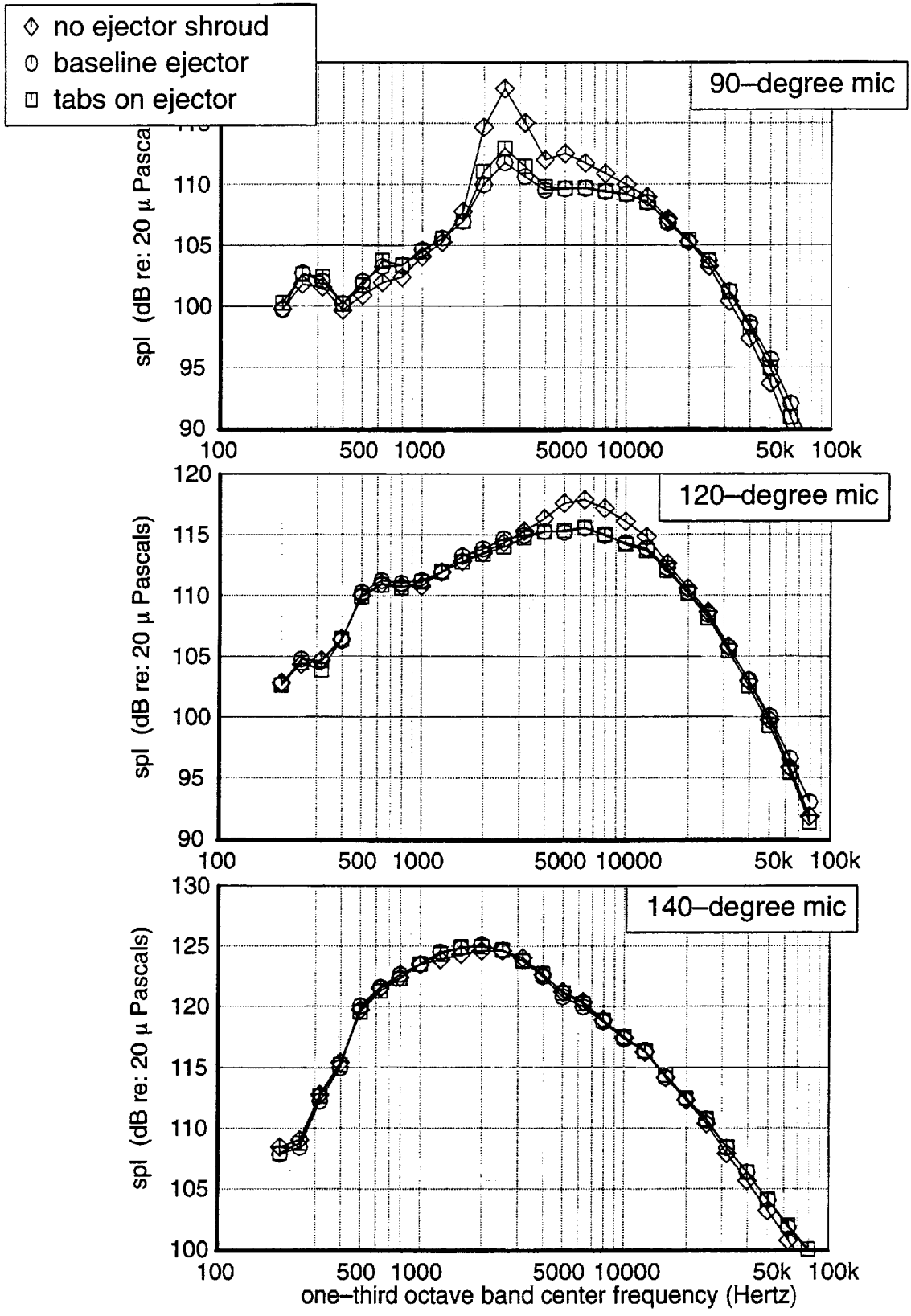

Figure 56. Model–scale Spectra: Baseline Primary, Various Ejectors, NPR 3.5 20–ft sideline mics, tunnel Mach 0.245

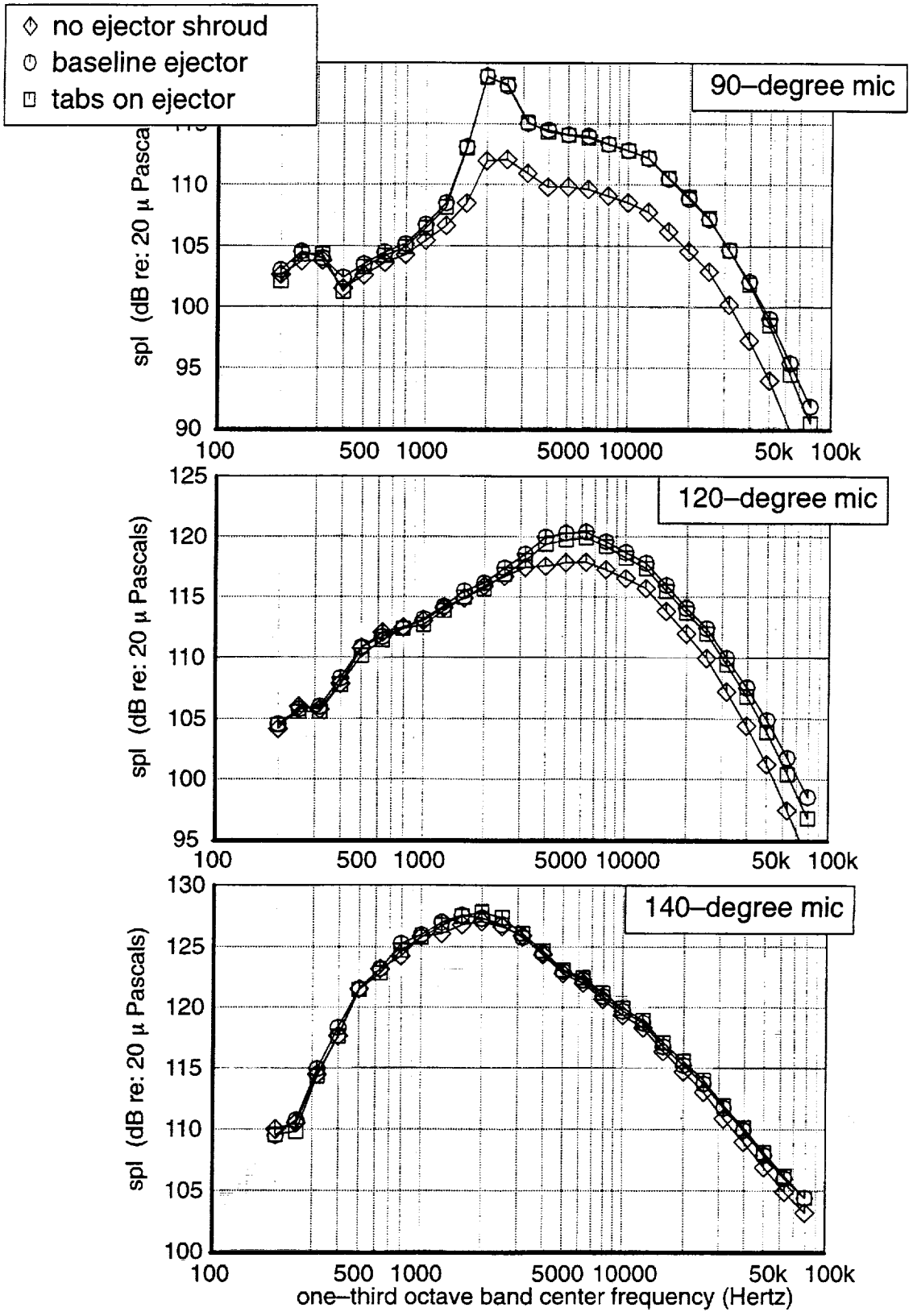

Figure 57. Model–scale Spectra: Baseline Primary, Various Ejectors, NPR 4.0 20–ft sideline mics, tunnel Mach 0.245

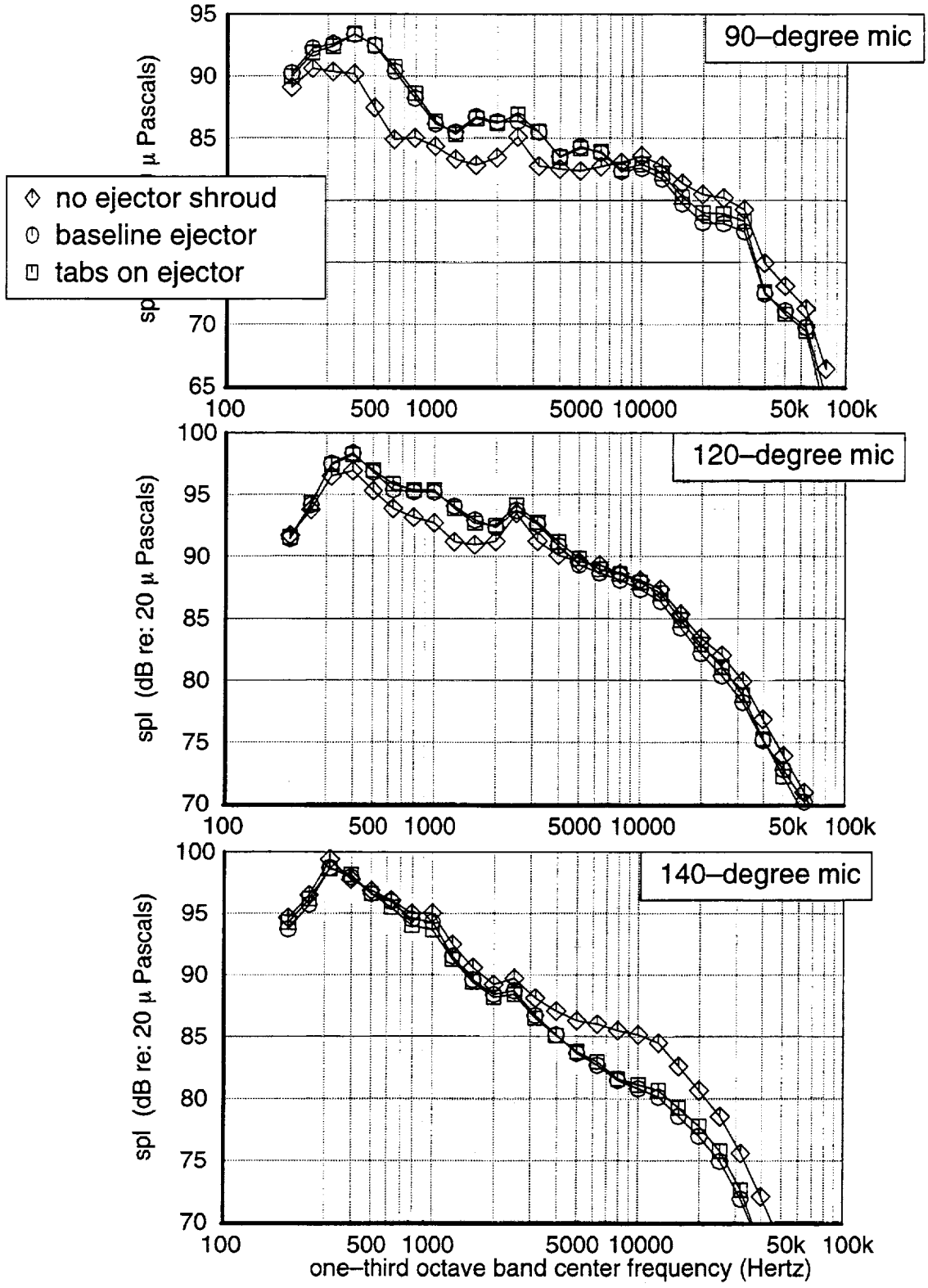

Figure 58. Model–scale Spectra: Tabs on Primary, Various Ejectors, NPR 1.5 20–ft sideline mics, tunnel Mach 0.245

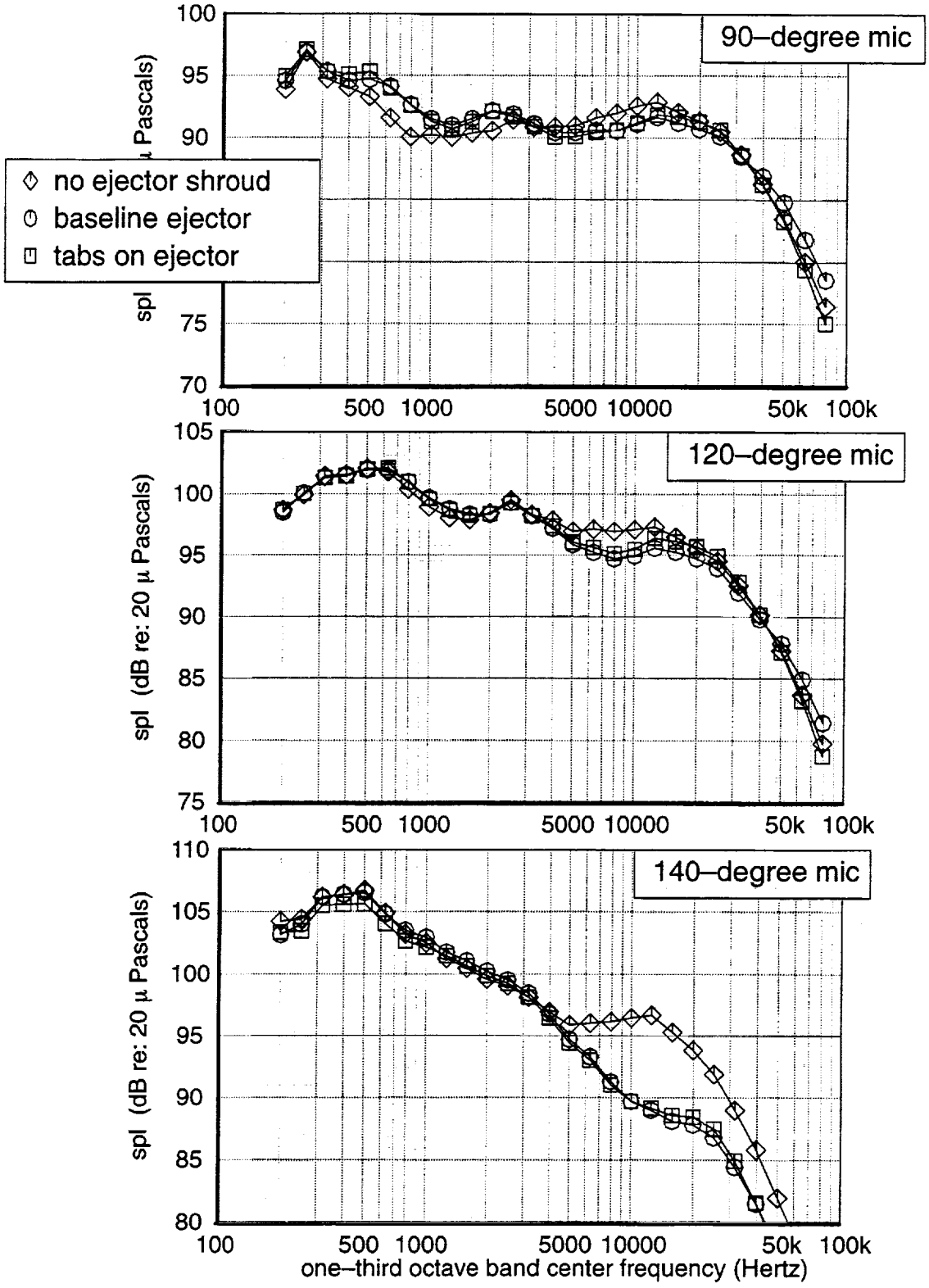

Figure 59. Model–scale Spectra: Tabs on Primary, Various Ejectors, NPR 2.0 20–ft sideline mics, tunnel Mach 0.245

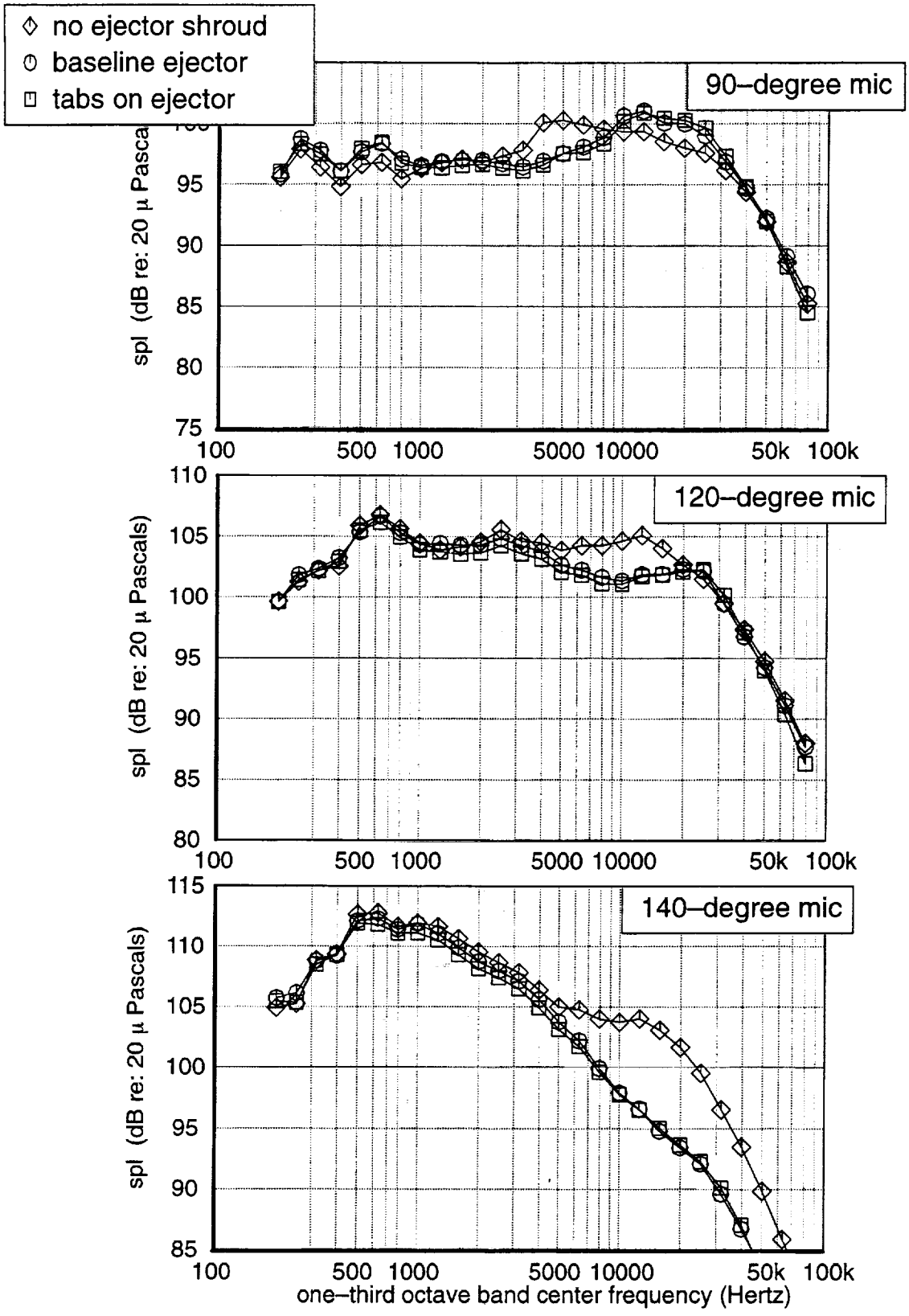

Figure 60. Model–scale Spectra: Tabs on Primary, Various Ejectors, NPR 2.5 20–ft sideline mics, tunnel Mach 0.245

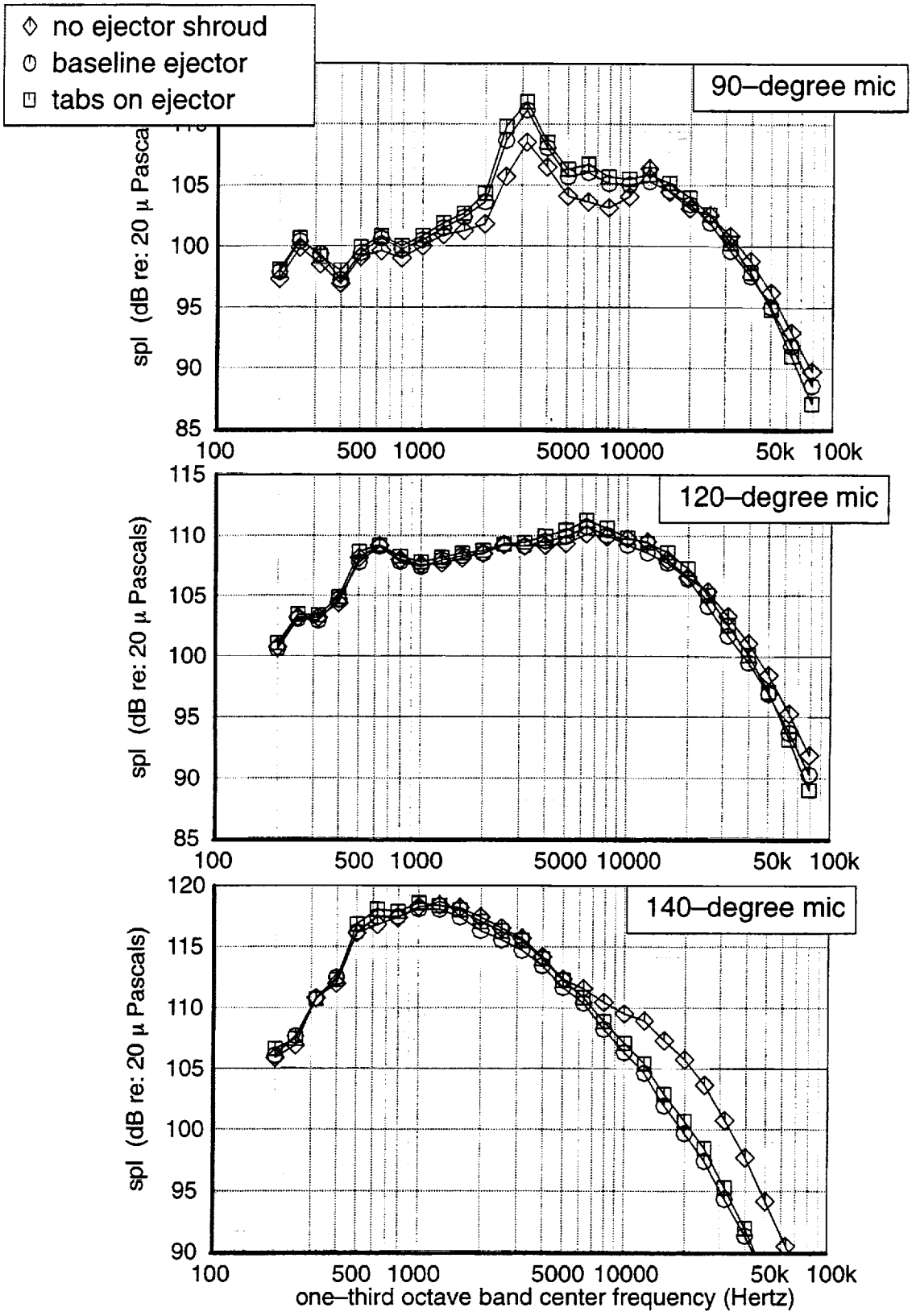

Figure 61. Model–scale Spectra: Tabs on Primary, Various Ejectors, NPR 3.0 20–ft sideline mics, tunnel Mach 0.245

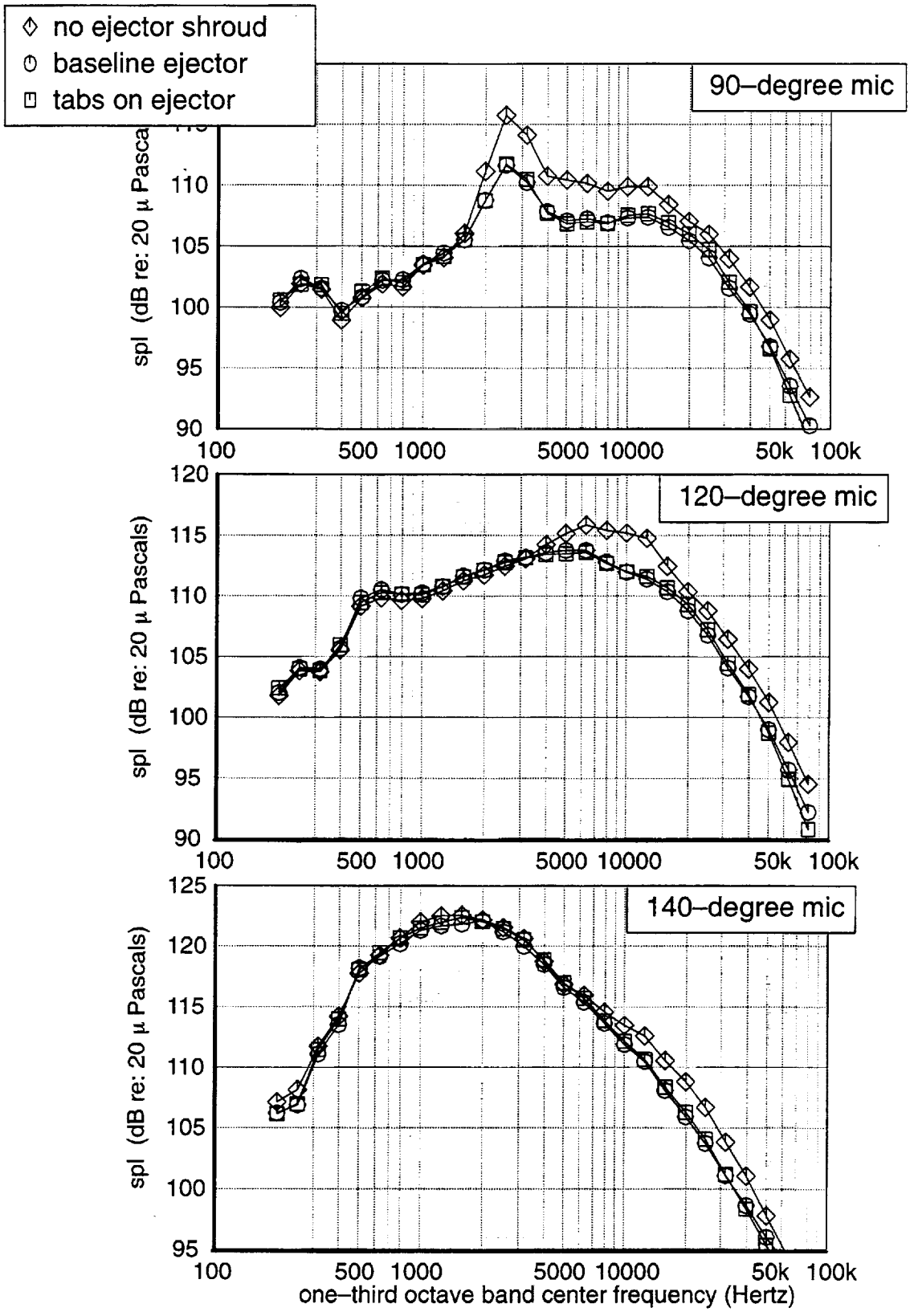

Figure 62. Model–scale Spectra: Tabs on Primary, Various Ejectors, NPR 3.5 20–ft sideline mics, tunnel Mach 0.245

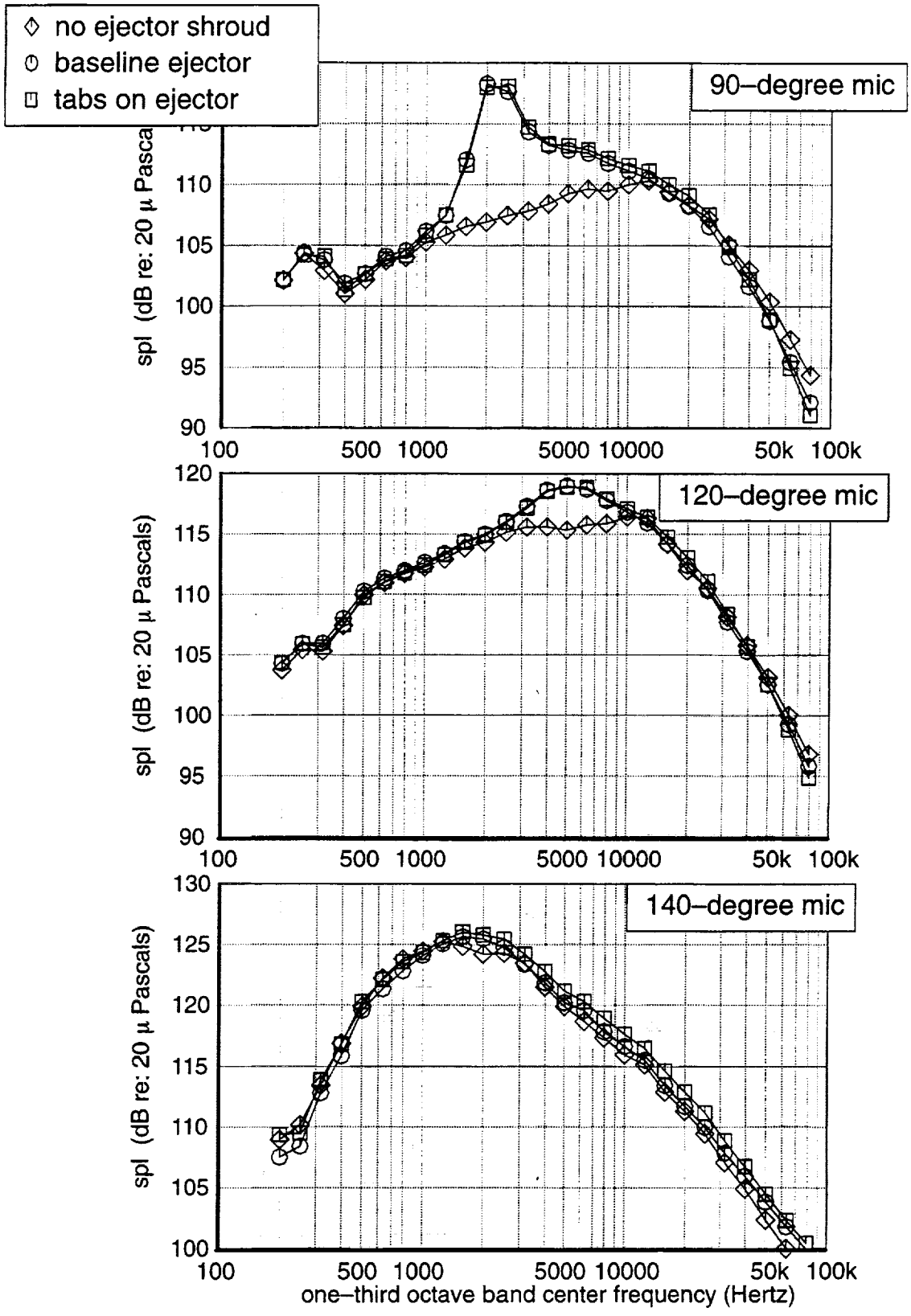

Figure 63. Model–scale Spectra: Tabs on Primary, Various Ejectors, NPR 4.0 20–ft sideline mics, tunnel Mach 0.245

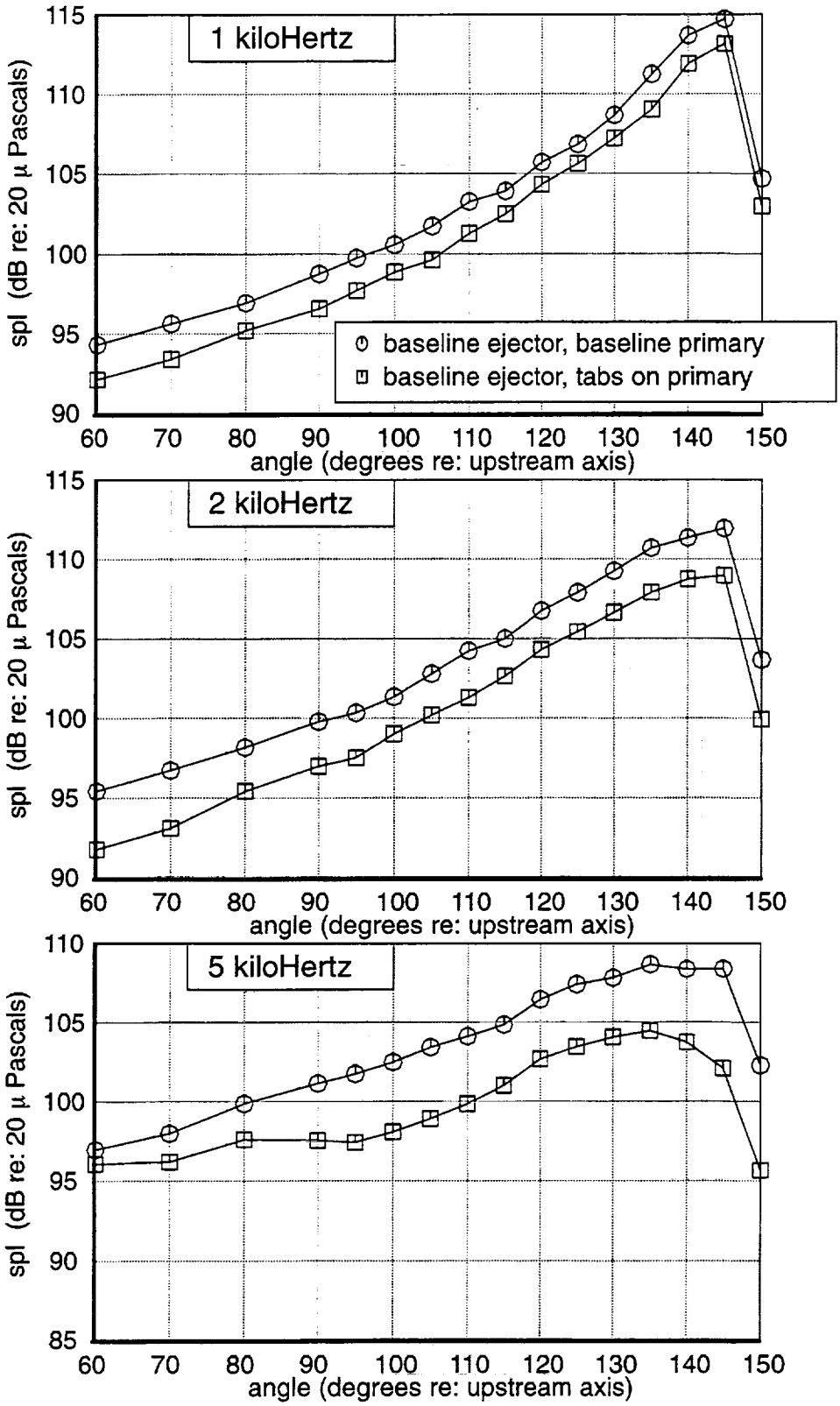

Figure 64. Effect of Tabs on Directivity; Mid Frequencies

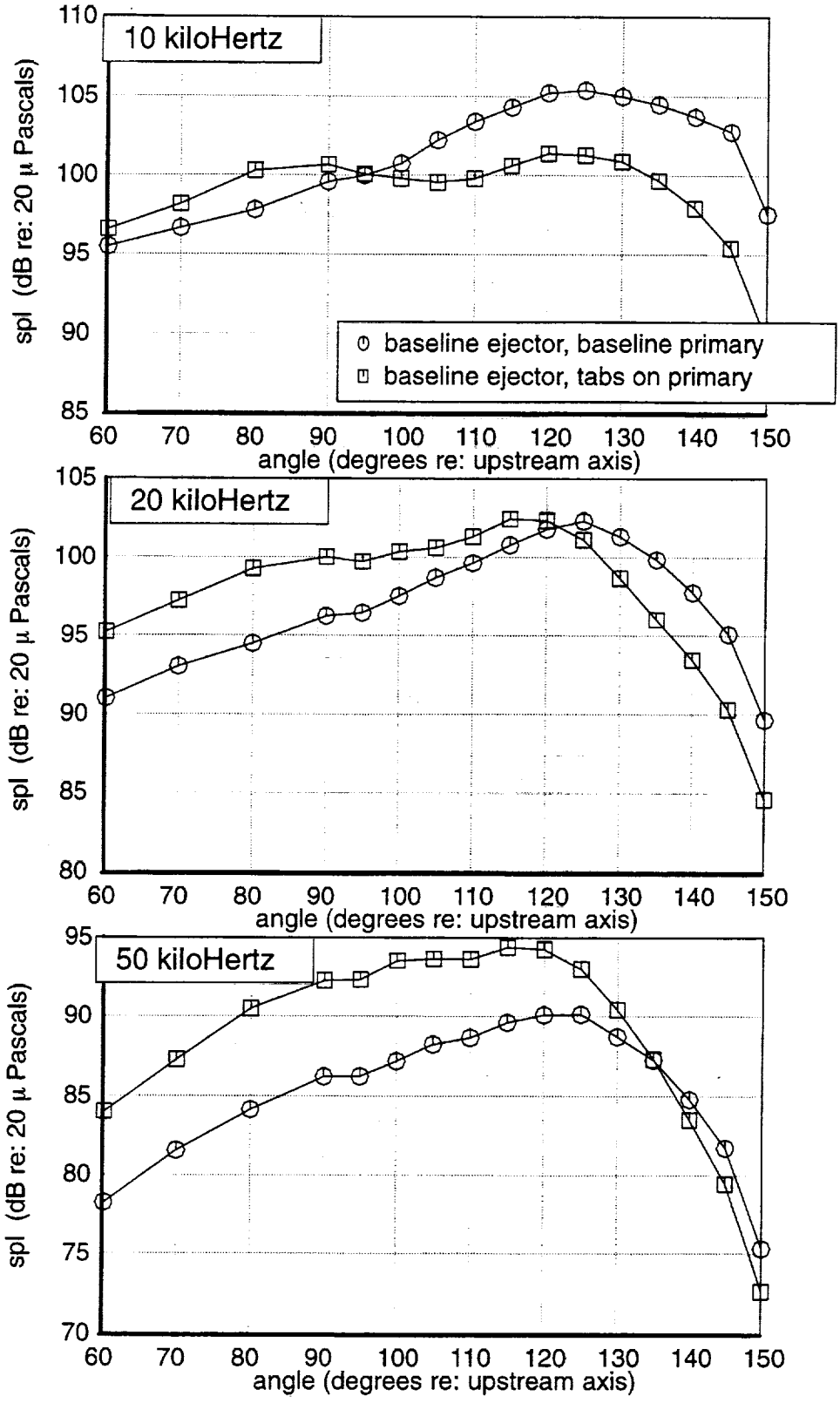

Figure 65. Effect of Tabs on Directivity; High Frequencies

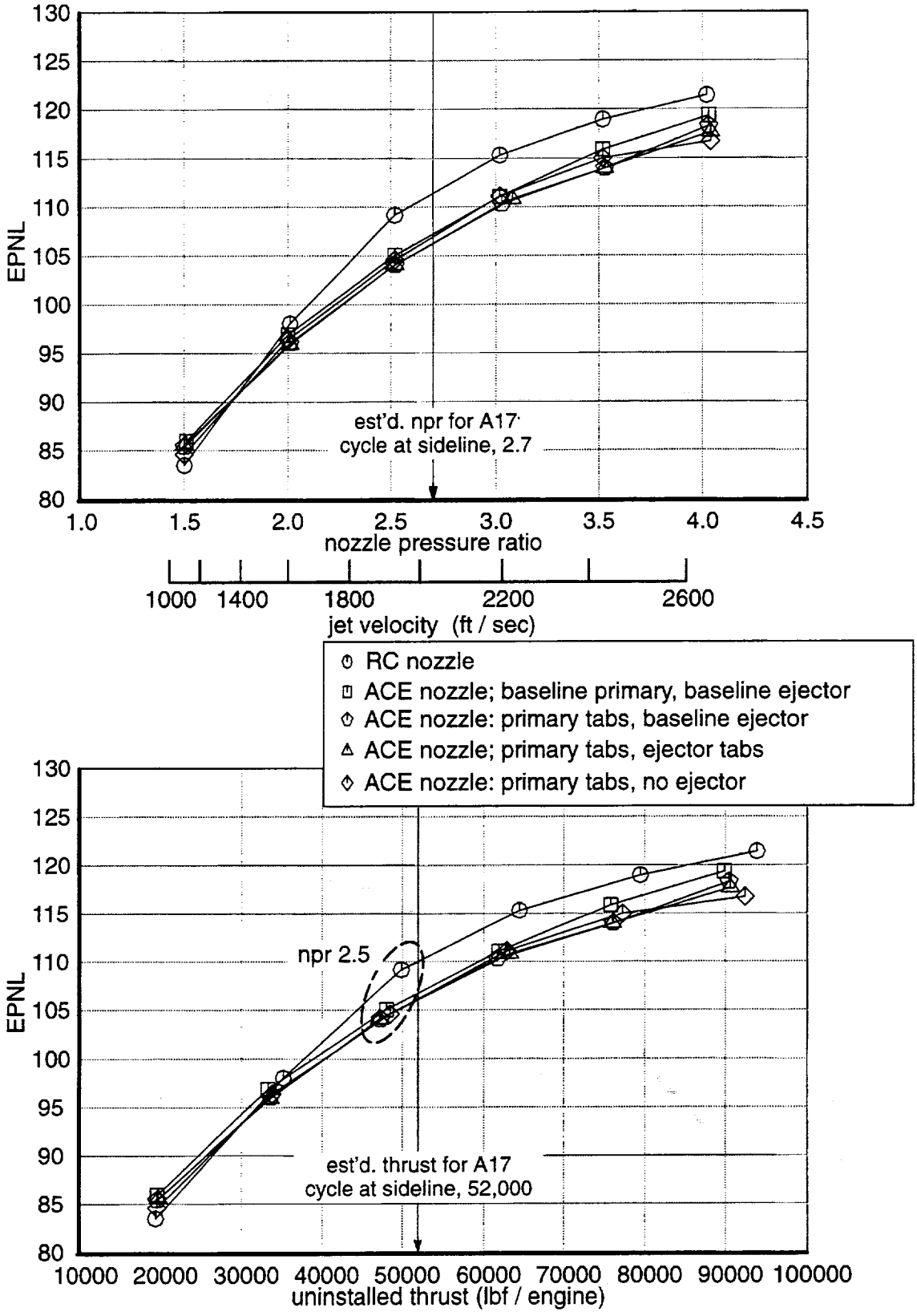

Figure 66. EPNLs for RC Nozzle and Selected ACE Nozzle Configurations at Sideline tunnel Mach 0.245, 20–ft mics

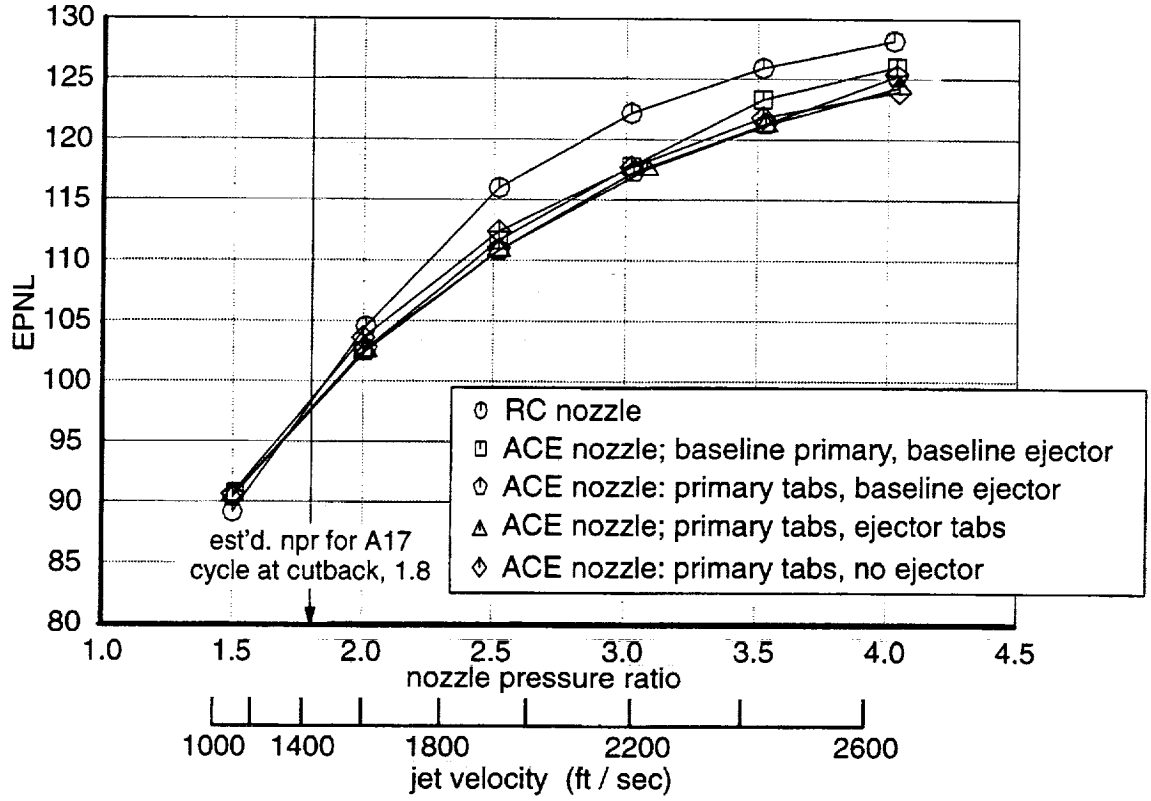

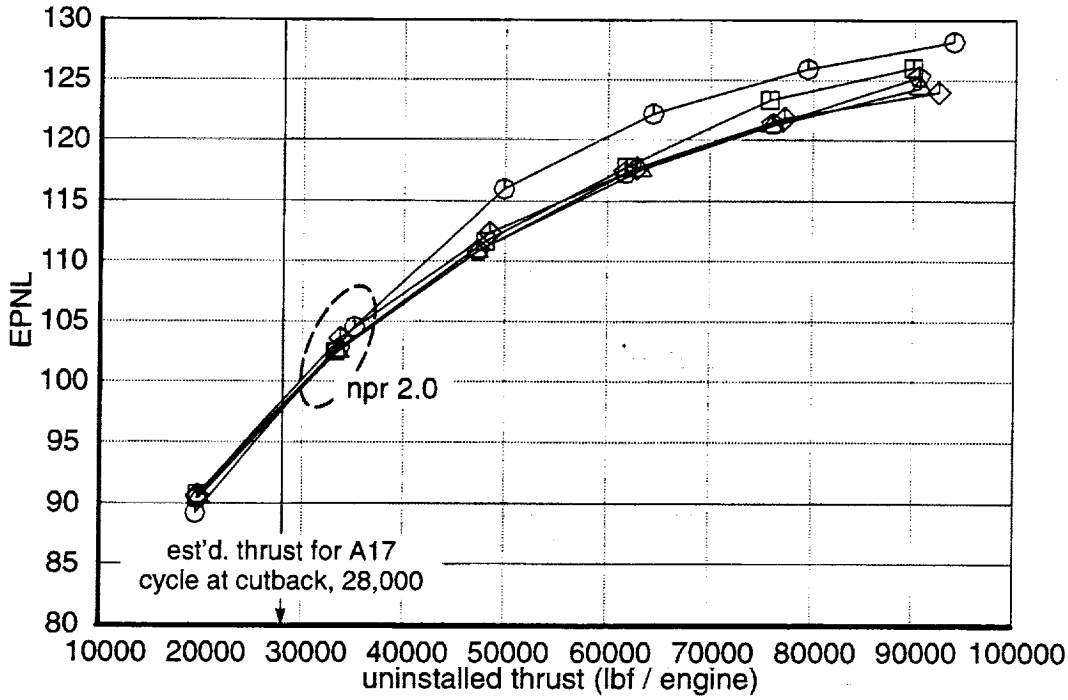

Figure 67. EPNLs for RC Nozzle and Selected ACE Nozzle Configurations at Cutback tunnel Mach 0.245, 20–ft mics

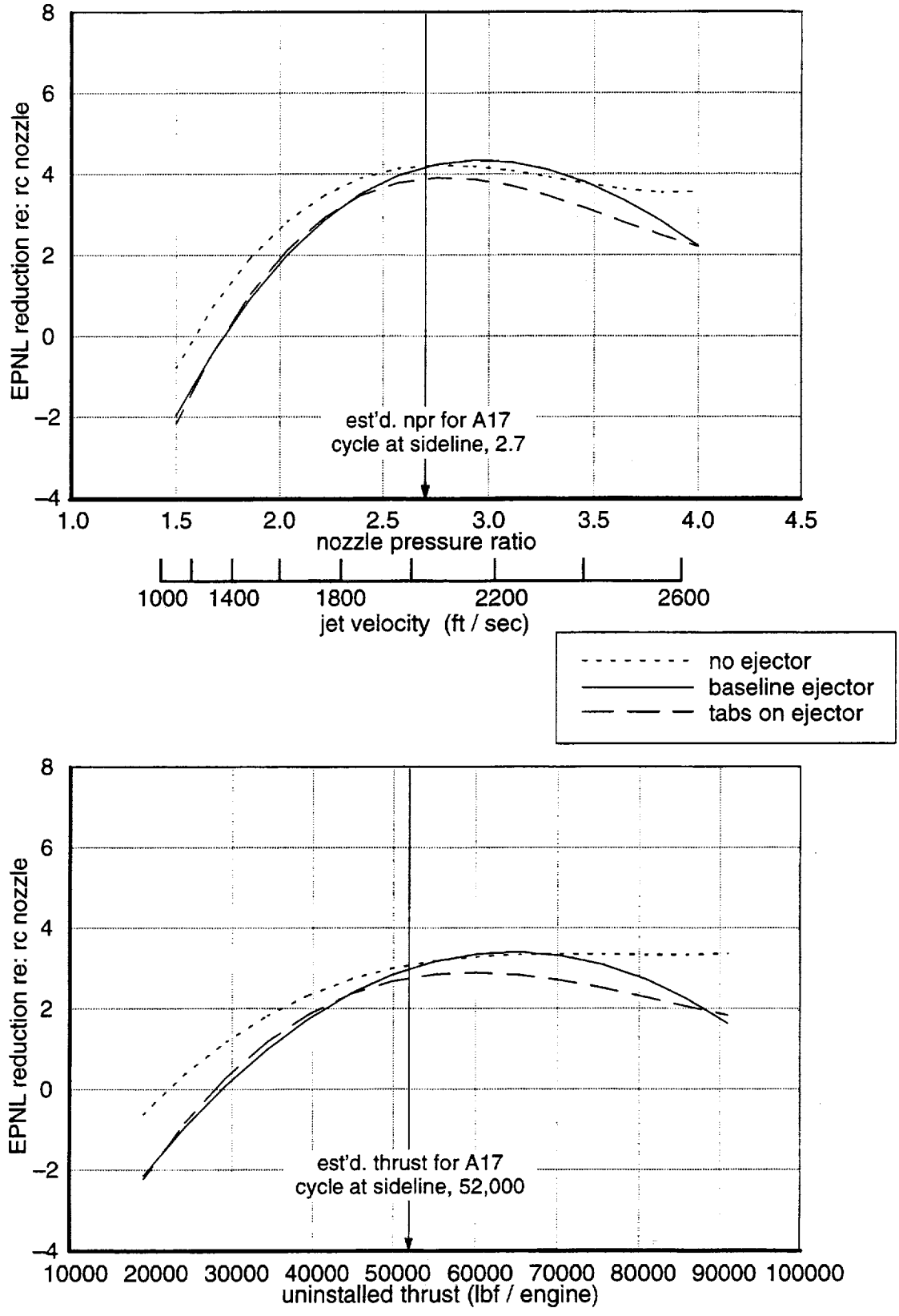

Figure 68. EPNL Reduction, Baseline Primary Nozzle at Sideline
tunnel Mach 0.245, 20–ft mics, corrected data

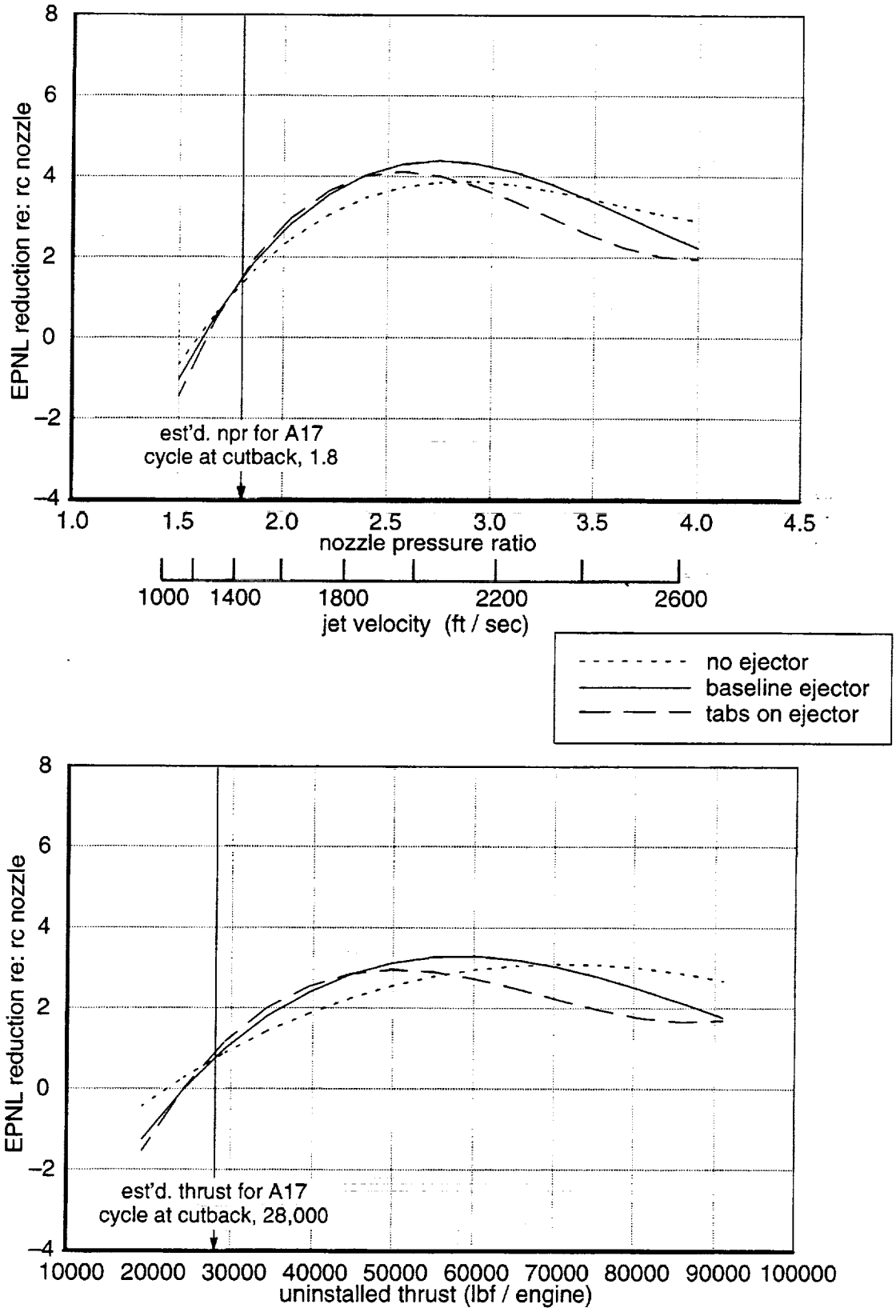

Figure 69. EPNL Reduction, Baseline Primary Nozzle at Cutback
tunnel Mach 0.245, 20–ft mics, corrected data

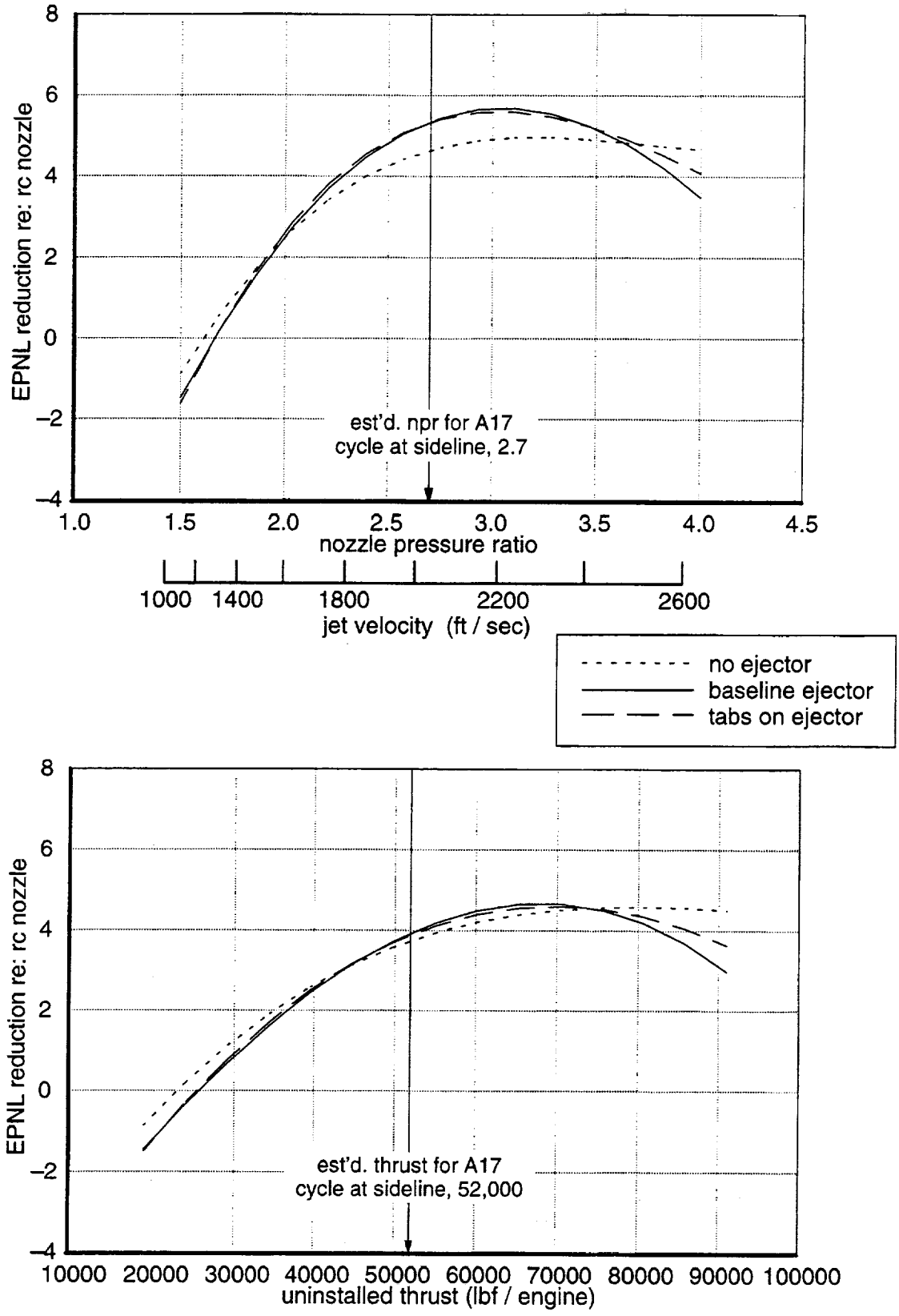

Figure 70. EPNL Reduction, Tabs on Primary Nozzle at Sideline
tunnel Mach 0.245, 20–ft mics, corrected data

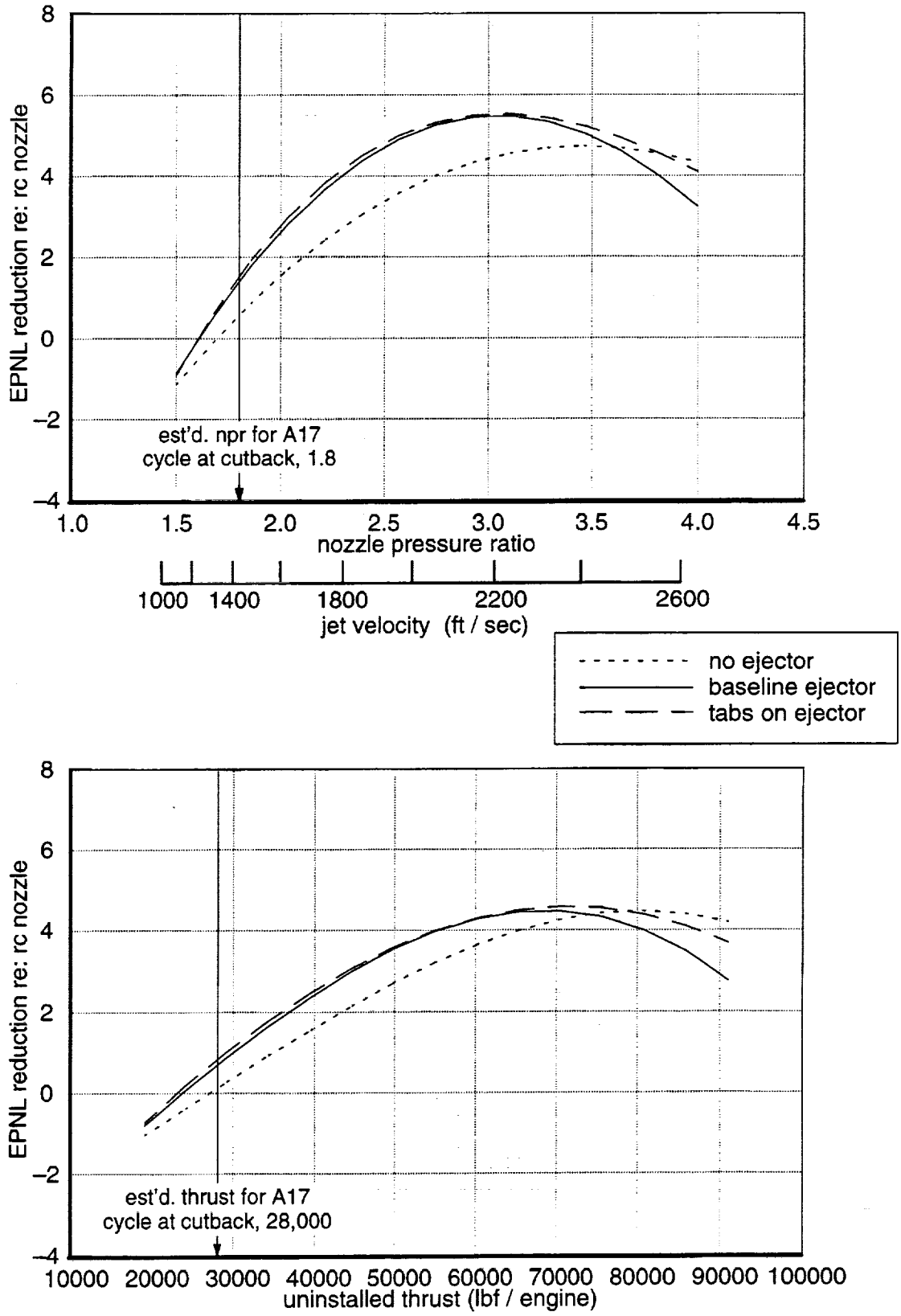

Figure 71. EPNL Reduction, Tabs on Primary Nozzle at Cutback
tunnel Mach 0.245, 20–ft mics, corrected data

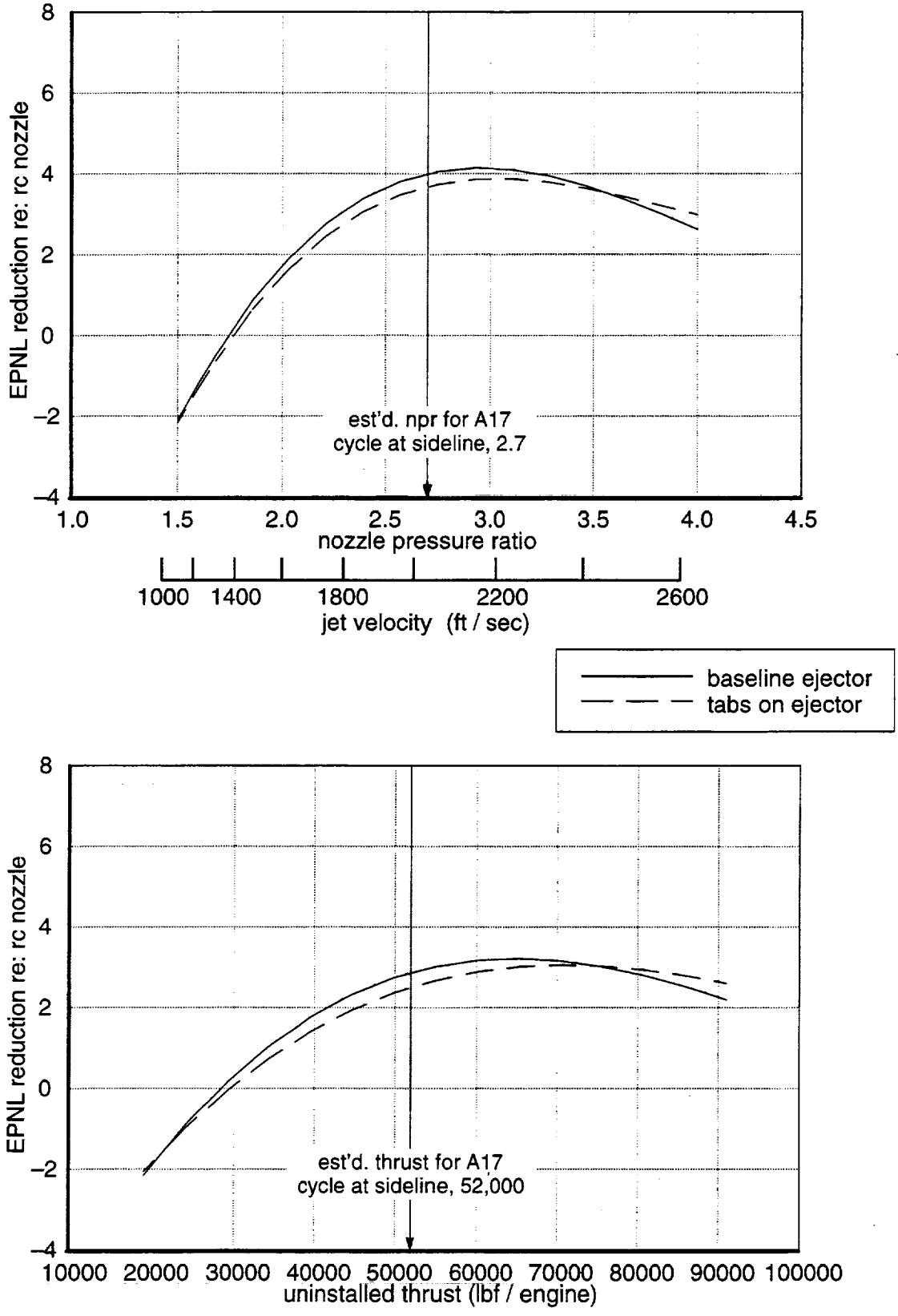

Figure 72. EPNL Reduction, Rods on Primary Nozzle at Sideline
tunnel Mach 0.245, 20–ft mics, corrected data

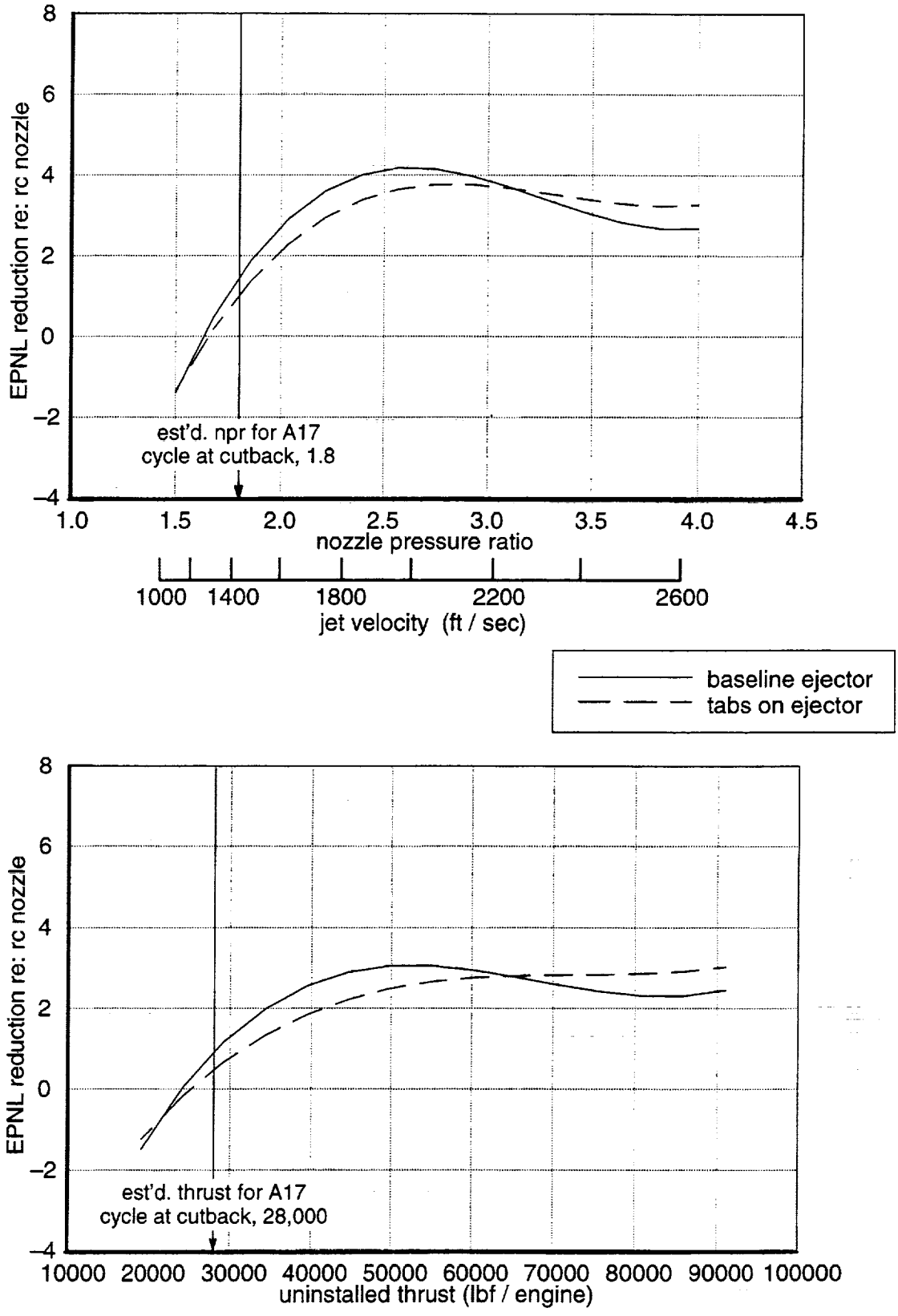

Figure a73. EPNL Reduction, Rods on Primary Nozzle at Cutback
tunnel Mach 0.245, 20–ft mics, corrected data

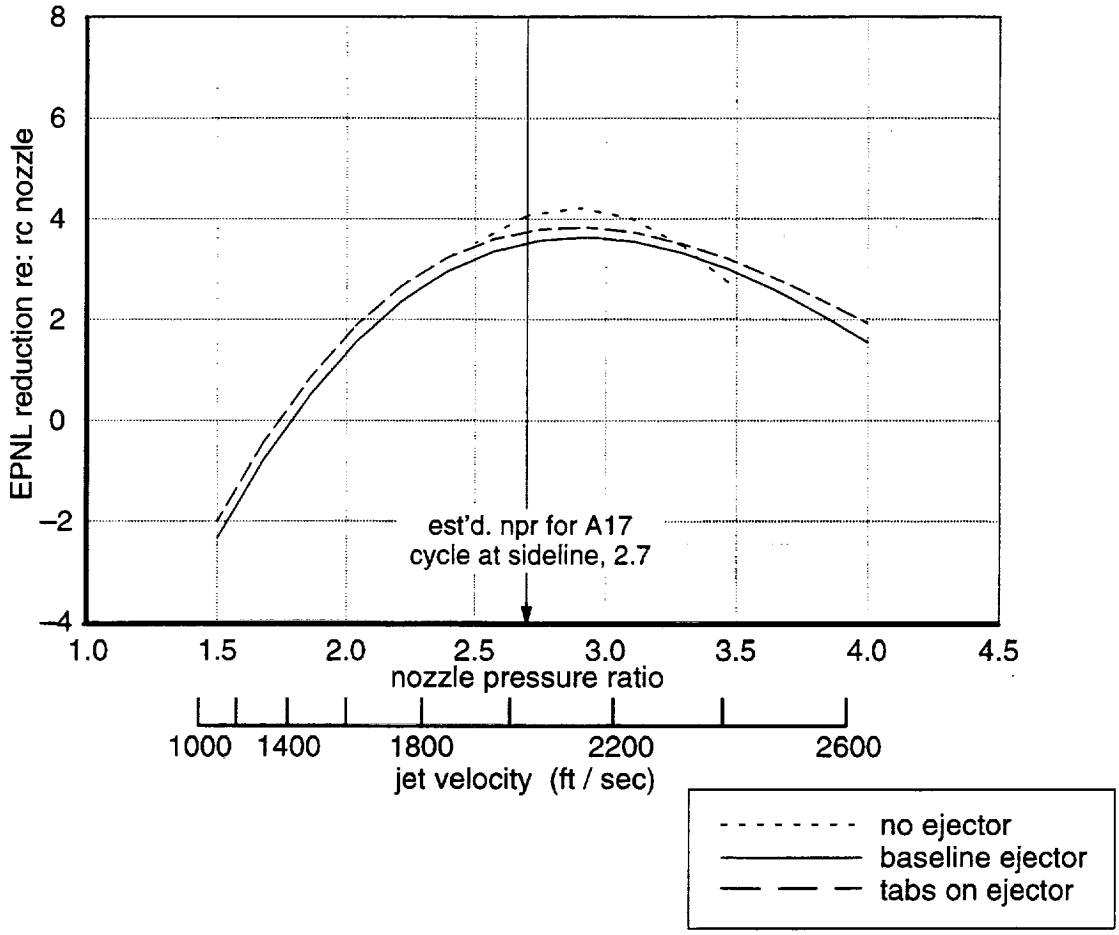

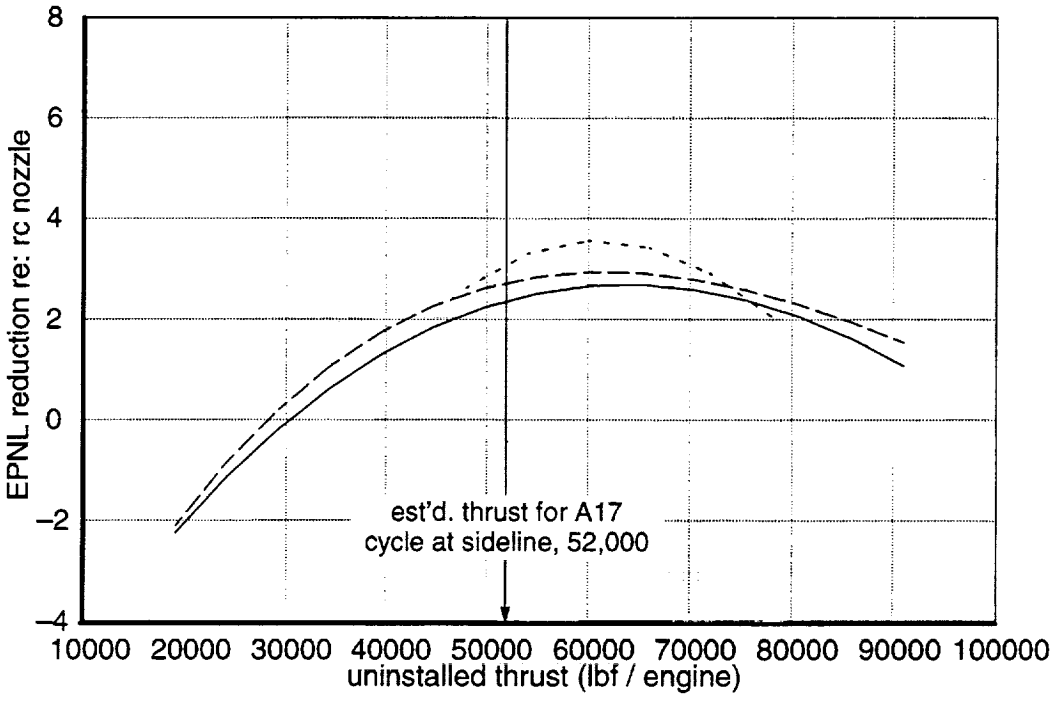

Figure 74. EPNL Reduction, Wheeler Ramps on Primary Nozzle at Sideline tunnel Mach 0.245, 20–ft mics, corrected data

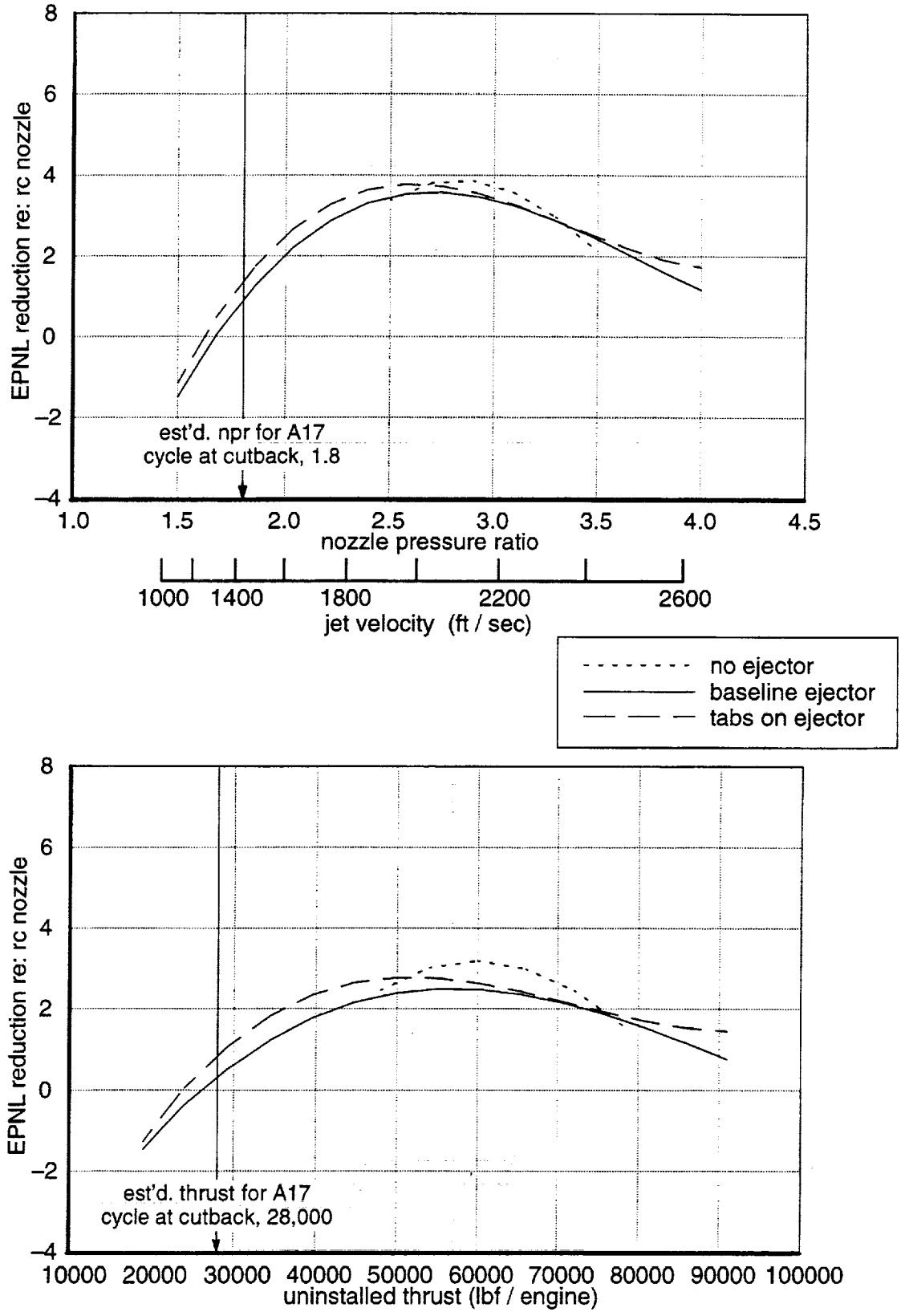

Figure 75. EPNL Reduction, Wheeler Ramps on Primary Nozzle at Cutback tunnel Mach 0.245, 20–ft mics, corrected data

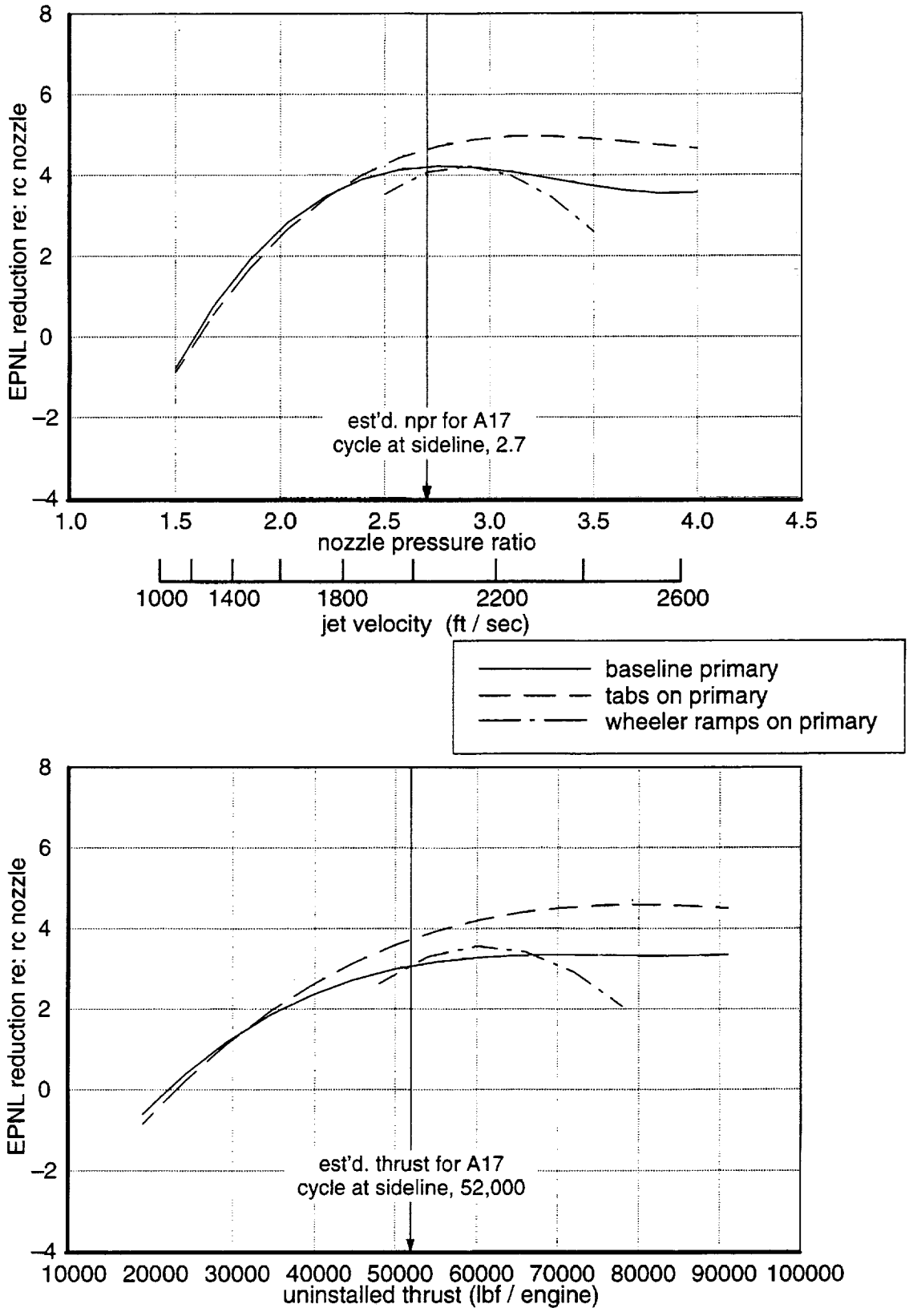

Figure 76. EPNL Reduction, No Ejector at Sideline
tunnel Mach 0.245, 20–ft mics, corrected data

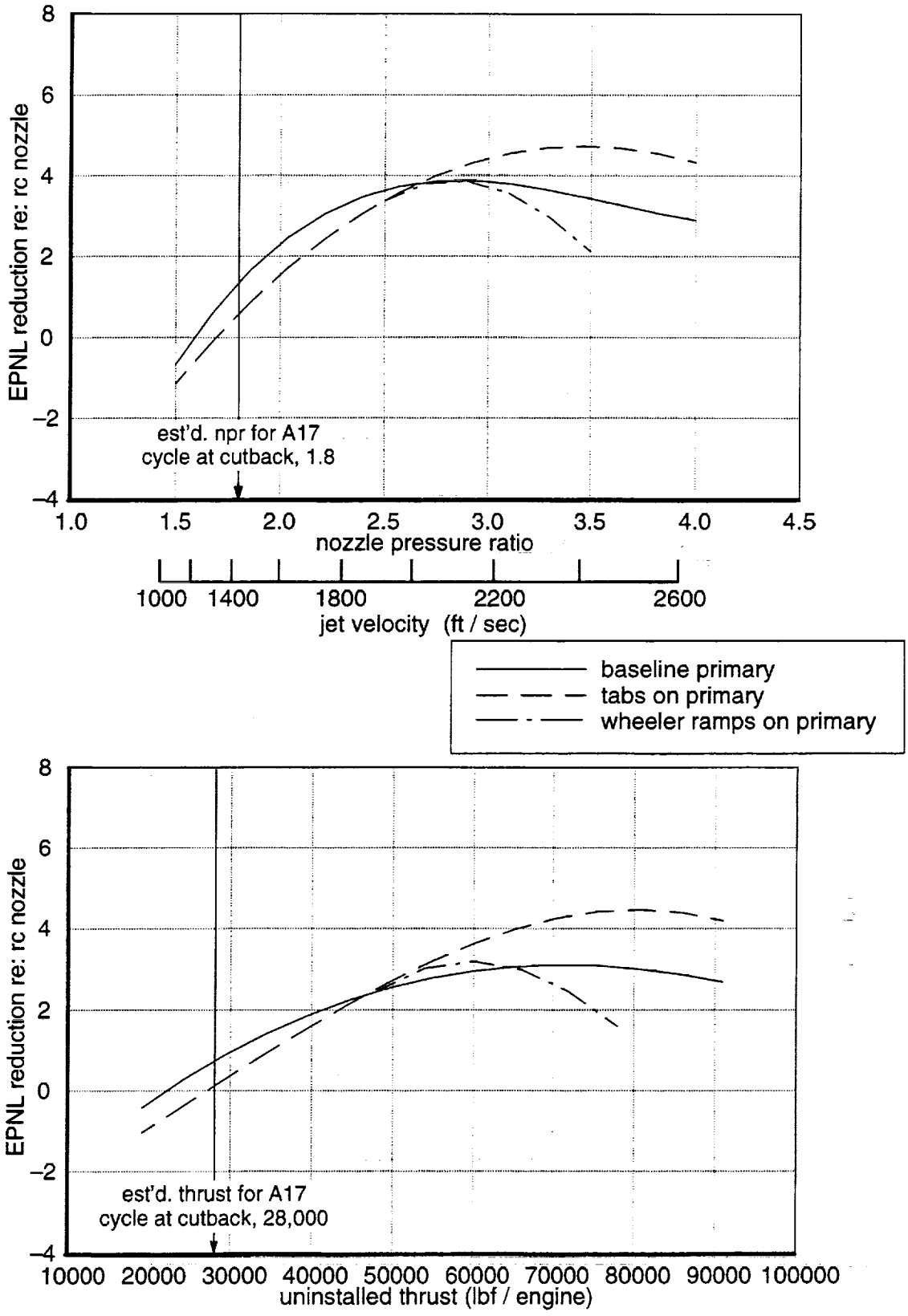

Figure 77. EPNL Reduction, No Ejector at Cutback
tunnel Mach 0.245, 20–ft mics, corrected data

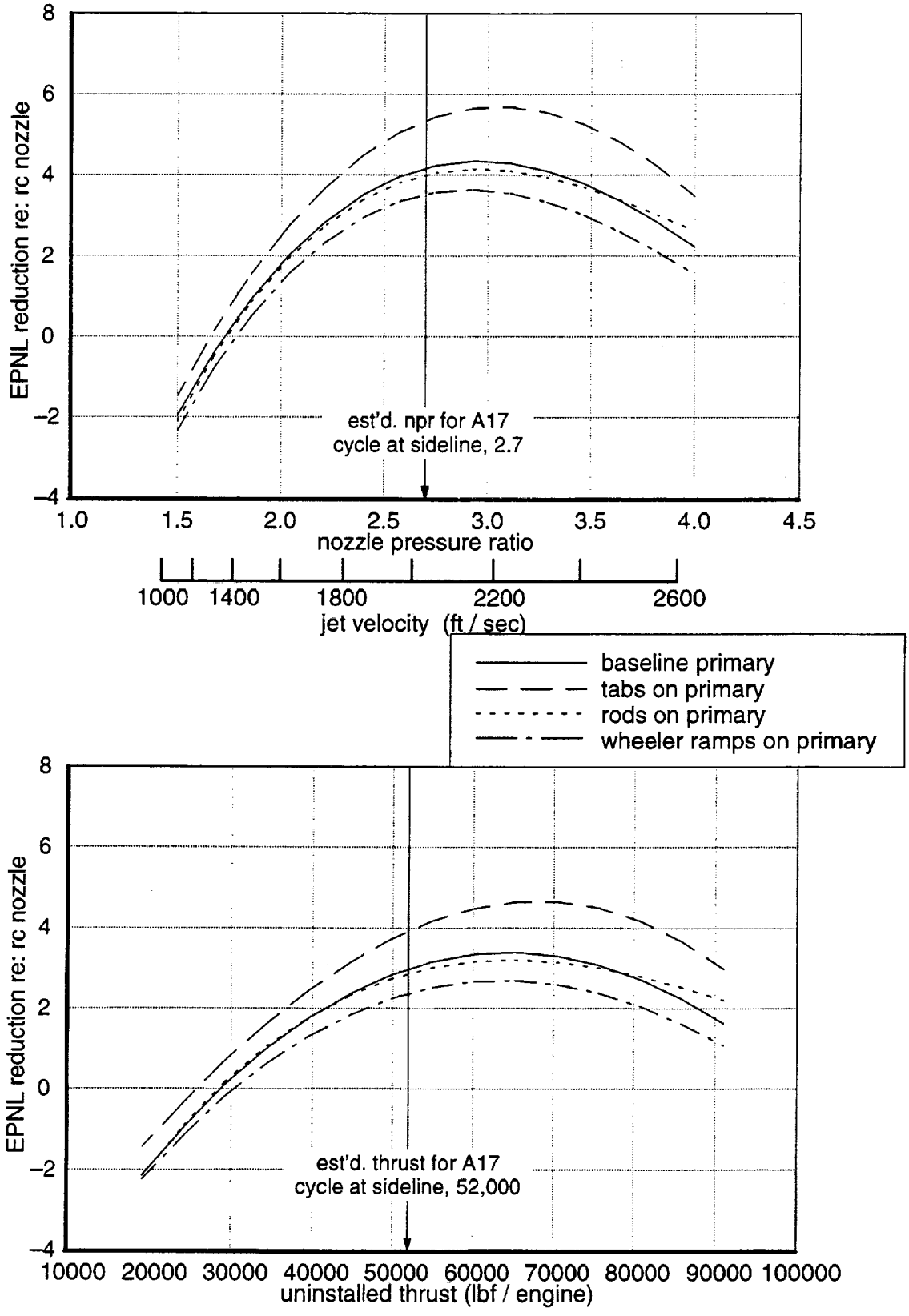

Figure 78. EPNL Reduction, Baseline Ejector at Sideline
tunnel Mach 0.245, 20–ft mics, corrected data

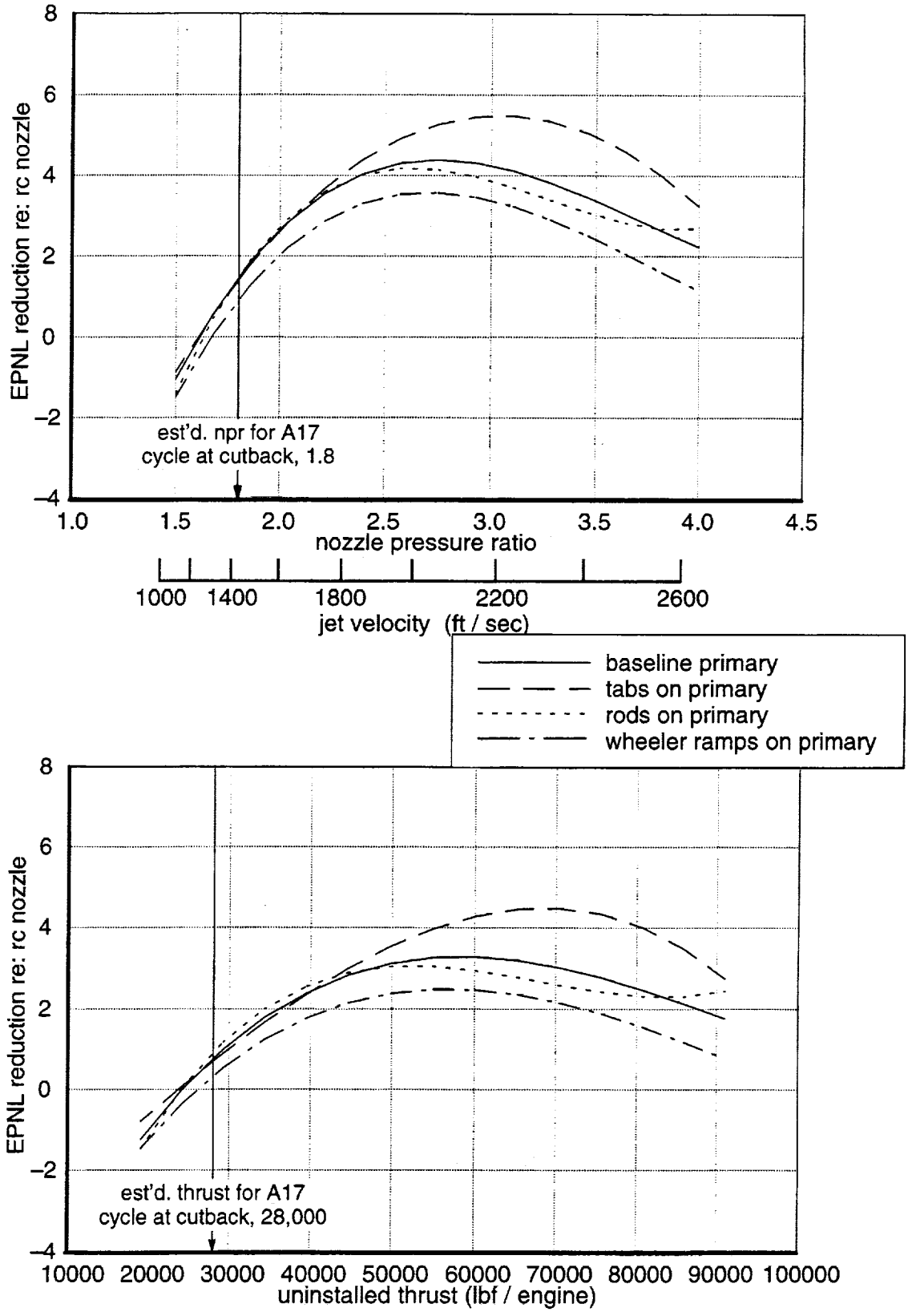

Figure 79. EPNL Reduction, Baseline Ejector at Cutback
tunnel Mach 0.245, 20–ft mics, corrected data

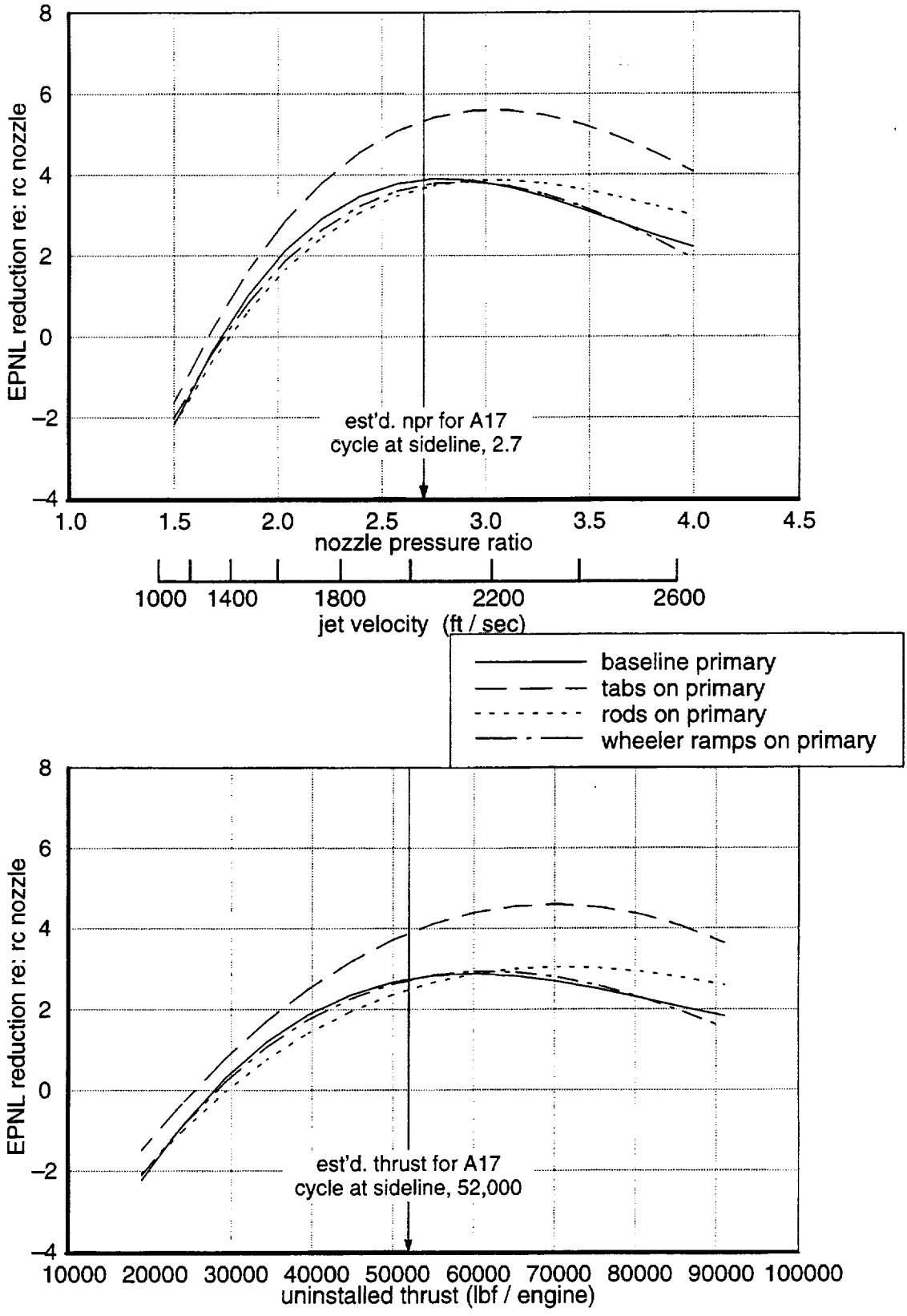

Figure 80. EPNL Reduction, Tabs on Ejector Shroud at Sideline
tunnel Mach 0.245, 20–ft mics, corrected data

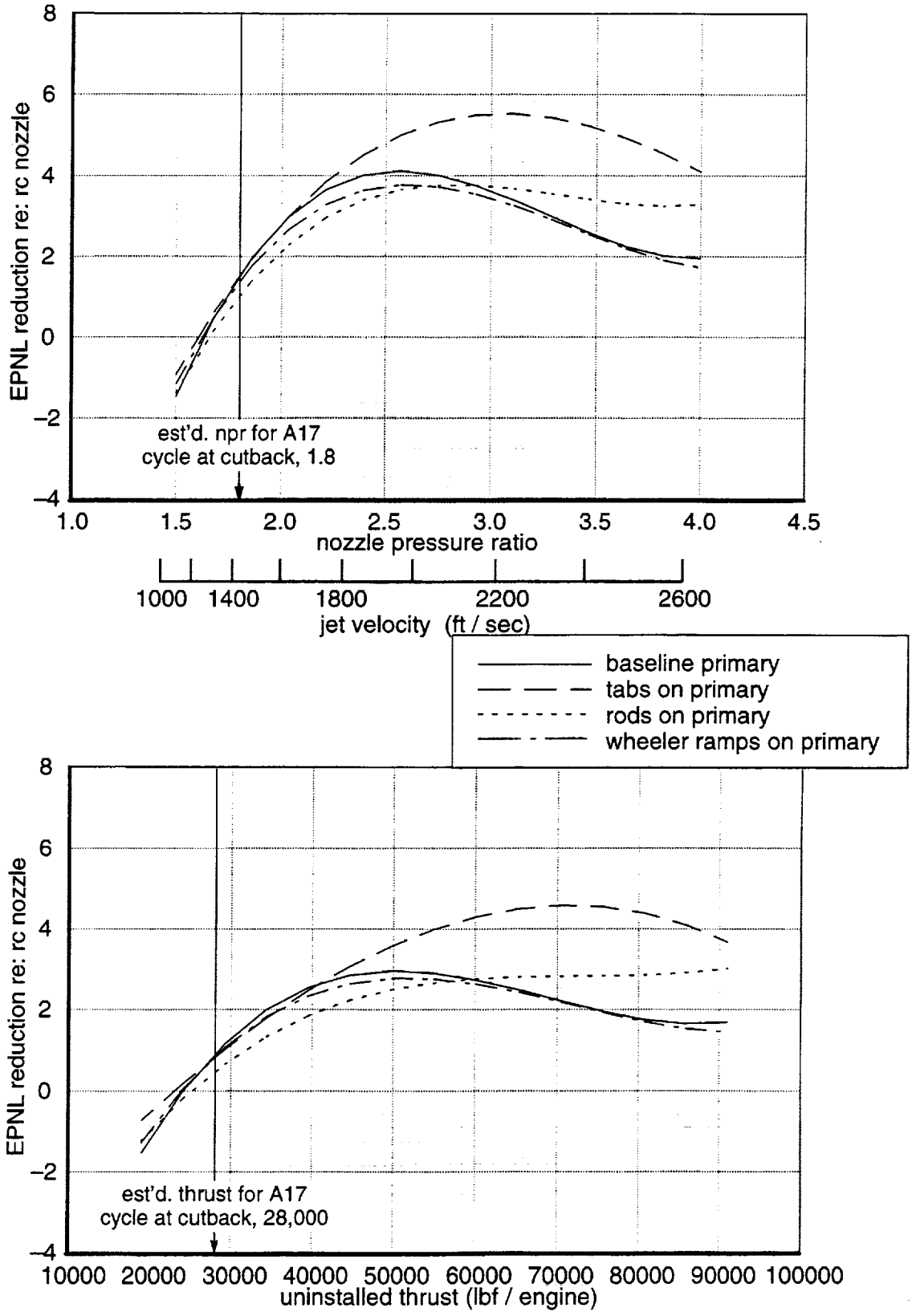

Figure 81. EPNL Reduction, Tabs on Ejector Shroud at Cutback
tunnel Mach 0.245, 20–ft mics, corrected data

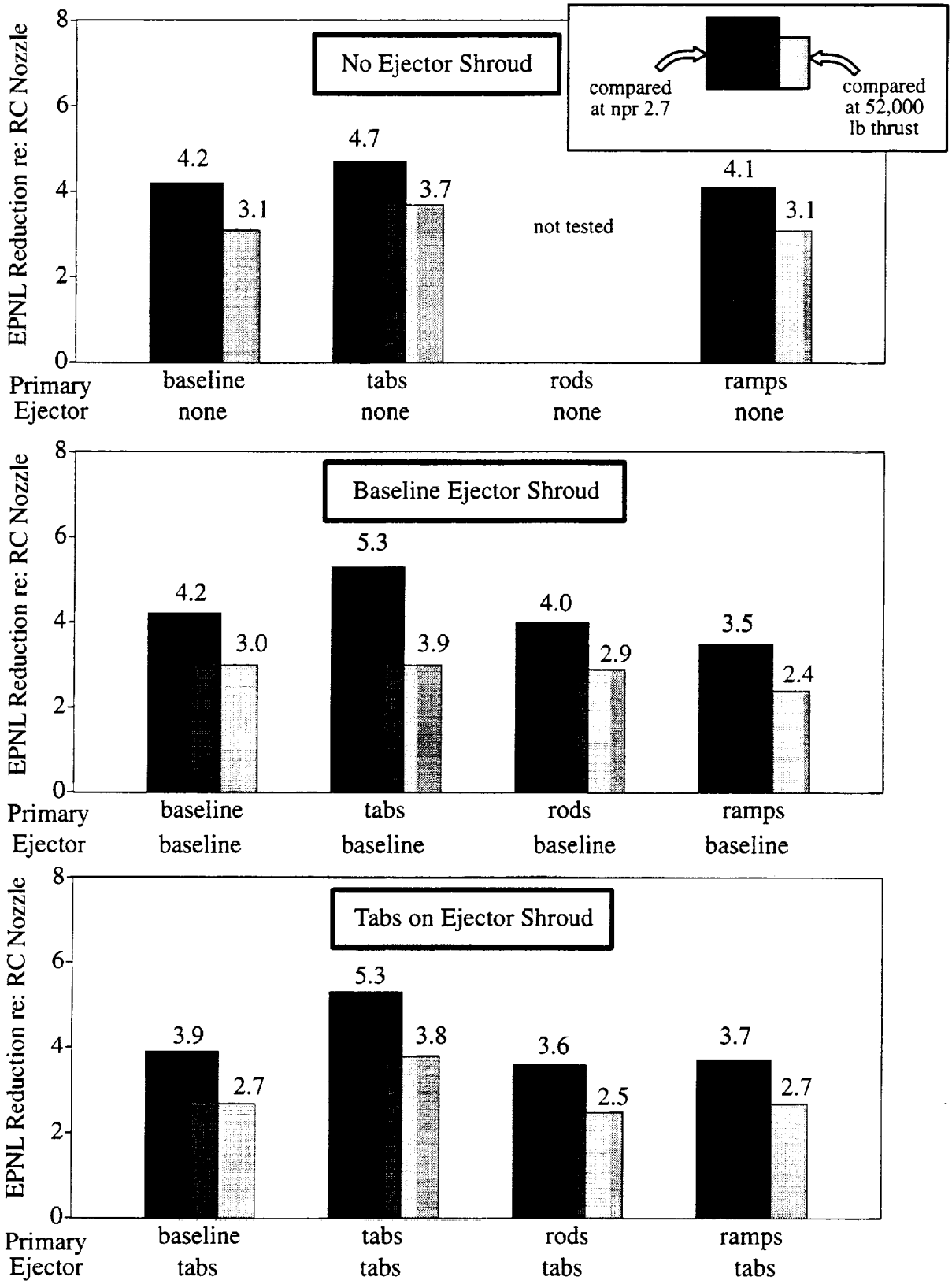

Figure 82. Summary of EPNL Results, Extrapolation to Sideline Condition tunnel Mach 0.245, 20–ft mics, corrected data

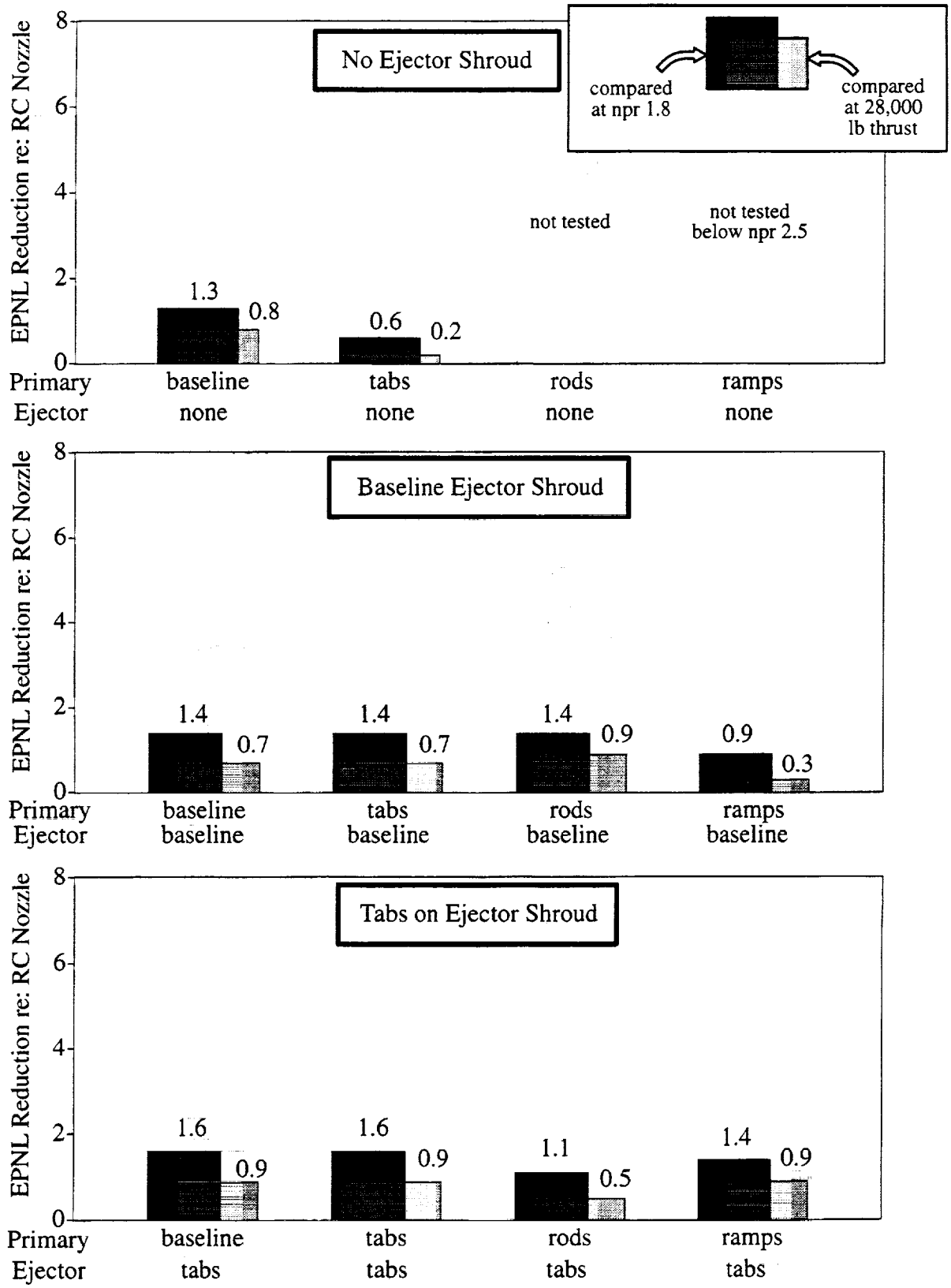

Figure 83. Summary of EPNL Results, Extrapolation to Cutback Condition tunnel Mach 0.245, 20–ft mics, corrected data

REPORT DOCUMENTATION PAGE

Form Approved
OMB No. 0704-0188

1. AGENCY USE ONLY (*Leave blank*)	2. REPORT DATE	3. REPORT TYPE AND DATES COVERED
	February 2000	Final Contractor Report

4. TITLE AND SUBTITLE

Acoustic and Aerothermal Performance Test of the Axisymmetric Coannular Ejection Nozzle Volume II—Acoustic Performance

5. FUNDING NUMBERS

WU–714–04–50–00
NAS3–25963

6. AUTHOR(S)

William Herkes

7. PERFORMING ORGANIZATION NAME(S) AND ADDRESS(ES)

The Boeing Commercial Airplane Group
Division of The Boeing Company
Seattle, Washington 98124–2207

8. PERFORMING ORGANIZATION REPORT NUMBER

E–12122

9. SPONSORING/MONITORING AGENCY NAME(S) AND ADDRESS(ES)

National Aeronautics and Space Administration
John H. Glenn Research Center at Lewis Field
Cleveland, Ohio 44135–3191

10. SPONSORING/MONITORING AGENCY REPORT NUMBER

NASA CR—2000-209813

11. SUPPLEMENTARY NOTES

Project Manager, MaryJo Long-Davis, Aeronautics Directorate, NASA Glenn Research Center, organization code 2300, (216) 433–8708.

12a. DISTRIBUTION/AVAILABILITY STATEMENT

Unclassified - Unlimited
Subject Category: 02 Distribution: Nonstandard

This publication is available from the NASA Center for AeroSpace Information, (301) 621–0390.

12b. DISTRIBUTION CODE

13. ABSTRACT (*Maximum 200 words*)

Acoustic and propulsion performance testing of a model–scale Axisymmetric Coannular Ejector nozzle was conducted in the Boeing Low–speed Aeroacoustic Facility. This nozzle is a plug nozzle with an ejector design to provide aspiration of about 20% of the engine flow. A variety of mixing enhancers were designed to promote mixing of the engine and the aspirated flows. These included delta tabs, tone-injection rods, and wheeler ramps. This report addresses the acoustic aspects of the testing. The spectral characteristics of the various configurations of the nozzle are examined on a model–scale basis. This includes indentifying particular noise sources contributing to the spectra and the data are projected to full–scale flyover conditions to evaluate the effectiveness of the nozzle, and of the various mixing enhancers, on reducing the Effective Perceived Noise Levels.

14. SUBJECT TERMS

High speed civil transport; HSCT; Nozzle; HSCT propulsion nozzle, Mixer; Ejector; Analysis; Jet noise, Noise suppression; Acoustics

15. NUMBER OF PAGES

118

16. PRICE CODE

A06

17. SECURITY CLASSIFICATION OF REPORT	18. SECURITY CLASSIFICATION OF THIS PAGE	19. SECURITY CLASSIFICATION OF ABSTRACT	20. LIMITATION OF ABSTRACT
Unclassified	Unclassified	Unclassified	